

**BIOMIMETIC SUPERSTRUCTURES FROM AMPHIPHILIC
ABA - TRIBLOCK COPOLYMERS**

Inauguraldissertation

zur

Erlangung der Würde eines Doktors der Philosophie

vorgelegt der

Philosophisch-Naturwissenschaftlichen Fakultät

der Universität Basel

von

Julie GRUMELARD

aus Saint-Louis, Frankreich



BASEL, 2004

Genehmigt von der Philosophisch-Naturwissenschaftlichen Fakultät
Auf Antrag der Herren

Prof. Dr. Wolfgang Meier (Universität Basel)

Prof. Dr. Marcus Textor (ETH Zurich)

Prof. Dr. Hanspeter Huber (Universität Basel)

Basel, den 21. Oktober 2004

Prof. Dr. Hans-Jakob Wirz
Dekan

« La science restera toujours la satisfaction du plus haut désir de notre nature, la curiosité; elle fournira à l'homme le seul moyen qu'il ait pour améliorer son sort. Elle préserve de l'erreur plutôt qu'elle ne donne la vérité; mais c'est déjà quelque chose d'être sûr de n'être pas dupe. »

Ernest RENAN, *L'Avenir de la science*, Pensées de 1848 (1890), Flammarion 1995

Table of contents

1	<u>ABSTRACT</u>	6
2	<u>ABBREVIATIONS</u>	8
3	<u>INTRODUCTION</u>	9
	BIOLOGICAL MEMBRANES	9
	SYNTHETIC AMPHIPHILES AS BIOMEMBRANE MIMICS	10
	PMOXA-PDMS-PMOXA ABA-TRIBLOCK COPOLYMERS	11
	AIM OF THE PhD THESIS	14
4	<u>NANOVESICLES</u>	16
4.1	ETHANOL METHOD	16
4.2	DETERGENT METHOD	32
4.2.1	DIALYSIS	34
4.2.2	DILUTION METHOD	36
4.2.3	BIO-BEADS METHOD	38
4.2.4	MEMBRANE PROTEIN RECONSTITUTION	45
4.3	BULK SWELLING	50
4.4	REMINDER OF MAIN RESULTS	53
5	<u>NANOTUBES</u>	54
5.1	BULK DISSOLUTION OR BULK SWELLING	54
5.2	FILM REHYDRATION OR FILM SWELLING	57
5.3	CRYO-TEM	65
5.4	FLUORIMETRY	70
5.5	GOLD LOADED NANOTUBES	72
5.5.1	GOLD PARTICLES ENCAPSULATION	72
5.5.2	GOLD TEMPLATED FORMATION	73
5.6	REMINDER OF MAIN RESULTS	81
6	<u>CONCLUSION AND OUTLOOKS</u>	82
7	<u>MATERIAL AND METHODS</u>	84
7.1	POLYMERS	84
7.2	COMPLEX I RECONSTITUTION EXPERIMENTS	85
7.3	ETHANOL METHOD	86
7.4	DETERGENT REMOVAL WITH BIO-BEADS	86
7.5	ATOMIC FORCE MICROSCOPY	87
7.6	DIALYSIS	87
7.6.1	DIALYSIS MEMBRANES	87

7.6.2	TEMPERATURE-CONTROLLED, CONTINUOUS OPEN-FLOW DIALYSIS APPARATUS	87
7.7	DILUTION METHOD	88
7.7.1	THE DILUTION CELL WITH OPTICAL DETECTOR	88
7.7.2	CONTROL UNIT	89
7.8	DETERMINATION OF THE FREE DETERGENT CONCENTRATION USING THE SITTING-DROP METHOD	90
7.9	TRANSMISSION ELECTRONIC MICROSCOPY	91
7.9.1	PREPARATION OF CARBON-PARLODION* COMPOSITE POLYMER FILMS ON COPPER GRIDS	91
7.9.2	NEGATIVE STAINING	91
7.9.3	CRYOELECTRON MICROSCOPY (CRYO-EM)	92
7.9.4	FREEZE FRACTURE PREPARATIONS FOR ELECTRON MICROSCOPY.	92
7.10	DYNAMIC LIGHT SCATTERING	92
7.11	FLUORESCENCE MEASUREMENTS	93
7.11.1	FLUORESCENCE MICROSCOPY	93
7.11.2	FLUORIMETRY	93
8	<u>APPENDIX I: OTHER ABA-TRIBLOCK COPOLYMER SUPERSTRUCTURES</u>	94
8.1	GIANT VESICLES	94
8.2	MONOLAYERS	95
9	<u>APPENDIX II: FREE-STANDING FILMS – BILAYERS</u>	106
9.1	INTRODUCTION	106
9.2	EXPERIMENTAL	106
9.3	RESULTS	108
9.4	CONCLUSION AND PERSPECTIVES	110
10	<u>APPENDIX III: POLYMER NANOCONTAINERS FOR SELECTIVE IMMOBILIZATION AT SURFACES</u>	111
11	<u>PUBLICATIONS AND POSTERS</u>	113
	POSTER PRESENTATIONS	113
	PUBLICATION LIST	113
12	<u>ACKNOWLEDGMENTS</u>	116
13	<u>REFERENCES</u>	118

1 Abstract

The spontaneous formation of nanostructured materials by molecular self-assembly of block copolymers is an active area of research, driven both by its inherent beauty and by a wealth of potential technological applications. The so-called “supramolecular” structures can be used to build functional materials with nanoscopic dimensions, such as sensors for biochips or smart drug delivery vehicles.

Block copolymer vesicles have attracted increasing interest, particularly in view of possible applications in drug delivery and in protein reconstitution. Conventional methods utilizing synthetic lipid membranes for protein functionality assays have yielded much information with respect to the membrane protein behavior. Furthermore, amphiphilic block copolymer membrane, allowing proper protein refolding while preserving protein function, have been developed to improve the efficiency of these proteins in robust devices.

Even if spherical structures are still the most common supramolecular structures generated by self-assembly of block copolymers, a remarkable variety of other morphologies have now been demonstrated, such as rod-like micelles and nanotubes. Soft nanotubes made from biocompatible organic molecules and polymers could find applications in biotechnology and medicine. However, polymer hollow tubes are rare and have so far only been described in organic solvents where their fabrication often requires elaborate procedures.

Recently, a series of ABA triblock copolymer composed of poly(dimethylsiloxane)-*block*- poly(2-methyloxazoline)-*block*- poly(dimethylsiloxane) (PMOXA-*b*-PDMS-*b*-PMOXA) able to mimic biomembranes has been introduced. The PMOXA blocks have hydroxyl end groups that allow functionalization with methacrylic acid. In aqueous solution, the triblock macromonomers form supramolecular assemblies that can be chemically cross-linked by polymerization of the methacrylic acid groups.

Established and new preparation methods have been used to prepare superstructures in water with various hydrophobic-hydrophilic ratios of the PMOXA-*b*-PDMS-*b*-

PMOXA ABA-triblock copolymers. Suitable choice of the block lengths and preparation method allowed controlling the shape of the self-assemblies.

We have particularly introduced a preparation method for nanovesicles using detergents and bio-beads that is a suitable alternative devoid of organic solvents leading to improved reconstitution of functional membrane proteins.

We have also developed a simple method for the preparation of soft, water-filled nanotubes via self-assembly of PMOXA-b-PDMS-b-PMOXA in aqueous media.

Polymer nanotubes have been loaded with water-soluble substances and used as highly specific templates for inorganic synthesis.

2 Abbreviations

AFM	Atomic Force Microscopy
BLM	Black Lipid Membrane
CAC	Critical aggregation concentration
CF	Carboxyfluorescein
CMC	Critical micellar concentration
DDM	Dodecylmaltoside or n-Dodecyl- β -D-maltopyranoside
2-D	Two-dimensional
DLS	Dynamic Light Scattering
DNA	Deoxyribonucleic acid
DPHPC	Diphytanoylphosphatidylcholine
E. coli	Escherichia coli
EPR	Electron Paramagnetic Resonance
HEPES	4-(2-hydroxyethyl)-1-piperazineethanesulfonic acid, or “Free Acid”
LamB	Maltoporin
MscL	Large mechanosensitive channel
NMR	Nuclear Magnetic Resonance
OG	Octylglucoside or n-Octyl- β -D-glucopyranoside
OmpF	E. coli Outer membrane porin
o-POE	Octyl-POE or n-octyl polyoxyethylene
PBS	Phosphate Saline Buffer
PDMS	Poly (dimethylsiloxane)
PEG	Polyethylene glycol
PMOXA	Poly (2-methyloxazoline)
SDS-PAGE	Sodium dodecyl sulfate-polyacrylamide gel electrophoresis
SEC	Size Exclusion Chromatography
TEM	Transmission Electron Microscopy
T X100	Triton X100

3 Introduction

Biological membranes

The function of **biological membranes** [1] is to organize biological processes by compartmentalizing them. Indeed, the cell, the basic unit of life, is essentially defined by its enveloping plasma membrane. Moreover, in eukaryotes, many subcellular organelles, such as nuclei, mitochondria, chloroplasts, the Golgi apparatus and the endoplasmic reticulum, are likewise membrane bound. Many fundamental biochemical processes, e.g. electron transport and oxidative phosphorylation, occur on or in the membrane scaffold.

A biological membrane is composed of proteins and other molecules associated with a phospholipid bilayer matrix (Figure 1). The lipids are arranged tail to tail so that only the hydrophilic heads are exposed to the aqueous medium on both sides of the membrane. This is the minimum-energy configuration for a suspension of lipids in water.

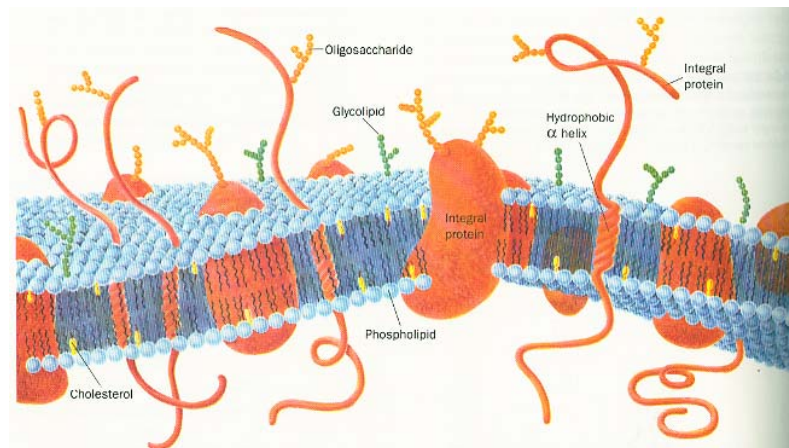


Figure 1: Schematic presentation of a cell membrane. Integral proteins (orange) are embedded in a bilayer of phospholipids (blue, shown in higher proportion than in nature for clarity) and cholesterol (yellow). The carbohydrate components of glycoproteins (yellow beaded chains) and glycolipids (green beaded chains) occur only on the external face of the membrane. From [1] p 292

Plasma membrane has various functions; (i) it acts as a semi-permeable barrier, (ii) it regulates the transport in and out of the cell, (iii) and it is responsible for communication and adhesion between the cells.

The **lipid bilayer** accounts for the basic barrier functions of the plasma membrane. It is permeable to water, oxygen, small hydrophobic molecules such as steroids, and ethanol; it is impermeable to highly charged molecules and ions such as Na^+ , K^+ .

Membrane proteins carry out most of the functions of the membrane. They are channels, receptors, enzymes etc., as shown in Figure 2. The functions of membrane proteins include transport of substances across membranes, enzymatic activity (e.g. smooth endoplasmic reticulum), signal transduction (e.g. cell communication), intracellular joining, cell-cell recognition (e.g. cell communication), and attachment to the cytoskeleton and extracellular matrix.

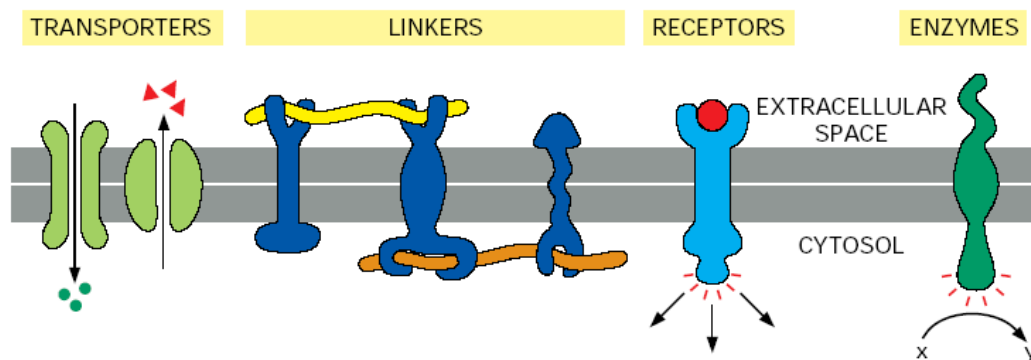


Figure 2: Some functions of plasma membrane proteins ©1998 by Alberts, Bray, Johnson, Lewis, Raff, Roberts, Walter <http://www.essentialcellbiology.com> Published by Garland Publishing.

Synthetic amphiphiles as biomembrane mimics

Artificial lipid membranes are widely studied as a model system for biological membranes. They are useful to study the physical properties of membranes, such as elasticity and permeability, but also the structure and the function of membrane proteins; their functional insertion and moreover their crystallization in lipid bilayers is of a great interest. In addition, **liposomes** (closed, self-sealing, solvent-filled vesicles surrounded by a single lipid bilayer) have attracted considerable interest for drug delivery [2], cosmetic formulation [3], or non-viral gene delivery vectors [4].

However, such liposomes are generally rather unstable [5, 6]. Various strategies have been developed to **stabilize liposomes** [7], such as steric stabilization [8, 9] or polycondensation of liposomes [10, 11]. The use of polymers has been also investigated [12-14]. A stabilization strategy of lipid membranes where the lateral mobility of the lipid molecules in the membrane is preserved was also proposed [15]: a 2D-polymer network is formed in the middle of the membrane on which the lipid molecules can freely glide. A **bioreactor** was thus introduced by incorporating natural channel proteins into polymer-stabilized liposomes [16]. The concept of this new kind of **nanoreactor** (illustrated in Figure 3), combining the protective ability of membrane and permeability control by natural channels, has recently been extended to a block copolymer system [17].

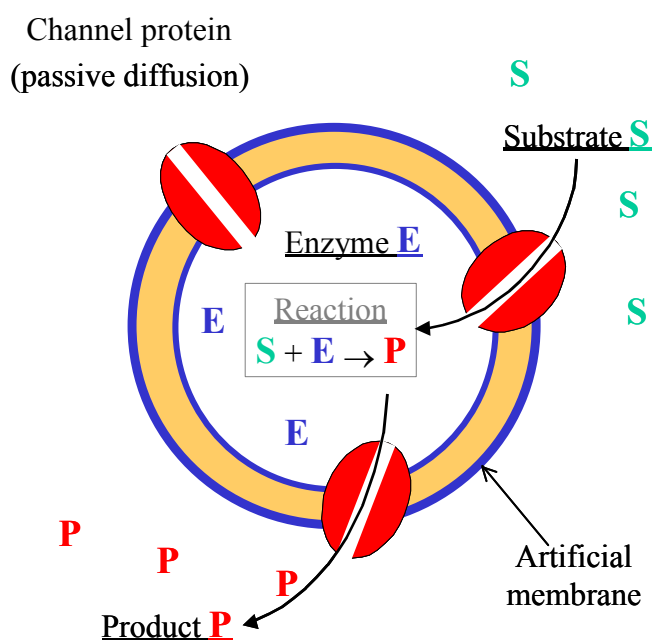


Figure 3: Nanoreactor. Nanovesicle act as a nanoreactor by release or incorporation of molecules through transport proteins inserted in the membrane

PMOXA-PDMS-PMOXA ABA-triblock copolymers

Recently, the self-assembly properties of a new amphiphilic **ABA-triblock copolymer**, composed of a hydrophobic middle block of poly(dimethylsiloxane) and two hydrophilic side blocks of poly(2-methyloxazoline) (Figure 4), into planar [18] or vesicular bilayers [19] was used to mimic biological membrane and to reconstitute functional membrane proteins (especially porins) [20, 21].

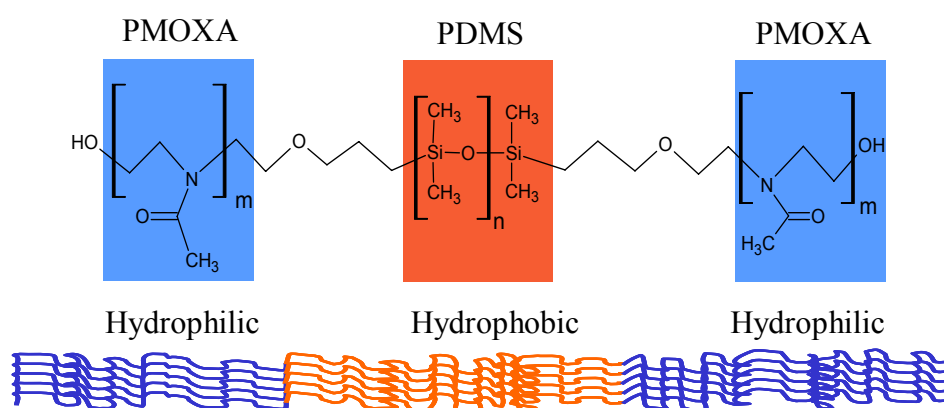


Figure 4: ABA-triblock copolymer formula and schematic bilayer

The amphiphilic PMOXA-b-PDMS-b-PMOXA (2-methyloxazoline-block-dimethylsiloxane-block-2-methyloxazoline) used for those studies was initially formulated by Ciba-Vision[®] as a material for contact lenses, because of its biocompatibility and low-protein binding surface. As shown in the phase diagram in Figure 5, it forms nanostructured hydrogels in concentrated solution and self-assembles into nanovesicles in dilute aqueous solution [22]. Giant vesicles (sub-micron range) can also be obtained by electroformation [23].

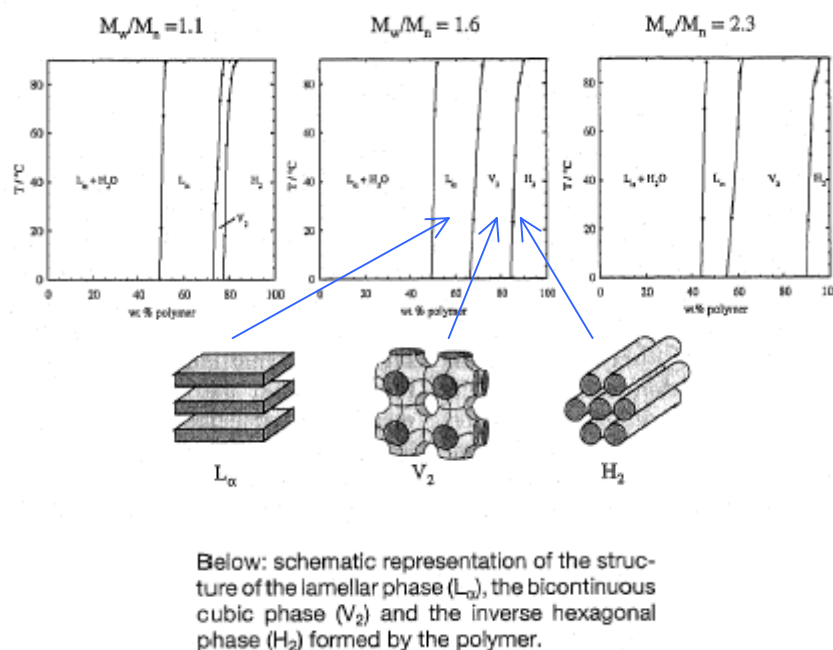


Figure 5: Phase diagrams of PMOXA-PDMS-PMOXA in water. Influence of the polydispersity of the hydrophilic blocks (M_n PDMS=5400g.mol⁻¹, M_n PMOXA=2100 g.mol⁻¹) [22]

The main advantage of the ABA-triblock copolymer is the versatility of the self-assembled vesicles illustrated in Figure 6; (i) the shell has a hydrophilic, biocompatible low-protein-binding onto surface, and an extremely high mechanical, chemical and thermal stability, (ii) the shell can act as a biomembrane for protein reconstitution, (iii) the nanovesicle can encapsulate hydrophilic substances, and (iv) the shell material has enormous possibilities for molecular functionalization. The nanovesicles can thus be employed as specific targeted drug delivery systems (e.g. biotinylated vesicles), stimuli responsive nanocontainers (e.g. pH sensitive) or nanoreactors.

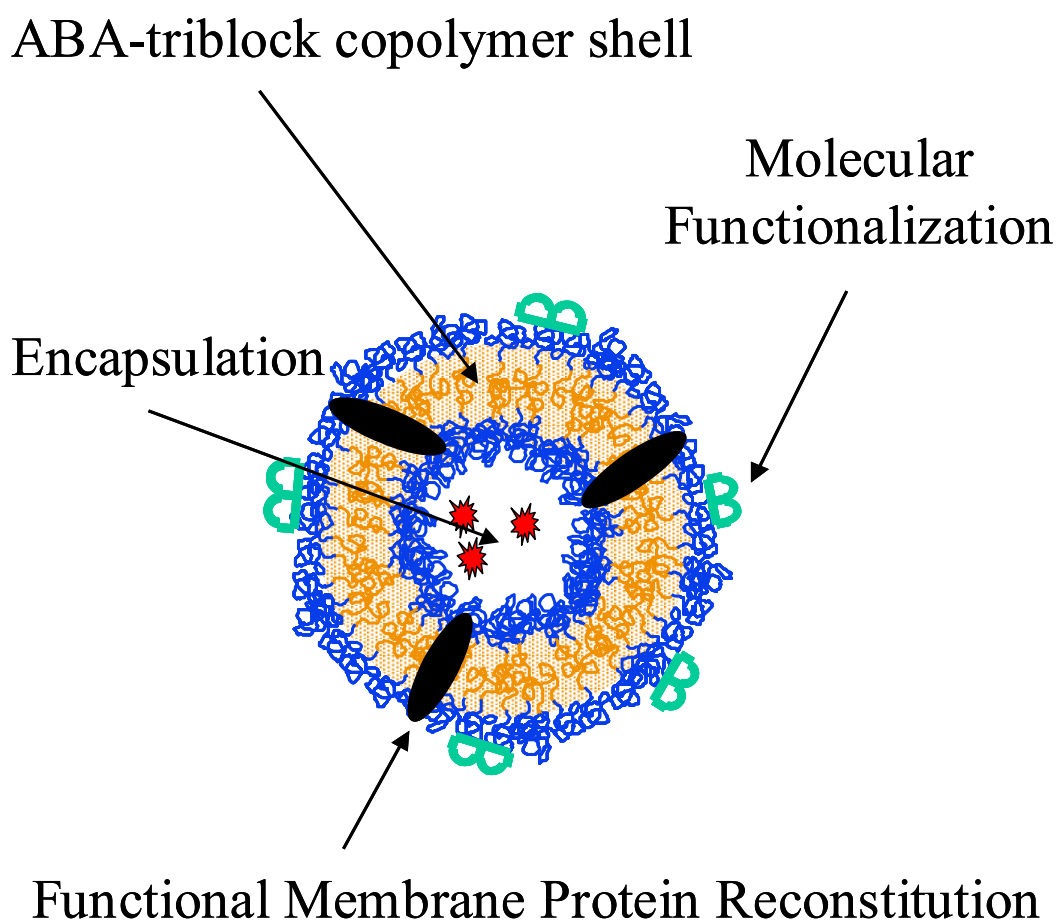


Figure 6: Schematic of an ABA-triblock copolymer vesicle with various modifications

This is highly promising for applications such as drug delivery, biosensors, and also gene therapy. Figure 7 illustrates one example of a so-called “**proteovesicle**”, where a virus recognizes its receptor on the inserted membrane protein and loads its DNA into the polymer nanocontainer [21].

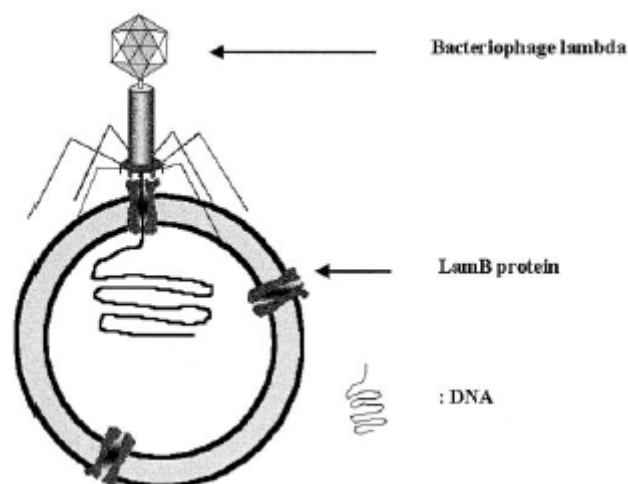


Figure 7: DNA-loaded vesicle; Lambda phage binds a LamB protein (receptor) and the DNA is transferred across the membrane [21]

The amphiphilic PMOXA-PDMS-PMOXA triblock copolymer is synthesized via cationic ring-opening polymerization of 2-methyloxazoline onto an activated telechelic PDMS block [19]. The length of each block can be adjusted by the amount of monomer added to the reaction mixture and the -OH end groups of the PMOXA blocks allow for further functionalization.

Aim of the PhD thesis

Based on previous investigations on ABA-triblock copolymer vesicles, 2 main questions became apparent.

The first question concerns the influence of the block length ratio on the morphology of the self-assembled superstructures. Micelles and vesicles are commonly observed in dilute solution. The possibility of preparing also tubular structures, that might be suitable as synthetic mimics of protein channels, was investigated by using established and newly developed sample preparation methods, and by a systematic study of various available PMOXA-PDMS-PMOXA block copolymers presented in Table 1. Were compared the morphologies in diluted solution as a function of polymer composition and preparation method.

Table 1: Description of the ABA triblock copolymers

Name	Mn	End group	Formula ^a
HP 708	9000	Methacrylate	A ₂₁ B ₆₉ A ₂₁
JW 08	7500	OH	A ₁₅ B ₆₂ A ₁₅
JW 03	4150	Methacrylate	A ₂₆ B ₄₈ A ₂₆
T 02	8500	OH	A ₁₆ B ₇₂ A ₁₆
TD 01	8500	Methacrylate	A ₁₆ B ₇₂ A ₁₆
TD 02	8500	Methacrylate	A ₁₆ B ₇₂ A ₁₆
S 125	9300	OH	A ₂₁ B ₇₂ A ₂₁
S 104	6700	OH	A ₁₁ B ₆₂ A ₁₁
S 131	8660	OH	A ₁₈ B ₇₂ A ₁₈

^a A: PMOXA, B: PDMS

The second question deals with improving membrane protein reconstitution procedures for synthetic polymeric membrane. The objective was to develop a procedure that allows also the insertion of sensitive proteins, that are not resistant to organic solvents, and that allows a high proportion of functional proteins incorporated in vesicles.

The structure of the thesis is divided in two main parts illustrating the two main superstructures we have studied: nanovesicles and nanotubes. The preparation methods and their applications in biology, such as protein reconstitution, are presented for both structures. Additional morphologies are presented in the appendix, together with additive experiments on lipid membrane and core-shell nanocontainers.

4 NANOVESICLES

As stated above, the first goal of this thesis was to reproduce the formation of nanovesicles with the new polymers synthesized in the group. The superstructures obtained via the established ethanol method [19] have been characterized and the reproducibility is discussed.

4.1 Ethanol method

Typical vesicles obtained via the ethanol method (chapter 7.3) are shown in Figure 8. The diameters measured in TEM were below 50 nm (from 10 to 50 nm) with all the polymers; this means that we have probably micelles and/or vesicles with an extremely small intravesicular space, in which only low encapsulation rate is possible.

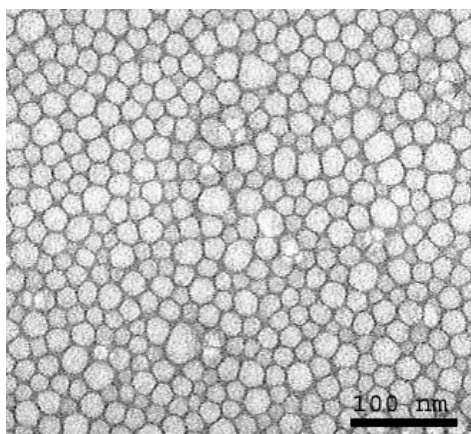


Figure 8: ABA-triblock copolymer (TD01) vesicles obtained via the ethanol method and subsequent filtration

We performed Dynamic Light Scattering (DLS) measurements on samples prepared via the ethanol method with different polymers in order to characterize spheres observed in TEM.

Theory

According to the semi-classical light scattering theory when light impinges on matter, the electric field of the light induces an oscillating polarization of electrons in the

molecules. The molecules then serve as secondary source of light and subsequently radiate (scatter) light. The frequency shifts, the angular distribution, the polarization, and the intensity of the scattered light are influenced by the size, shape and molecular interactions in the scattering material.

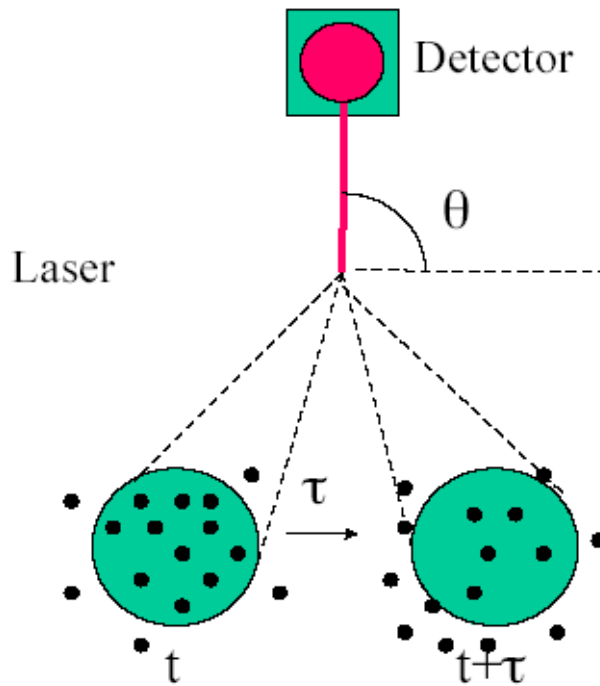


Figure 9: Scheme of the fluctuation of the scattered light in DLS; τ is the delay time and θ the angle of scattering measurement

DLS makes use of the Brownian motion (translational diffusion) of the molecules by measuring the intensity fluctuations of the scattered light, as explained in Figure 9.

The function $g_2(t)$, called intensity autocorrelation function, is derived from intensity fluctuation over time. A valid autocorrelation function is smooth, continuous, and exponentially decaying from a maximum value of 2 to 1. The parameter obtained is the **decay time**, which is dependent on molecule size.

If the population is monodisperse, a single exponential can fit the autocorrelation.

$$g_2(t) \propto e^{-t/\tau}, \quad \text{Equation 1}$$

If the population is polydisperse, we observe a decay time distribution. The overall diffusive process is not the sum of the individual ones due to cooperative motions.

$$g_2(t) \propto \int e^{-t/\tau} \cdot d\tau \quad \text{Equation 2}$$

The decay time is directly correlated to the diffusion coefficient of the molecules D

$$\tau = \frac{1}{D \cdot q^2}, \quad \text{Equation 3}$$

where q is the wave vector depending on the observation angle θ , the refractive index of the medium n and the wavelength of the incident beam λ .

$$q = \frac{4\pi \cdot n}{\lambda} \sin\left(\frac{\theta}{2}\right) \quad \text{Equation 4}$$

By fitting the autocorrelation curve, the diffusion coefficient can be calculated, and D_0 is extrapolated to angle 0 and concentration 0. Assuming that our vesicles behaves as hard spheres, D_0 could be related to the hydrodynamic radius R_h using the Stokes - Einstein equation:

$$R_h = \frac{k_B T}{6\pi\eta D_0} \quad \text{Equation 5}$$

where k_B is Boltzmann constant, T temperature, η solvent viscosity.

For hard sphere, the hydrodynamic radius R_h is equivalent to the gyration radius R_s . However, for other particles, we can consider R_h as the radius of a hypothetical hard sphere that diffuses with the same speed as the particle under examination. Figure 10 gives a few examples of R_h for different particles, such as charged sphere, rod or gaussian coil.

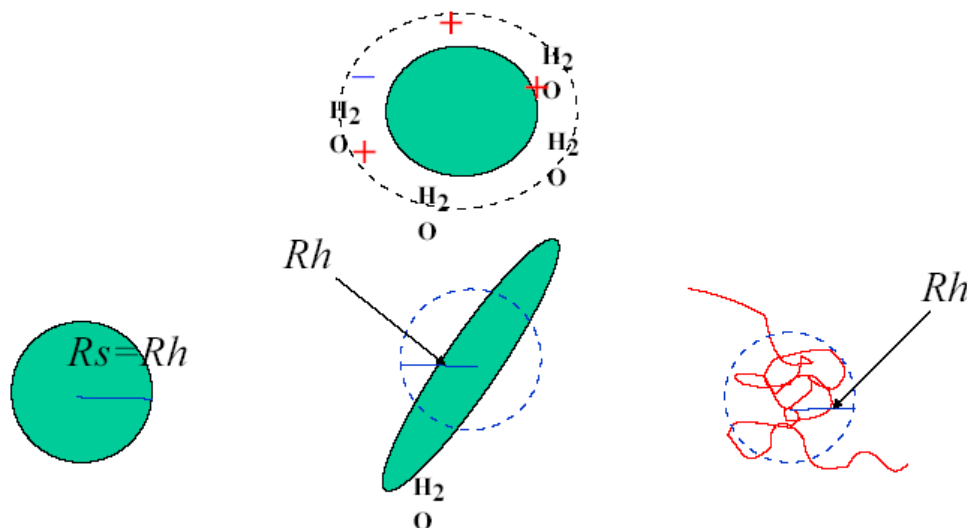


Figure 10: Hydrodynamic radius R_h for different molecules. For a hard sphere, the hydrodynamic radius R_h is equivalent to the gyration radius R_s .

If more than one decay is observed in the autocorrelation function, there is a multimodal population. A faster one represents a smaller particle and a slower one represents a larger particle.

Results and Data analysis

Figure 11 shows the autocorrelation function of 0.5% ABA copolymer (TD01) sample. The sample was prepared at 1% with the ethanol method, i.e. dissolution of polymer in ethanol and dropwise addition to water, and further dilution to 0.5 % in water. Multiple filtrations have been performed to eliminate dust.

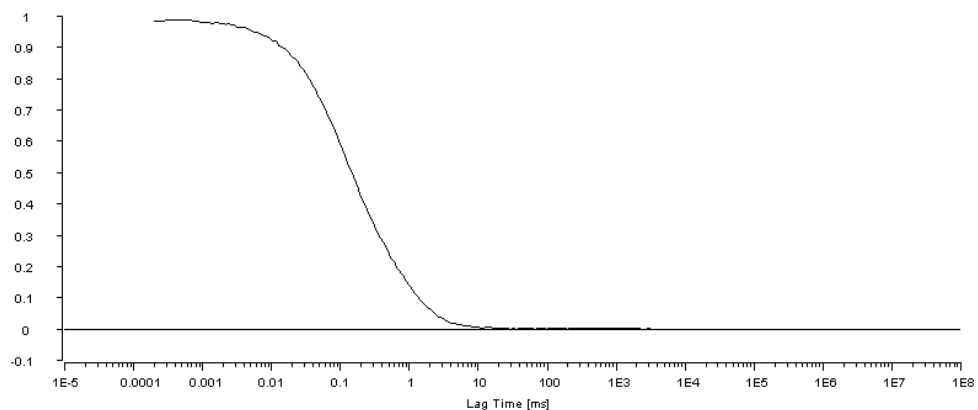


Figure 11: Autocorrelation for 0.5% TD01 sample prepared with the ethanol method, measured in DLS at 90°

Different models are available to fit the autocorrelation (Software ALV-5000) and to determine the decay time τ . We have tried the different model functions to fit our data and compared them by looking at the residuals. A fit was considered satisfactory if there were no systematic deviations in the plot of the residuals of the fitted curve.

We used first a cumulant analysis. The analysis of the cumulant expansion of the correlation function is based on a series expansion of the exponential functions.

$$\ln(g_2(t)-1) = \ln(A) - \frac{t}{\tau} + \frac{k_2}{2}t^2 - \frac{k_3}{6}t^3 \quad \text{Equation 6}$$

It allows obtaining the average decay rate of a system with a reasonable polydispersity. If we have only one size in the system (i.e. also one τ), the cumulant analysis should be good. As it is shown on the Figure 12, this is not the case: the residuals are clearly correlated.

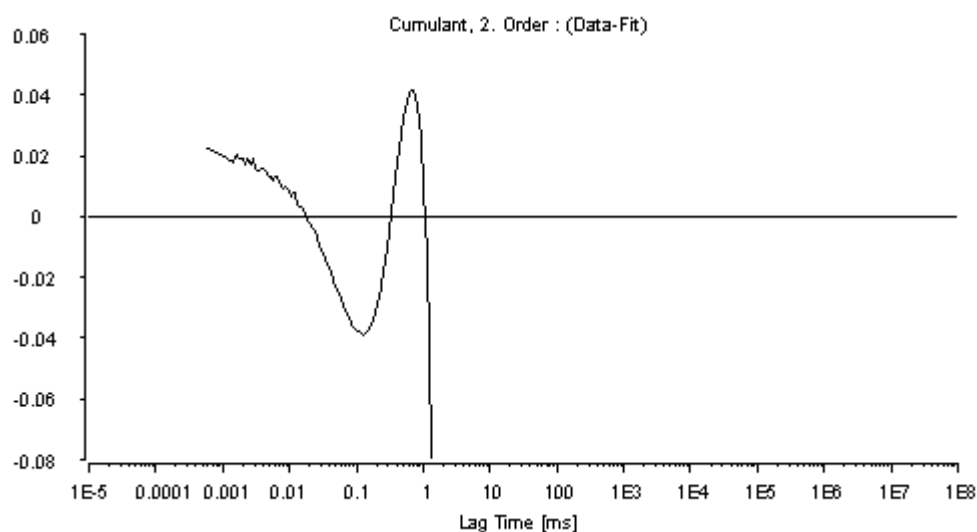


Figure 12: Residuals from simple fit (cumulant) of data shown in Figure 11

We should thus use non-linear analysis of the data. We tried exponential functions (Sum up to 4 exponential functions) and stretched exponential functions, called Kohlrausch-Williams-Watts functions (KWW), where the overall diffusive process is not the sum of the individual ones due to cooperative motions

$$g_2(t) \propto e^{(-t/\tau)^\alpha} \quad \text{Equation 7}$$

The one model giving acceptable fit (random distribution of fit residuals), as shown in Figure 13, is KWW using 2 stretched exponentials plus 1 exponential.

$$g(t) - 1 = a(0) + [a(1) * \exp(-(a(2)*t)^{a(3)}) + a(4) * \exp(-(a(5)*t)^{a(6)}) + a(7) * \exp(-a(8)*t)]^2$$

This indicates that we have 2 populations with a broad size distribution and a third population more monodisperse.

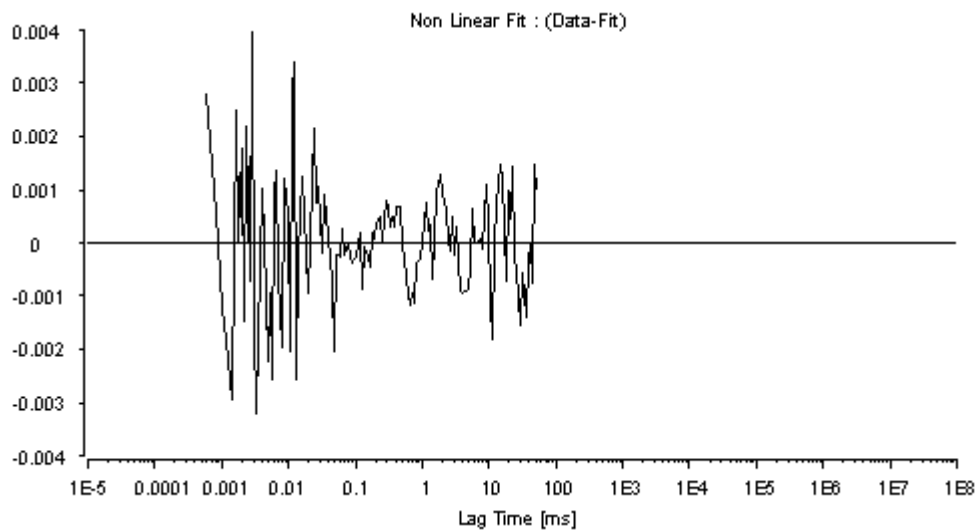


Figure 13 Residuals from non-linear fit (KWW) of data shown in Figure 11

We obtained thus 3 decay times with corresponding weights, as reported in Figure 14. We see clearly that none of those populations is negligible

2 Stretched Exponentials + 1 Exponential (DLS)	
1. Exponent:	56 % at 1.194 [ms]
2. Exponent:	16 % at 11.07 [ms]
3. Exponent:	28 % at 0.1228 [ms]

Figure 14: Fit Result (KWW) for Figure 11

We reported the 3 apparent diffusion coefficients D (D_1 , D_2 , D_3) calculated from those 3 decay times for different angles, as shown in Figure 15.

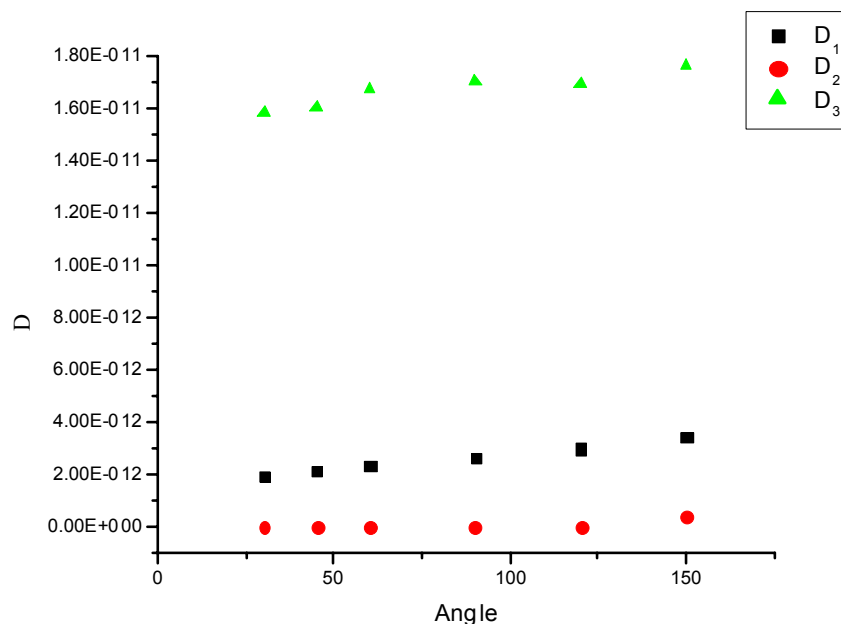


Figure 15: Diffusion coefficients versus angles calculated via the KWW fit for 0.25 % TD01 sample.

When a linear dependence of the values is observed, as shown in Figure 15, we could extrapolate the values of D at angle $\theta = 0$. We can thus determine the cooperative translatory diffusion coefficient D_m at a concentration c :

$$D_m = D_0(1 + k_d c) \quad \text{Equation 8}$$

where D_m is a z -averaged cooperative translational diffusion coefficient and k_d the diffusion virial coefficient. [24]

Unfortunately, this example is not representative of the majority of the samples. Often, it was hard to find a linear dependence between the data, even eliminating $\theta = 30^\circ$ that is the most influenced by impurities.

However, when a linear dependence of the D_m values is observed, the extrapolation to zero concentration yields a diffusion coefficient D_0 , which allows the calculation of the hydrodynamic radius R_h via the Stokes-Einstein equation.

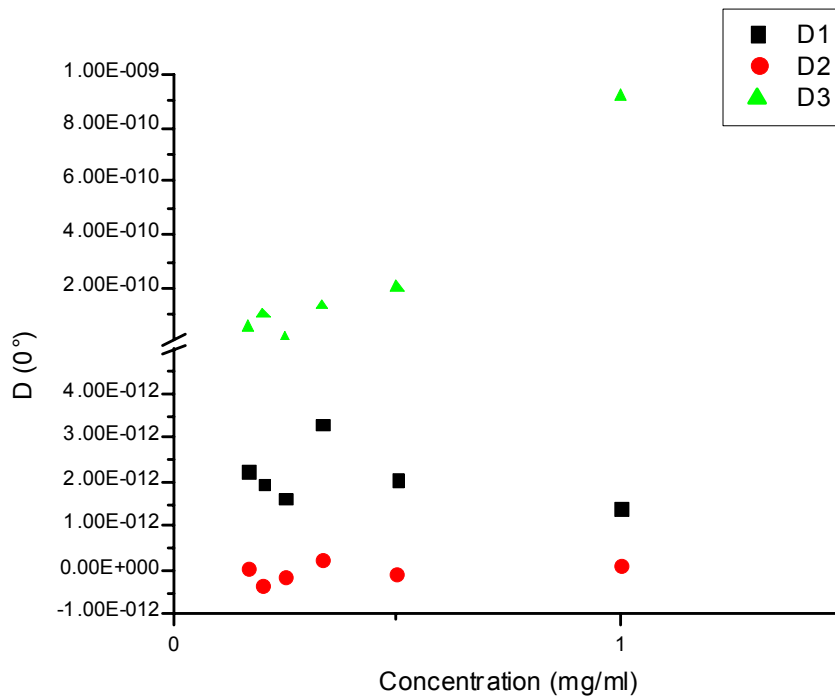


Figure 16: Diffusion coefficients at $\theta = 0$ versus concentration for TD01 sample.

Figure 16 shows the D_m (estimated from the Figure 15) versus concentration. It is impossible to find a linear dependence of the data. This means that the diffusion process is more complicated and radii cannot be estimated with this model.

We thus decide to use the regularized fit (Contin) to have at least an approximation of particle size in the sample. It fits an integral type model function to the correlation function using a constrained regularization method. Contin has poor physical meaning but allows us to fit properly all the data.

If we looked the size distribution obtained at 90° , as shown in Figure 17, we observed 3 peaks, one centered around 12 nm, one around 180 nm and one beyond the range observable with the DLS setup (> 400 nm).

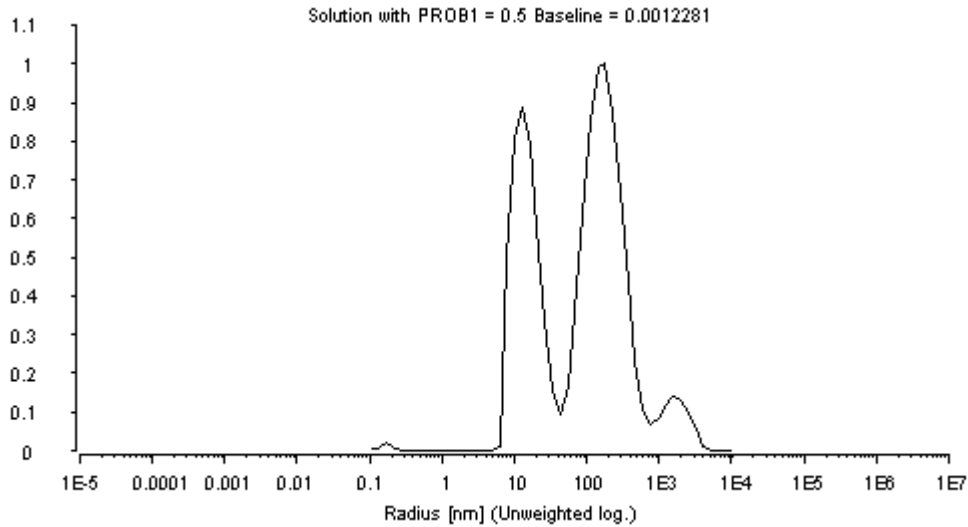


Figure 17: Distribution function of the radius obtained with regularized fit of the data (0.5 % TD01) at 90°

We have compared the distribution functions obtained for different polymers at 1% in the Figure 18. We did not report absolute sizes, but just the size ranges and the proportion (%) for each population. Population under 0.1 (10 %) will not be reported because they are just a mathematic artefact of the contin fit. We also take out sizes over 400 nm because they are not in the experimentally accessible range of the setup.

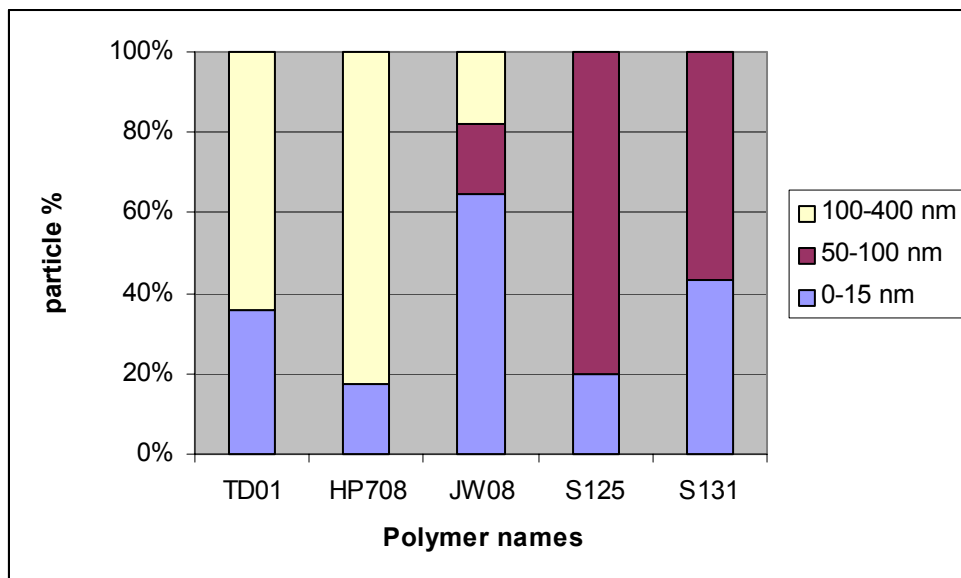


Figure 18: Size distribution in samples prepared with the ethanol method for 1% ABA-copolymers.

The small size (0-15 nm) could be attributed to micelles. We observe also vesicles (50-100 nm) that fit with results previously obtained.[19] A bigger size population (100-400 nm) is observed in some samples (TD 01, HP 708, JW 08). This could not be correlated to block lengths; as shown in Table 2, hydrophobic/hydrophilic ratio is the same for JW 08 and S 131, and they do not aggregate in the same size range. This bigger size population could correspond to bigger vesicles or aggregates.

Table 2: Hydrophobic/Hydrophilic ratio of ABA-triblock copolymers

Name	Formula ^a	Hydrophobic/Hydrophilic ratio (Mw/Mw)
HP 708	$A_{21}B_{69}A_{21}$	1.6
JW 08	$A_{15}B_{62}A_{15}$	2
TD 01	$A_{16}B_{72}A_{16}$	2.25
S 125	$A_{21}B_{72}A_{21}$	1.7
S 131	$A_{18}B_{72}A_{18}$	2

^a A: PMOXA, B: PDMS

The hypothesis of aggregation of the vesicles (for the bigger sizes) is corroborated by the results obtained after dilution of the samples. As shown in Figure 19, if we measure the size distribution of the same sample after consecutive dilutions, the vesicle sizes decrease.

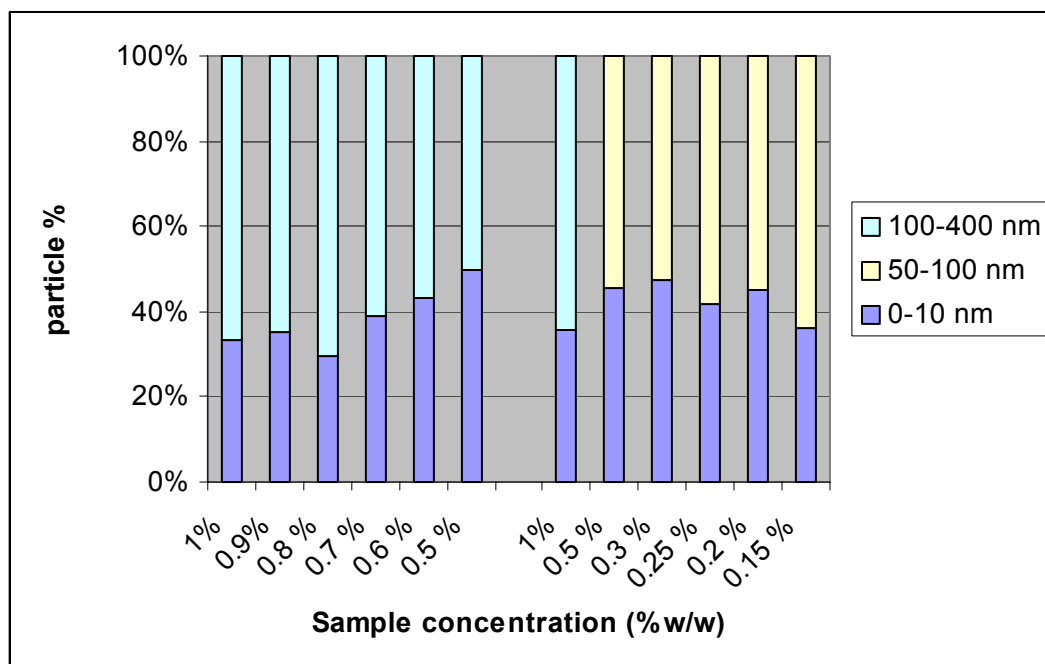


Figure 19: Size distribution of 1 % TD01 samples before and after consecutive dilutions; first dilution series from 0.9 % to 0.5 %, second dilution series from 0.5 % to 0.15 %

Furthermore, all size distributions are broad. In particularly for the sample JW08 in Figure 18, we observed 3 populations, but the separation between the 2 largest one could be only due to the mathematical fit; we can expect also a broad distribution of vesicles between 50 and 400 nm radii.

The interpretation of DLS data is quite hard because of the broad distribution of the samples. We cannot determine an accurate size for the particles. We can however conclude that the samples obtained via the ethanol are a mixture of micelles (radius around 10 nm) and vesicles with a radius between 50 and 100 nm that tend to aggregate at above 1% concentration.

The sizes of small spheres obtained in DLS fit with the TEM results, as shown in Figure 8. The difference of the sizes obtained with DLS and TEM for the bigger vesicles can be explained as follows: in TEM, sample grid preparation (chapter 7.9.2) requires multiple (3 times) washing of the microscopy grid probably leading to removal of big vesicles. Small spheres adhere more strongly to the microscopy grid surface (higher surface per volume), and we can expect that they will stick strongly to the grid during the adsorption time. The successive washings probably eliminate the big vesicles, less strongly adsorbed on the grid. To corroborate this hypothesis, as

shown in Figure 20, we have observed from time to time for diluted samples, vesicles whose size was in agreement with DLS results, which means a distribution of sizes and not only small spheres. We thus recommend diluting at least 10 times the samples before TEM observation in order to minimize the abovementioned preparation artifacts. This is unfortunately not enough to have reproducible pictures. This could also be explained by the TEM technique itself. A glow-discharge is performed to render the grid surface hydrophilic, but this procedure is for sure not uniform. After sample drop deposition on the grid, vesicles sedimentate on the grid but they will prefer the more hydrophilic places and the vesicles will not be well distributed on the grid surface. Only a spray deposition (opposed to drop) allows a homogeneous repartition of the sample on a TEM grid [25], but we were not able to find the right conditions to obtain good pictures with this technique.

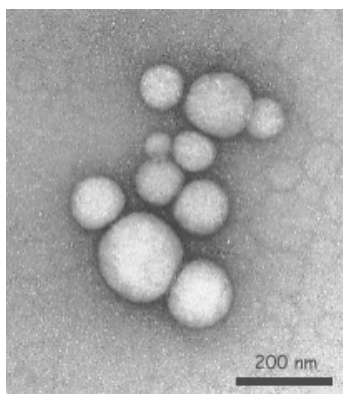


Figure 20: TEM picture of nanovesicles prepared with the ethanol method, filtered and diluted 10 times before grid preparation.

We have also performed freeze-fracture microscopy (chapter 7.9.4). As shown in Figure 21, we observed a few spheres with diameters around 200 nm, but above all a lot of small structures with diameters below 20 nm.

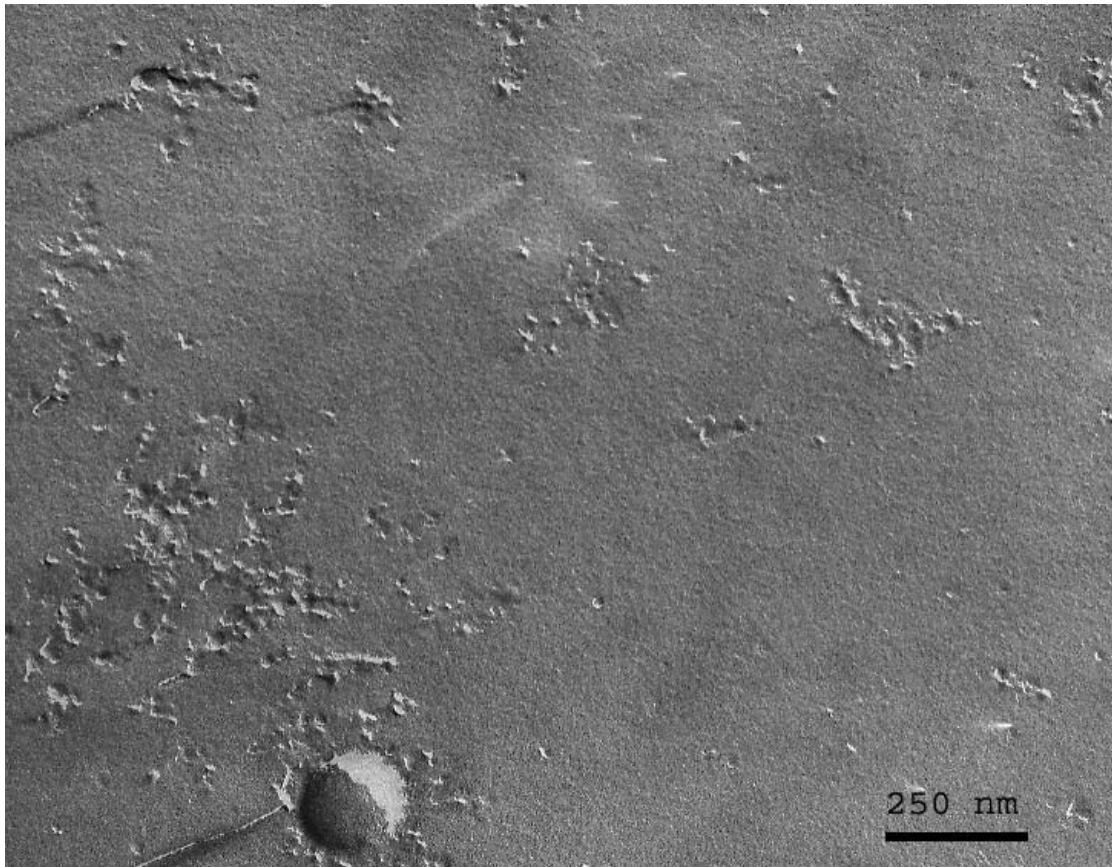


Figure 21: Freeze-fracture image of ABA-copolymer vesicles prepared with the ethanol method

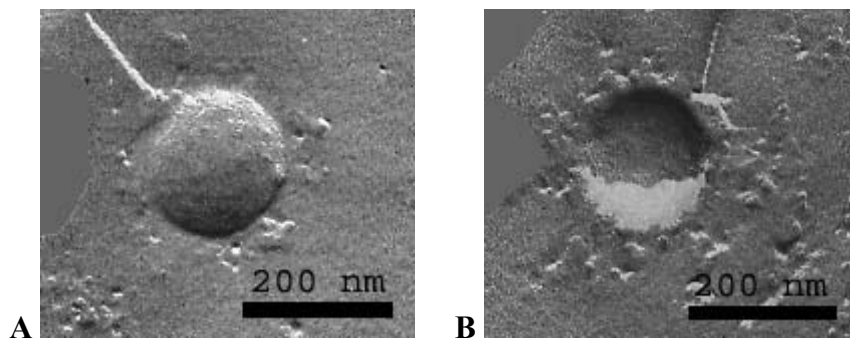


Figure 22: Freeze fracture TEM picture of nanovesicles from JW 08 formed by the ethanol method; A shows a convex vesicle, B a concave one.

Figure 22 shows a concave and a convex vesicle with a diameter of 200 nm. In phospholipid bilayers the fracture selectively propagates along the membranes, permitting the visualization of intra-membrane features. Even if we cannot completely exclude in case of copolymers that the vesicles are pulled out of the fracture plan, we can assume that we have a fracture plan in the middle of the ABA-membrane. This is possible if a majority of the ABA molecules are “U” shaped, with a hydrophobic

centre and both hydrophilic segments of the amphiphilic copolymer towards the outside, as schematized in Figure 23. This hypothesis is reasonable because the “U shape” is thermodynamically favored compared to the “I shape” as demonstrated for symmetric triblock copolymers in [26, 27].

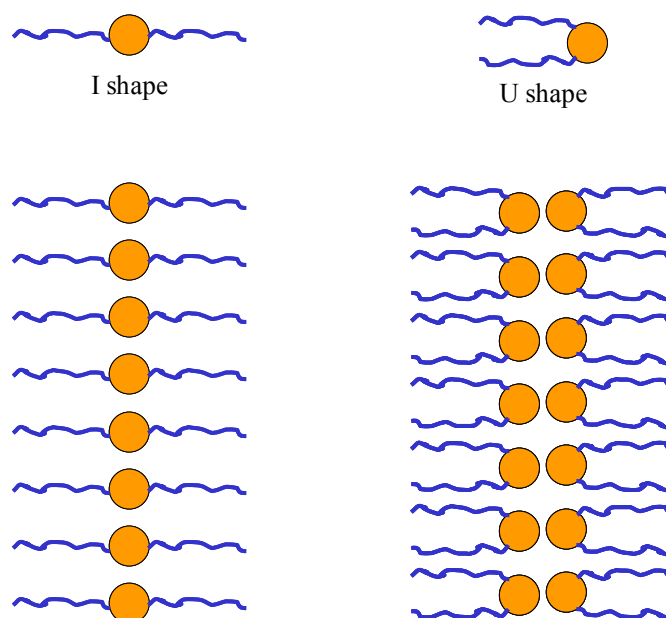


Figure 23: Conformations of the ABA molecules in the membrane.

According to previous experiments [17, 18] we can assume a membrane thickness around 10 nm. Micelle diameters are thus expected to measure around 10 nm. Small spheres observed in freeze fracture can thus be micelles, taking in account the effect of the shadowing (increased size), or vesicles with a small water-filled inner pool. Furthermore, the diameter observed in freeze-fracture microscopy should be considered as a minimal diameter and does not necessary reflect the true diameter. Indeed, as explained in Figure 24, the fracture plane is not necessarily in the center of the vesicle, and thus does not reflect the total diameter. As a result, the true diameter may be larger, which decreases the proportion of micelles in the small spheres observed.

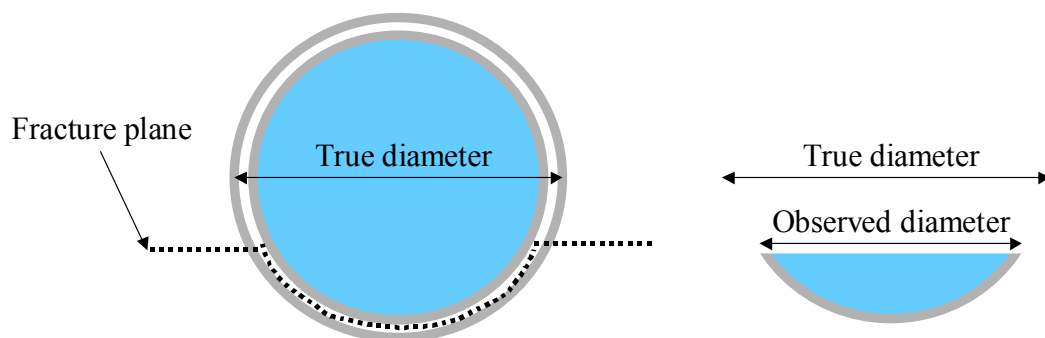


Figure 24: Schematics of the fracture plane in Freeze-fracture microscopy

Figure 25 shows the results of AFM experiments (chapter 7.5). Below the critical aggregation concentration (c_{ac}), i.e. the lower concentration at which the vesicles are stable, no structure could be observed. At concentrations of about 0.2 mg / ml, the vesicles form and could be transferred to the surface.

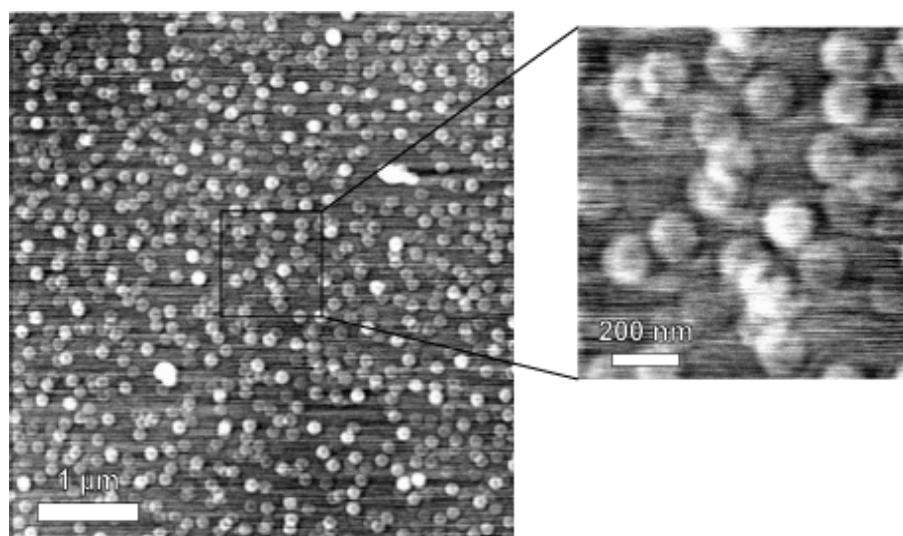


Figure 25: AFM picture of ABA-polymer nanovesicles (TD01, 0.2 mg/ml) prepared with the ethanol method

The vesicles are randomly but densely distributed on the surface. The diameter of the vesicles is 136 nm, with a very low polydispersity. The apparent height is only a few nanometers (line-scan not shown), which would indicate that the vesicles collapse upon removal of the solvent, as already observed in SEM [19]. This could be confirmed from the observation that the center of the circular shapes in Figure 25 is

visibly lower and the shape of the vesicles resembles a deflated ball, as represented in Figure 26.



Figure 26: Schematic of a deflated ball

In conclusion, the ethanol method is a fast and easy method to prepare nanovesicles. However, it yields to a mixing of micelles and vesicles with diameters broadly distributed mainly between 50 and 100 nm. The main radius of the vesicles is not well defined and reproducible for a same polymer with this method. This can be explained by the presence of ethanol, which acts as a fluidizer or co-amphiphile and interferes significantly in the self-assembly process. Vesicle formation depends thus not only on the molecular parameters of the polymers, but also on the ethanol concentration, the mixing rate, etc. This was widely studied by Adi Eisenberg [28]. The copolymer is first dissolved in ethanol, which is a favorable solvent for both PMOXA and PDMS blocks. Water acts as a precipitant for the hydrophobic block in the ethanol. At the critical water concentration, the single polymer chains present in the solution start aggregating into spherical micelles. As more water is added to the polymer solution, morphologies are transformed from micelles to vesicles. It was proven recently that vesicles are potentially equilibrium structures [29] and that sizes of block copolymer vesicles are also under thermodynamic control [30]. Furthermore, kinetics of increases in the vesicle size of diblock copolymers have been shown to be dependent to water content and magnitude of water perturbation [31].

4.2 Detergent method

It is of a great interest to establish a reconstitution method for membrane proteins into ABA-polymer membrane, in particular for those that are sensible to environmental conditions, like G-Protein Coupled Receptors (GPCR) whose major role is to transmit signals into the cell. We have previously demonstrated that the ethanol method is suitable to produce nanovesicles, which can successfully be used for membrane protein incorporation [21, 32]. In order to optimize the proportion of functional proteins incorporated per vesicle, we wanted to develop nanovesicle preparation methods devoid the presence of organic solvent in the solution. Here the methods employed for 2D crystallization of membrane proteins into liposomes appear to be of high interest.

The most commonly used strategy for proteoliposome preparation involves the use of detergents, since most membrane proteins are extracted and purified through the use of detergents [33]. Indeed, because of their amphiphilic nature, membrane proteins need to be isolated, purified and crystallized in detergent solution. The protein, kept in a detergent solution after purification, can then be added to a lipid – detergent mixture without aggregation. Figure 27 is a schematic representation of the different aggregation states during detergent mediated liposome formation, proposed by Rigaud [34].

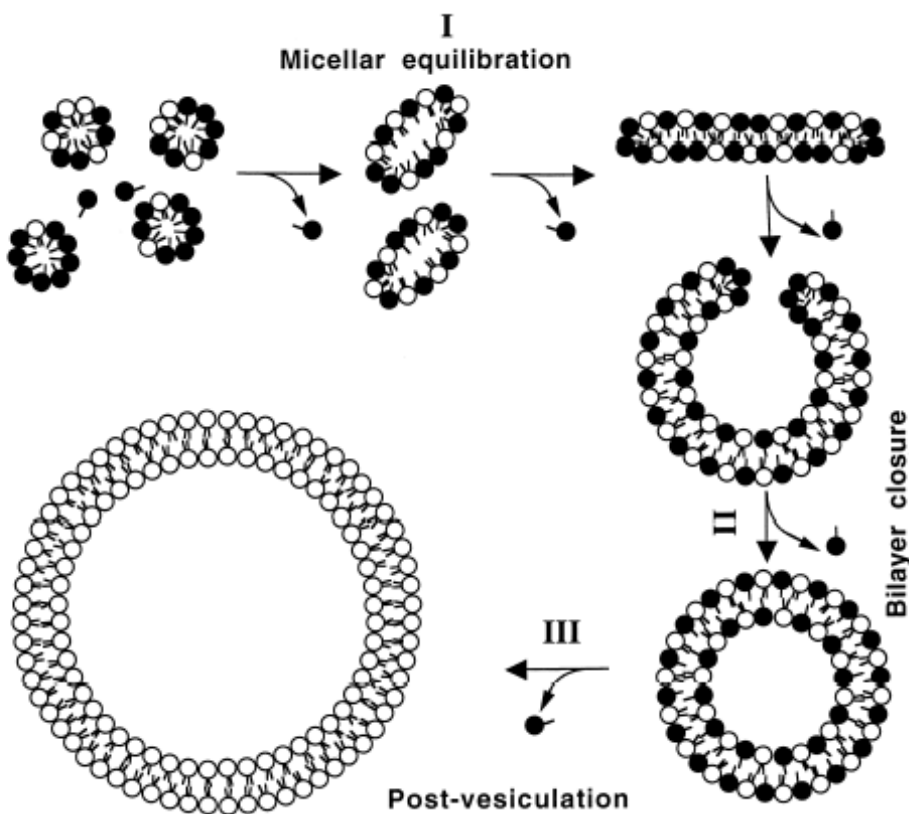


Figure 27: Schematic representation of the different aggregation states during detergent mediated liposome formation; detergent is black, lipid is white. [33]

Detergent removal from lipid-detergent micelles causes the transformation of small micelles to larger ones (I), which bend to form curved mixed micelles. Then detergent saturated vesicles are formed (II) which undergo size growth (through fusion and lipid exchange mechanisms (III), leading ultimately to larger unilamellar liposomes.

In proteoliposome formation, the relevance of the detergent nature is not clear since systematic studies have not been performed and/or reported, and the choice is generally empirical and relies mainly on the detergent chosen to purify the membrane protein of interest [34]. To adapt this procedure for (proteo-)polymersome formation with our ABA-triblock copolymer, we need a detergent able to dissolve it.

We have tested several detergents (o-POE, DDM, Triton X100 and OG). We used each detergent at the concentration that is employed for the purification of the membrane protein that we want to reconstitute. For e.g. octylglucoside at 3% in aqueous solution was a good candidate; polymer solutions with this detergent are homogeneous after 2h of stirring at room temperature. The other detergents, which

could be needed for protein compatibility, required longer and stronger agitation (sonication, ultraturax).

After dissolution of the polymer different strategies are available to remove the detergent and form vesicles. We have tested 3 techniques used for 2D-crystallization of membrane proteins: dialysis, dilution and “bio-beads”. We will discuss here the formation of polymer nanovesicles which each technique.

4.2.1 Dialysis

Dialysis is the most widely used technique in 2D-crystallization trials, as we can see in Table 3, which is a review of detergent and removal strategies for detergent for various membrane proteins. [33] The sample is placed into a small compartment dialyzed against large buffer volumes. The dialysis method has been successfully applied to many membrane proteins, but could be unsuitable for detergents with low cmc's, which would require very long dialysis times. Indeed, long exposure times could be incompatible with membrane proteins of poor stability. Using a more sophisticated device flow-through dialysis cell can be advantageous as the rate of detergent removal can be carefully controlled and dialysis time largely decreased [35].

Detergent	Protein	Strategy
Triton X-100	outer membrane phospholipase A	dialysis
	glutathione transferase	dialysis
	cytochrome bo ubiquinol oxidase	dialysis
	mechano-sensitive channel	bio-beads
	cytochrome bcl	bio-beads
		dialysis
	ubiquinone: cyt c reductase	bio-beads
	PSI	bio-beads
	cytochrome reductase	dialysis
		dialysis
C12E8	band 3	dialysis
	Ca-ATPase	bio-beads
C8E4	rhodopsin	dialysis
Dodecylmaltoside	lactose permease	dialysis
	Na ⁺ /H ⁺ antiporter	dialysis
	melibiose permease	bio-beads
	LH2	dialysis
	KcsA K ⁺ channel	dialysis
Decylmaltoside	cytochrome oxidase	dialysis
Octylglucoside	aquaporin	dialysis
	LH1 <i>Rhodospirillum rubrum</i>	dialysis
	LH2 <i>Rhodobacter sphaeroides</i>	dialysis
	LH2 <i>Rhodovulum sulfidophilum</i>	dialysis
	rhodopsin	dialysis
	cytochrome b6f	bio-beads
		dialysis
Hecameg	PSI	bio-beads
Octylthioglucoside	PSI	bio-beads
	PSII	dilution
	PSII	bio-beads
Heptylthioglucoside	PSII	bio-beads
	PSII	dialysis
Hexadecyl PC	LH1 <i>R. sphaeroides</i>	dialysis
	LH1 reaction center	dialysis
OctylPOE	porin OmpF	dialysis
	porin OmpF	dilution
	band 3	dialysis
	maltoporin	dialysis
LDAO	rhodopsin	dialysis
	LH2 <i>R. gelatinosus</i>	bio-beads
	reaction center	dialysis
	reaction center	bio-beads
LDAO+OTG	FhuA	bio-beads
	LH2	bio-beads
SDS	porin PhoE	dialysis
CHAPS	mannitol transporter	dialysis

Table 3: Use of detergents in 2D-crystallization of proteins [33]

We have dialyzed our polymer samples dissolved in various detergents (chapter 7.6.1) over several days without success; detergent was still present in solution. To improve this technique, we have also used a temperature-controlled, continuous-flow apparatus (chapter 7.6). Even here, we were unable to completely eliminate the detergent using dialysis.

This could be explained as follows: flexible polymers chains are well known for the strength of intermolecular forces, which slow down polymer motion; this will lead to long times to eliminate the detergent molecules strongly entrapped in the polymer chains. It was shown recently that the dominant mechanism for the surfactant-dissolution of polymer vesicles is the surfactant transport through the polymeric bilayer [36]. We can thus think that the detergent removal is also limited by the thickness of the polymer membrane.

The complete removal of the detergent from the polymer will probably take several weeks. As a result, this method is not efficient for polymersome formation; we have thus tested dilution as a second strategy for detergent removal.

4.2.2 Dilution method

Although widely used, another procedure for obtaining proteoliposomes from micellar solutions consists of diluting the reconstitution mixture (lipid-protein-detergent micellar solution). [37] Dilution lowers the detergent concentration below its cmc and proteoliposomes form spontaneously. The dilution is followed by a centrifugation to concentrate the proteoliposomes. Dilution is only useful for high cmc detergents, like OG. This technique has two main advantages: (i) it requires a relatively short time for decreasing detergent concentration and (ii) it offers the possibility to control the dilution rate by progressive addition of buffer. However it requires a high protein concentration since the protein is also diluted.

Diluting a solution of amphiphile and detergent decreases equally the concentrations of all the components, until the free detergent drops below “saturation”. Figure 28 shows an example where the concentration of o-POE was decreased by dilution and the formation of structures of different sizes was monitored using light scattering [37]. The dilution experiment led to the formation of vesicles with lipids, or vesicles and 2D-crystals with lipids and of porin. The latter assembled only if the dilution rate was slow.

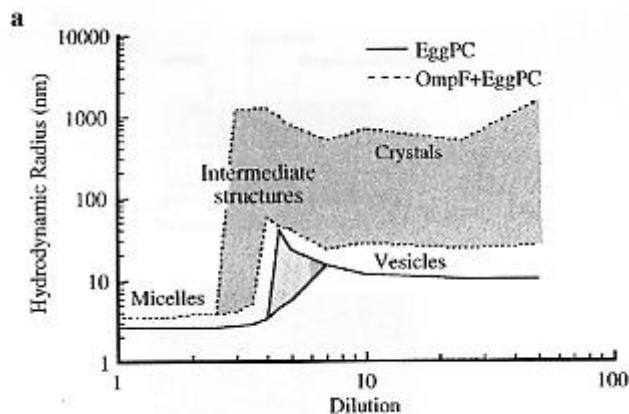


Figure 28: Protein reconstitution and formation of lipidic structures of different sizes monitored using dynamic light scattering upon dilution [37]

For our experiments, we have used a device designed by H.W. Rémigy [38] that allows controlled dilution of a protein-lipid-detergent mixture to induce formation of densely packed or crystalline proteoliposomes (chapter 7.7). Turbidity is used to monitor the progress of reconstitution in situ, while dilution is achieved by computer-controlled addition of buffer solution in sub-microliter steps. This system has mainly been tested with various membrane proteins and has resulted into large, highly ordered two-dimensional crystals [38].

In this dilution device, we have solubilized a pre-sonicated polymer suspension into detergent, and afterwards formed vesicles by dilution of the polymer-detergent mixture in buffer. Results are reported in Figure 29.

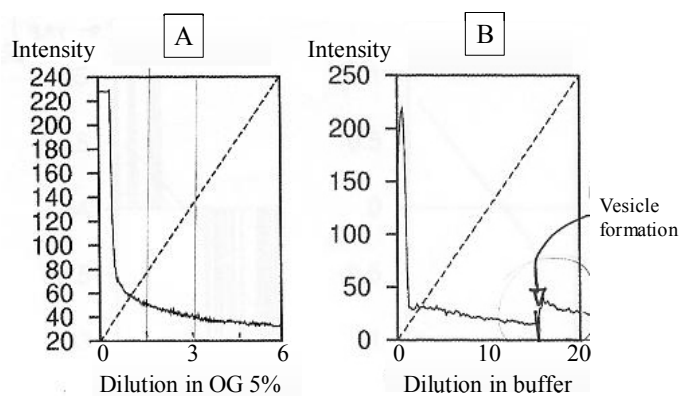


Figure 29: Turbidity curves for dilution of a 0.5% solution ABA-polymer (TD02); (A) 6 times dilution in 5% OG; (B) 20 times dilution in buffer.

Curve (A) represents the dilution of a polymer suspension (0.5% TD02 in Tris-buffer) by a detergent solution (5% OG); it shows a decrease of the intensity of the scattered light, which corresponds to a size reduction of the structures; the polymer is solubilized by formation of mixed polymer-detergent micelles. The final solution is 0.08 % TD02 – 4.1 % OG. Curve (B) represents the dilution of the polymer-detergent (TD02 - OG) mixture obtained in (A) by a buffer; it shows a continuous decrease of the intensity (simple dilution of the micelles) until an abrupt increase for a 14.2 times dilution, which is representative of the formation of vesicles (more scattering structures). This corresponds to $4.1\% / 14.2 = 0.29\%$ of OG in the solution. This is much lower than the CMC of OG (19 mM or 0.56 %); this illustrates again the difficulty for the detergent to get out of the polymer membrane.

Unfortunately the above observation, i.e. formation of vesicles by simple dilution of the sample, has poor reproducibility. This can be partly explained by long equilibrium time due to slow polymer dynamics (entrapment of detergent molecules in the thick polymer membrane). Moreover, the dilution rate is known to affect the morphology: slow removal is necessary to obtain sealed vesicles [33]. Removing detergent by dilution of polymer-detergent solution will thus require very large quantity of buffer and lengthy times.

Another drawback of this method is the sample dilution that will dramatically decrease the encapsulation rate and thus prohibit many applications where high encapsulation of hydrophilic substances within the vesicles is of great importance.

As adsorption of the detergent by porous polystyrene beads is a powerful alternative to the dilution and dialysis methods for preparing proteoliposomes [39], we tried bio-beads as a third strategy for detergent removal.

4.2.3 Bio-Beads method

Detergents with low cmc's, which consequently form large micelles, are not readily removed by dialysis or dilution but can be efficiently removed through adsorption on hydrophobic resins. Bio-Beads SM2 (BIO-RAD) are macroporous divinyl benzene cross-linked polystyrene beads with a high surface area for adsorbing organic

materials from aqueous solution. They are non-polar beads with average pore diameter of about 90 Å. They can be added in very small volumes with almost no dilution of the sample, and they are known to specifically adsorb detergent with a quite low non-specific adsorption (100-200 times lower adsorptive capacity for lipids and even less for proteins, as reported in Table 4) [39-41].

Compound	Adsorptive capacity (mg/g beads)
Detergent:	
Triton X100	185
C ₁₂ E ₈	190
Dodecyl maltoside	105
Cholate	80
Chaps, chaps0	85
Hecameg	110
Octyl glucoside	117
Phospholipid:	
Liposomes	1
Lipid-detergent micelles (Rsol)*	2
Lipid-detergent micelle (3×Rsol)	4
Lipid-detergent-protein micelles	0.5–1
Protein:	
BR, Ca ⁺⁺ ATPase, FOF1 ATPase, melibiose permease, cytochrome b6f	0–0.2

* Rsol represents the effective detergent to lipid ratio needed for total solubilization of preformed liposomes

Table 4: Adsorption capacities of Bio-Beads SM2 for detergents, phospholipids and proteins [34]

Rigaud [34] gives a reasonable explanation for the different adsorptive capacities for detergents, lipids and proteins by considering the accessibility of detergent monomers, binary or ternary micelles, liposomes or 2D crystals to the volume and/or surfaces within the pores of the absorbent beads (see Figure 30). The surface area available for adsorption onto beads is mainly represented by the surface area within the pores; the external surface of the beads is only a small fraction of the adsorptive surface. In our case, i.e. for bio-beads SM2, the surface area within the pore is about 10⁴ higher than the external surface of the beads. The accessibility within the pore will thus be a crucial parameter in determining the adsorptive capacity.

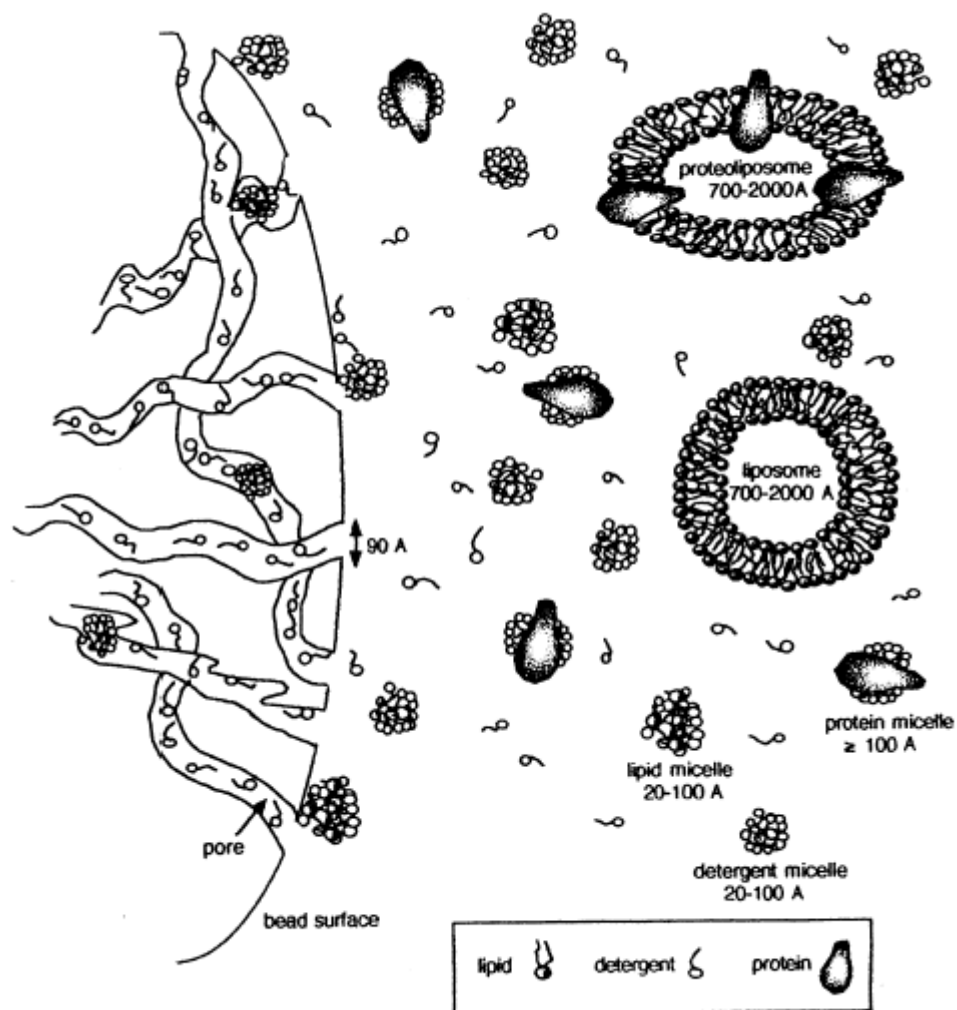


Figure 30: Proposed mechanisms of adsorption onto Bio-Beads. Adsorption of detergents, lipids and proteins depend upon the accessibility within the pores of the beads of detergent monomers, binary or ternary micelles, liposomes or proteoliposomes [34]

The average pore diameter of the beads, 90 Å, has been compared to the sizes of detergent micelles: about 20–40 Å diameter for ionic detergents and 90–100 Å for detergents with low cmc's. From such a comparison, it has been concluded that the access and/or the diffusion of micelles within the pores of the beads will be hampered and/or limited, explaining the large differences in the rates of monomer and micelle adsorption, but also the low phospholipid adsorption onto beads. Indeed, due to their very low cmc of about 10^{-8} M, phospholipids exist either in the form of lipid-detergent micelles, up to 2 times larger than pure detergent micelles, or in the form of liposomes with diameters of 800–2000 Å. Even if few lipid-detergent micelles can be adsorbed within the pores, upon detergent removal, the lipids rapidly re-associate into liposomes, which have no access to the pores of the beads and could only be adsorbed

on the external surface. A similar interpretation has been advanced to explain the negligible protein adsorption since proteins exist either as large lipid-detergent-protein micelles or as proteoliposomes, which cannot enter the low average diameter pore of the beads and can only be adsorbed to the surface of the beads. Hence we expect, because of the higher size of polymer molecules compared to lipids, that the non-specific binding to polymers would be also low.

Because the rate of detergent removal has been shown to be proportional to the amount of beads [34], bio-beads also offer an easy control of the rate of detergent removal, which is a key parameter for controlling protein insertion, protein orientation, and the size homogeneity of the formed vesicles. Detergent can be removed either by adding all the beads in one batch above their adsorptive capacity or by adding small successive amounts of beads, as illustrated in Figure 31.

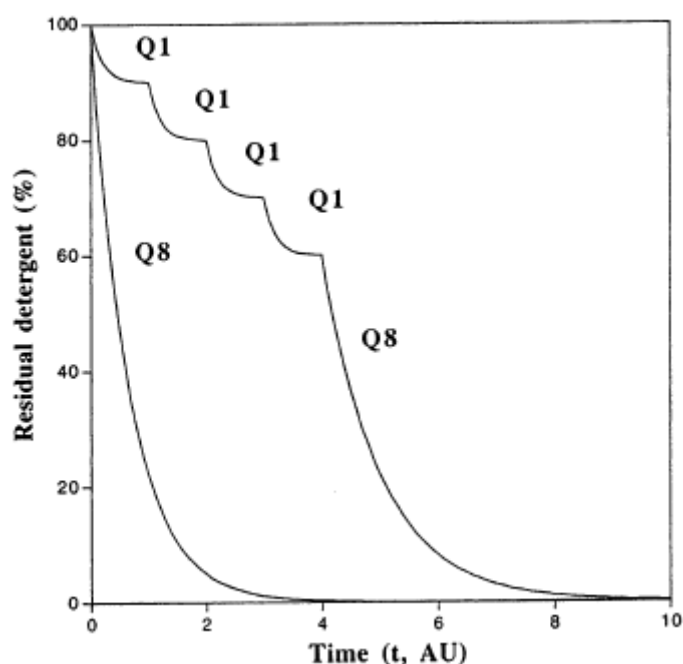


Figure 31: Use of Bio-Beads to control the rate of detergent removal; Q8 = 8 x Q1 mg of Bio-beads. [33]

We have thus added the bio-beads to the polymer-detergent solution in 3 consecutive steps, each addition containing 1/3 of the total bead quantity needed for complete detergent removal (values from Table 4 [33]). Each bio-bead addition is followed by at least 3h of slow stirring (we have increased this adsorption time, which is only 1h for lipids, because again of strong entrapment of detergent in the polymer matrix).

However, to prevent any detergent release from the saturated beads, they must be removed from the solution after the 3 h stirring following the last bio-beads addition. A final SEC cleaning is performed to eliminate the eventual remaining free detergent molecules (and also free proteins for reconstitution trials). Of course, SEC does not offer the possibility to control the rate of removal (detergent and polymer are separated immediately after loading) and cannot be used alone as an efficient detergent removal method to form proteovesicles.

The detergent removal has been followed by determination of the free detergent concentration using shape analysis of sitting drops [42] (chapter 7.8).

This method allows evaluating contact angle. Consider the drop of a liquid resting on a solid surface. The drop of liquid forming an angle may be considered as resting in equilibrium by balancing the three forces involved: namely, the interfacial tensions between solid and liquid, that between solid and vapor, and that between liquid and vapor. The angle within the liquid phase, as shown in Figure 32, is known as the contact angle or wetting angle. It is the angle included between the tangent plane to the surface of the liquid and the tangent plane to the surface of the solid, at any point along their line of contact.

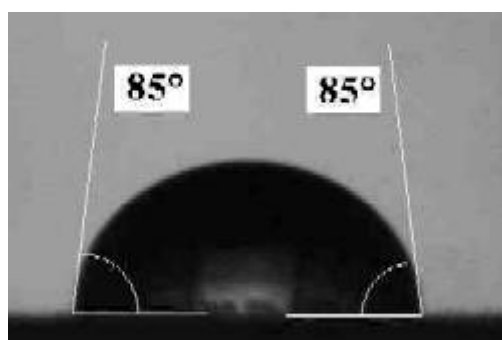


Figure 32: Contact angle

So, when the surface is smooth, homogenous and impermeable to the liquid, static contact angle measurement is a reliable method to characterize interaction between a liquid and a solid surface. The surface tension of the solid will favor spreading of the liquid, but this is opposed by the solid-liquid interfacial tension and the vector of the surface tension of the liquid in the plane of the solid surface. A droplet of a liquid with a high surface tension (like water) deposited on a low surface tension material (like

Teflon) makes a quite high contact angle. Contact angle can be modified by the addition of surfactant that lowers interfacial tension of the liquid: the droplet spreads more easily on the solid surface. A higher contact angle is thus obtained.

We used a “home-made” set-up that does not measure directly the contact angle but a focus point, evaluated from the shape of the droplets, correlated to the contact angle value. Photography of a sitting droplet is taken. Then software approximates the shape of the droplet with a parabola, as shown in Figure 33.

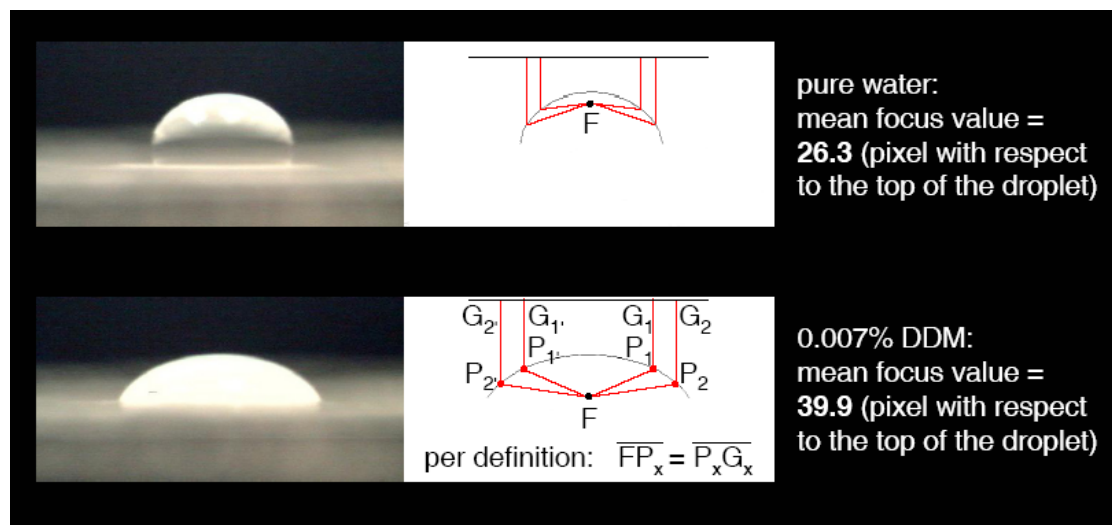


Figure 33: Sitting-drop method measurement

Per definition all the points of the parabola are at the same distance of a line and the focus point F. The focus value is the distance between F and the top of the droplet (in pixel). When the focus value decreases, the contact angle is also lower. It means that an increase in detergent concentration in water, that lowers contact angle, will decrease focus value.

Figure 34 shows the calibration curves (mean focus point F versus concentration) of Triton X 100 in water and in 0.1% ABA-polymer solution. The presence of polymer in water (without detergent) does not change considerably the contact angle (this is reasonable regarding the low cac of the polymer). But we observe clearly an influence of the polymer on the curvature of the focus point versus detergent curves. At a same detergent concentration, focus value is lower in presence of polymer, which means that a part of the detergent is used to solubilize the polymer.

Comparing those values to the curvature of a drop taken from time to time during bio-beads procedure, the quantity of free detergent remaining in solution can be measured and thus the removal followed step by step.

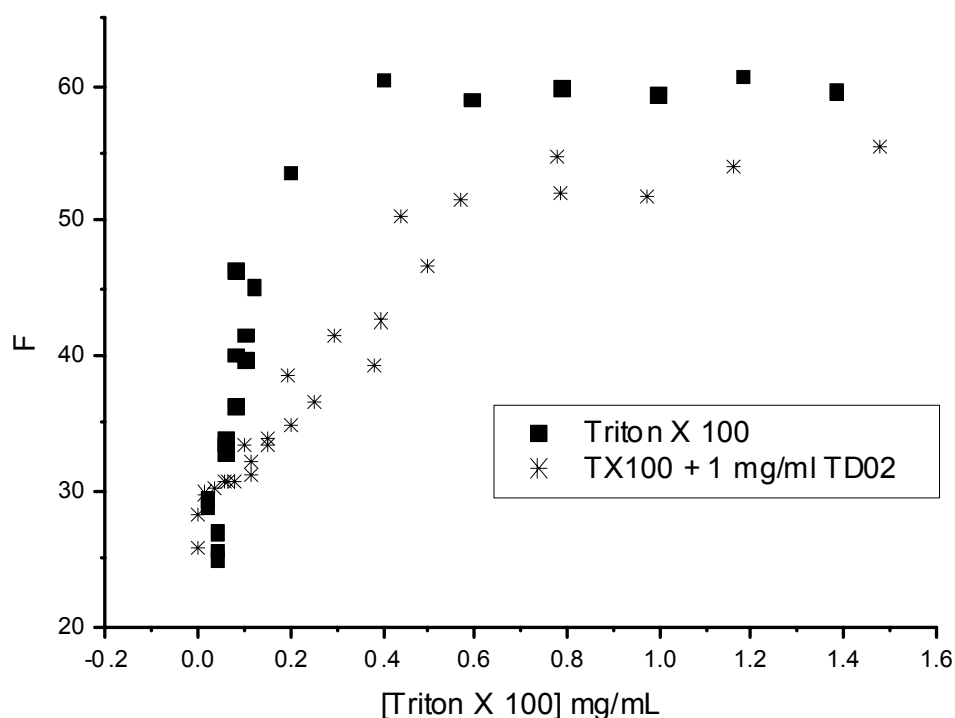


Figure 34: Calibration curve of Triton X 100 in water ■ and in a polymer solution* (F is the mean focus point)

Table 5 summarizes the focus point values measured after complete removal of the detergent by bio-beads method. We can see that the chromatography removes the remaining detergent to reach the same value as vesicles formed in pure water.

Samples	Focus point values						
	F1	F2	F3	F4	F5	F6	F (mean)
Vesicles prepared by:							
Detergent removal (Bio-Beads)	28.7	26.9	28.2	26.7	28.6	26.3	27.6
+ Size exclusion chromatography	27.5	27.4	27.4	26.9	27.4	27.1	27.3
Overnight dissolution in H ₂ O (Control)	28.3	26.8	28.0	26.8	27.9	26.6	27.4

Table 5: Focus point values of a drop of vesicle containing solution

Figure 35 shows the vesicles obtained with the bio-beads method. The sizes and corresponding distribution observed in TEM seem to be randomly distributed from 40

nm to 200 nm of diameter (whereas we observed 2 distinct populations with the ethanol method). This is perfectly reproducible using OG as a detergent for the polymer.

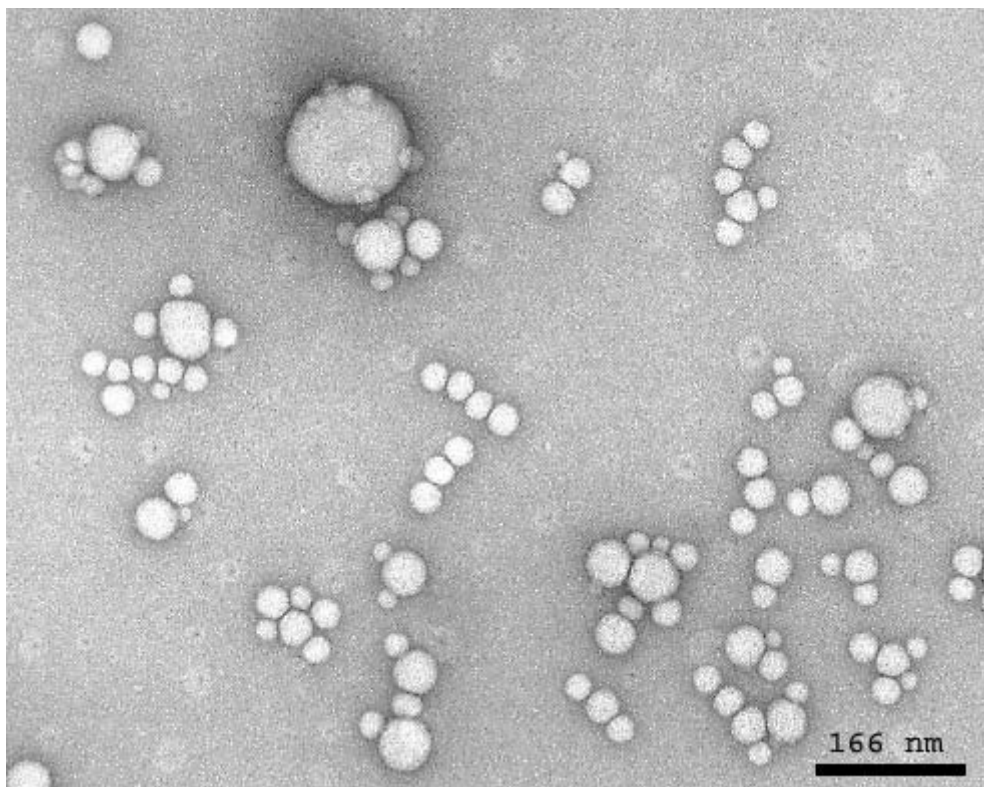


Figure 35: TEM picture of vesicles obtained by Bio-Beads method from ABA-copolymer (JW 08) dissolved in 3% OG.

In summary, we have demonstrated the ability of the bio-beads method to form nanovesicles from ABA-copolymers. As it is a method of choice for protein crystallization into liposomes, we expect to optimize our membrane protein reconstitution into polymer vesicles results using this method.

4.2.4 Membrane Protein reconstitution

As presented in the introduction, proteins are the active components of biomembranes. Their inclusion in synthetic membranes such as those of vesicle-based drug carriers imparts favorable, or unfavorable, functionalization. Incorporation of proteins into lipid bilayers has been widely studied [43, 44]. Reconstitution of membrane proteins in polymer-stabilized lipid membranes has been successful [16]. Recently, interest has been focused on block copolymer vesicles as drug delivery

vehicles, particularly because of their enhanced stability and greater flexibility to tailor bilayer properties such as thickness and chemical composition [45-48]. Little is known regarding protein incorporation into pure polymeric bilayers.

It can be expected that it is an inappropriate system for such insertions, due to their larger thickness. Lipid membranes have a ‘universal’ thickness of ca. 4 nm, which is also the height of channel proteins (e.g. OmpF). On the other hand, the thickness of polymeric membranes is several times that of lipid bilayers [49], and their size particularly depends on the polymer used. Such a thickness difference was considered too large to create a chemically favorable environment for the inserted protein, which may deform the bilayer significantly (Figure 36). The energetic penalty arising from this deformation may reduce the equilibrium concentration of proteins within the membrane, in addition to a slowdown of the protein adsorption kinetics similar to that of stealth liposomes.

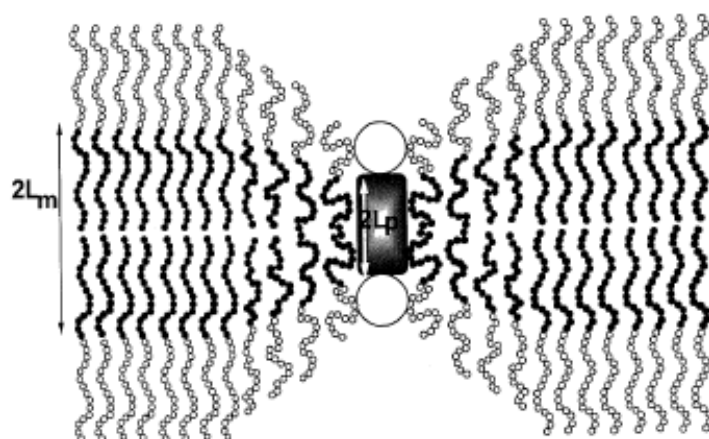


Figure 36: Conformation of AB diblock copolymer chains near a protein inserted in a polymeric bilayer. Matching a protein whose height, which is half the thickness of the membrane, is easily obtained through polymer chains stretching [50]

Pata and Dan have studied the above problem theoretically [50]. They proved via mean field calculations that protein insertion into polymer membrane can be possible. The main argument for their finding is that – contrary to other molecules – polymers possess a special feature, namely, the chain can assume various conformations.

If we imagine a triblock amphiphilic polymer membrane, the molecules will form a mono- or bilayer structure, in which the polymer chains are stretched in the form of ‘I’ conformation, or have a ‘U’ shape (see Figure 23). Such conformations will only

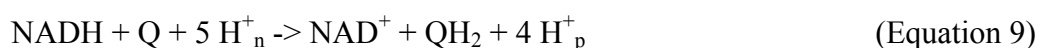
be favored in a membrane, whereas in diluted solution the macromolecules prefer an entropy-minimum coil conformation. After protein insertion into diblock or triblock (amphiphilic) polymer membranes, the height incompatibility will increase the energy of the system, yet this increase will be compensated immediately by the partial coiling of the neighboring chains to adapt to the protein size, as presented in Figure 36. Such coiling will decrease the free energy of the membrane and will stabilize such a polymer-protein system.

Various functional reconstitutions of membrane in block copolymer vesicles have been done in our group using the ethanol method [17, 21, 23], but without optimization concerning the number of functional proteins incorporated per vesicle. The detergent removal method using Bio-beads is one of the more powerful methods for 2D-crystallization of membrane proteins into liposomes. Using this method to prepare our ABA-copolymer proteovesicles we expect to insert more functional proteins.

The efficiency of the Bio-Beads procedure to reconstitute functional membrane proteins into ABA-copolymer vesicles has been compared with the same experiments performed via the ethanol method, using the membrane protein **NADH:ubiquinone oxidoreductase**, also named **Complex I**, which is interesting for electron transport through membranes [51]. Complex I was purified from *E. coli* (see chapter 7.2).

The aerobic respiratory chain of *Escherichia coli* contains several primary dehydrogenases. The Complex I links the electron transfer from NADH to ubiquinone with the translocation of protons across the membrane [52]. The resulting membrane potential is used to drive energy-consuming processes like ATP synthesis, solute transport, and flagellar motion.

Complex I is a **multi-subunit enzyme** and couples the electron transfer from NADH to ubiquinone with a proton translocation according to the overall equation:



where Q refers to ubiquinone, and H^+_{n} and H^+_{p} to the protons taken up from the negative inner and delivered to the positive outer side of the membrane. Complex I has a general 'L-shape' made of a peripheral arm and a membrane arm (Figure 37). The peripheral arm contains at least one flavin mononucleotide (FMN) and four iron-

sulfur (Fe-S) clusters and is able to catalyze the oxidation of NADH by artificial electron acceptor, such as **ferricyanide** or ruthenium (III) hexamine (the natural acceptor is ubiquinone).

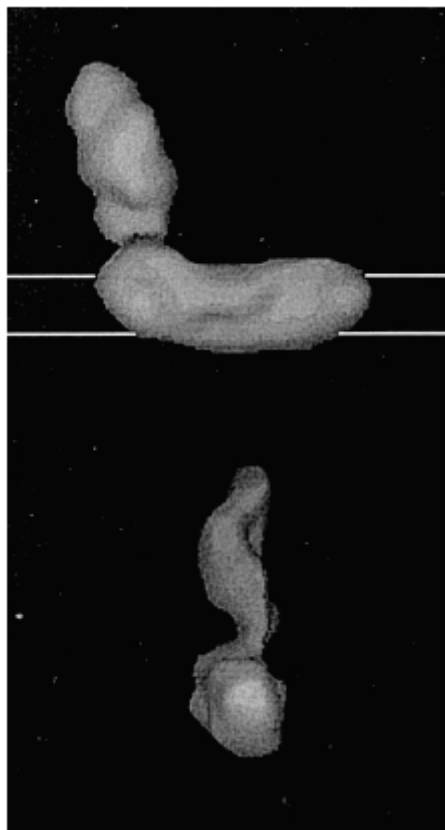


Figure 37: Three-dimensional model of the *E. coli* Complex I. The lower view is rotated by 90° clockwise about the axis of the peripheral arm with respect to the upper view. The membrane arm is shown horizontally. Two horizontal lines at the top separated by 4 nm symbolize the lipid bilayer. [52]

As mentioned above, the water-soluble NADH dehydrogenase fragment is capable for transferring electrons from NADH to ferricyanide, which is an artificial electron acceptor. This enzymatic activity is called **NADH:ferricyanide activity** and can be used to demonstrate the Complex I functionality [53].

Reconstitution trials

Proteovesicles are prepared via the ethanol method (chapter 7.3), where the protein is added dropwise in parallel with addition of the polymer/ethanol mixture into the solution; and via the Bio-beads method (chapter 7.4), where the protein is solubilized

together with the polymer in a 0.5 % Triton X 100 detergent solution before detergent removal with Bio-Beads.

To test the ferricyanide activity, and so the functionality of Complex I, the proteovesicles are prepared in a ferricyanide containing solution. The reduction of ferricyanide after NADH addition is followed by UV-spectroscopy.

Figure 38 shows the results for optimized reconstitution conditions with the bio-beads method (complex I concentration and bio-beads incubation time), and for the controls, i.e. same experiments reproduced with “free” Complex I and polymer vesicles without protein. We proved that the ferricyanide activity of Complex is preserved. Complex I is a highly asymmetric membrane protein: its functional reconstitution depends strongly on its orientation within the membrane. So at least a part of the proteins have been inserted in the right orientation.

With the ethanol method, no ferricyanide activity was recorded (data not shown). The proteins Complex I are not functional. They could have been denatured by ethanol (spatial conformation is crucial for enzymatic activity). They could also have been not inserted in the membrane or mainly inserted in the wrong orientation.

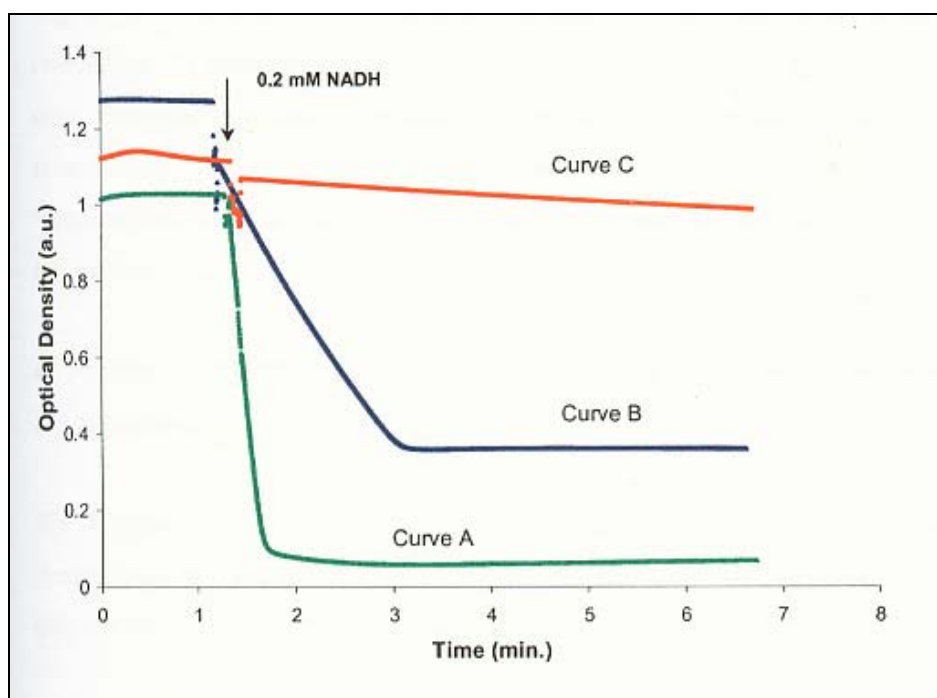


Figure 38: Time profile of the absorbance of ferricyanide solution reduced by NADH at 410 nm at 25°C. The reduction of ferricyanide started after addition of NADH to the different samples. **A:** free Complex I, **B:** Complex I reconstituted in polymer vesicles prepared via the bio-beads method, **C:** polymer vesicles (prepared via the bio-beads method) without Complex I.

In case of asymmetric membrane proteins, it will be much interesting to combine the bio-beads method (allowing a good protein preservation during reconstitution process) with asymmetric ABC triblock copolymers that would favor a unidirectional orientation of the protein within the membrane [54].

4.3 Bulk swelling

In order to exclude organic solvents, we have tried to form nanovesicles without solvent via solid rehydration (bulk swelling), where the amphiphile is directly hydrated as bulk powder in water. The dissolution is long; overnight stirring is necessary.

Figure 39 shows that bulk dissolution of ABA copolymer results in nanovesicles that have around 2 times larger average size in comparison with the ethanol or detergent methods, but also a higher size polydispersity, which has been also confirmed by DLS measurements.

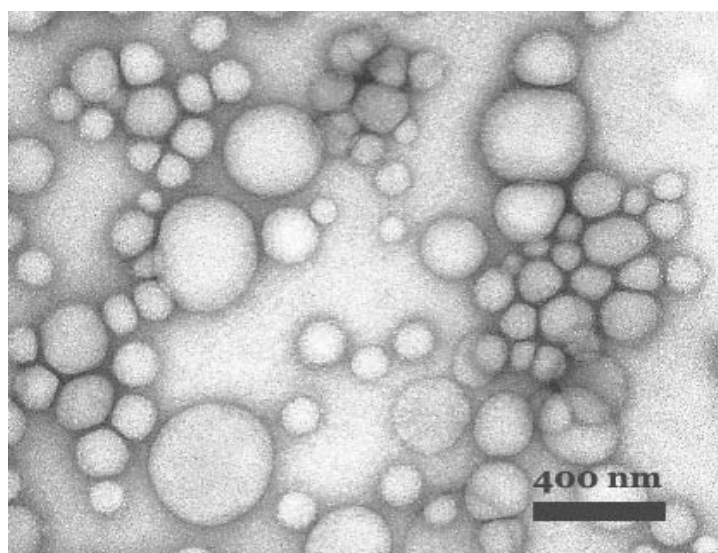


Figure 39: Nanovesicles from ABA-polymer formed by direct dissolution in water

We wanted to study the influence of the filtration on the size of the nanovesicles. On this purpose, samples with different concentrations (from 10 mg/ml to 2 mg/ml) have been examined in DLS, after consecutive filtrations (1 to 5 times) with decreasing pore size filters (0.45 to 0.2 μm). Results are summarized in Table 6.

Table 6: Radius and polydispersity of ABA- polymer nanovesicles prepared via bulk swelling

	Concentration	Consecutive filtrations (times number x pore size)			
		A	B	C	D
		1 x 0.45 μm	5 x 0.45 μm	1x 0.2 μm	5 x 0.2 μm
1	10 mg / ml	299* - 0.82**	310 - 0.82	209 - 0.86	217 - 0.86
2	`` diluted 2 times (5 mg / ml)	198 - 0.85	228 - 0.85	177 - 0.88	180 - 0.91
3	`` diluted 5 times (2 mg / ml)	123 - 0.90	222 - 0.89	224 - 0.88	
4	2 mg / ml	156 - 0.88	206 - 0.88	162 - 0.92	

* hydrodynamic radius in nm

** β_1 parameter from Williams-Watts fit of $g^2(t)$ in DLS; $\beta_1 = 1$ for a monodisperse sample

We can notice that multiple extrusions through the same filter are needed to “rinse” the filter; we see that the samples filtered only one time (column A and C) have smaller average sizes (with about same polydispersity) than the samples filtered 5 times (respectively column B and D); this means that biggest polymer vesicles can stuck in the filter. Thus we will discuss only the 5 times filtered samples (columns B and D).

For a same concentration (same line), multiple extrusions through filters from decreasing pore size allow for a decrease of the nanovesicle size (hydrodynamic radius) and also for a slight decrease of the polydispersity, i.e. β increases. This is mainly due to the elimination of the biggest vesicles (and/or vesicle aggregates).

For a same filtration (same column), the dilution of the 1 % sample (line 1 to 3) tends to decrease sample sizes. It is due to the dissolution of vesicle aggregates (formed at high concentration); the dissolution of aggregates is also responsible for the polydispersity decrease.

We can also observe that direct preparation of less concentrated polymer solutions (line 4) gives smaller sizes than the dilution of a 1 % stock solution until the same concentration (line 3). This could be attributed to the role of kinetics in self-assembly of macromolecules. In case of bulk swelling, only a part of the molecules are accessible to water (outer part of polymer powder aggregates) at the first instant of the dissolution. Nanovesicles forms spontaneously and then grow as the rest of the polymer become accessible to the water. A more concentrated sample will thus be able to produce larger vesicles, whereas the dissolution will take longer time. After

complete hydration of the polymer molecules, the self-assembled vesicles are in a semi-equilibrium state: a simple dilution will not influence significantly their size, unless reaching the cac (vesicle to micelle transition). The eventual size decrease observed is attributed to aggregates dispersion.

Bulk dissolution is a good method to produce vesicles in an easy way, especially for encapsulation applications (large inner volume). Hydrophilic substances to be encapsulated are simply dissolved in the same solution as the polymer. Non-encapsulated molecules are then removed by SEC.

It is however not ideal for membrane protein reconstitution because the proteins will be diluted in water and have a high probability to aggregate (similar to the ethanol method).

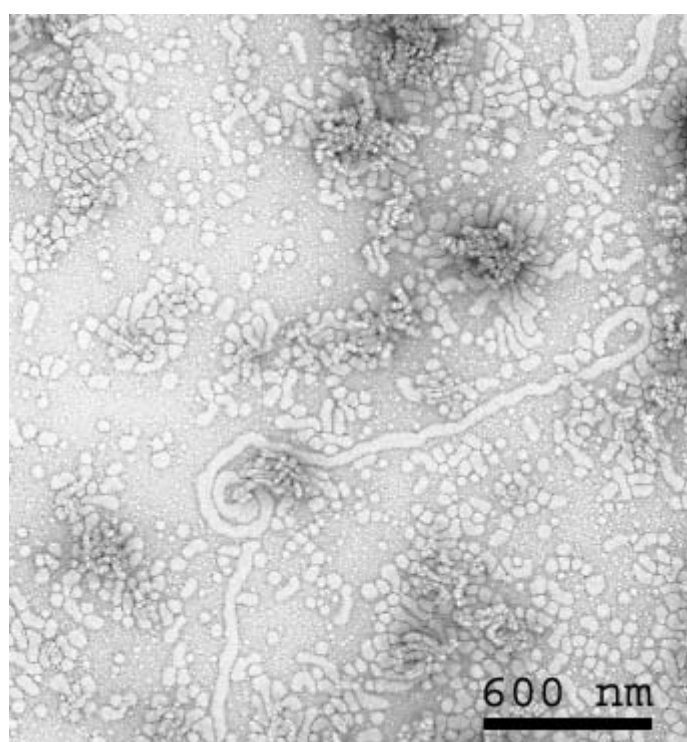


Figure 40: TEM image of ABA-copolymer (TD 01) self-assembled structures after bulk dissolution

For copolymers with shorter PMOXA blocks, observations in TEM revealed an interesting additional morphology besides vesicles: nanotubes (see Figure 40). Even if until now vesicles are the main common superstructure observed and studied from the self-assembly of block copolymers, this new type of superstructure appears of a great

interest, especially because soft nanotubes made from biocompatible polymers could find applications in biotechnology and medicine. ABA-triblock copolymer nanotubes study is presented in the chapter 5.

4.4 Reminder of main results

We have studied the morphologies adopted by different PMOXA-PDMS-PMOXA triblock copolymers in water. By using established and new preparation methods, we have demonstrated that (1) the ethanol method is a short and easy way to produce nanovesicles, (2) the detergent method with bio-beads is a powerful alternative to organic solvent use for nanovesicles preparation, and furthermore to improve reconstitution of functional membrane proteins in proteovesicles, and (3) bulk dissolution is also an easy way to produce nanovesicles without organic solvent, and highlights the possibility to prepare also nanotubes with our ABA-triblock copolymers.

5 NANOTUBES

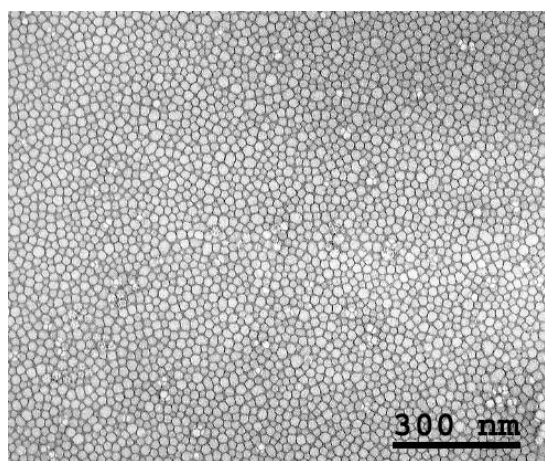
Nanotube research is currently one of the most active areas of Nanoscience.[55] Carbon nanotubes could have applications in miniature electronics and for hydrogen storage, but as they are stiff, difficult to process and purify, not biocompatible, and cannot be degraded by living organisms they are not well suited for biological applications; soft nanotubes made from biocompatible organic molecules and polymers however could find application in biotechnology and biomedicine.[56] Typical examples include self-assembled lipid nanotubes,[57] and peptide-based nanotubes.[58] Recently also block copolymers have been used to prepare vesicles and spherical or rod-like micelles.[59] Polymer *nanotubes* however have so far only been described in organic solvents where their fabrication often requires elaborate procedures;[60-62] however, the controlled preparation of water-filled polymer nanotubes in aqueous media has remained elusive.

Our interest in developing a reproducible method of polymer nanotube preparation, and furthermore in studying their behaviors is thus associated with the putative advantages of nanotubes in various fields of applications, such as optics or nanofluidics, where nanotubes can for e.g. be used as connections between compartments in a “lab on a chip” [63], but also with an interest from a basic scientific point of view.

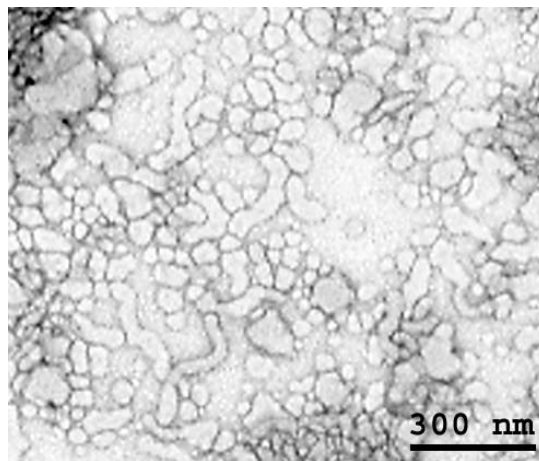
5.1 Bulk dissolution or bulk swelling

As mentioned in the previous chapter, observations in TEM for bulk dissolution of ABA-triblock copolymers with shorter PMOXA blocks, revealed an interesting additional morphology besides vesicles: nanotubes. This was never observed with the ethanol method, as shown in Figure 41. We can notice that nanotubes have a quite similar diameter (around 50 nm) and a broad length distribution. The diameter observed tend to exclude the possibility of formation of worm-like micelles, we expect only around 20-30 nm for a micelle. Furthermore the diameter of the tubes is

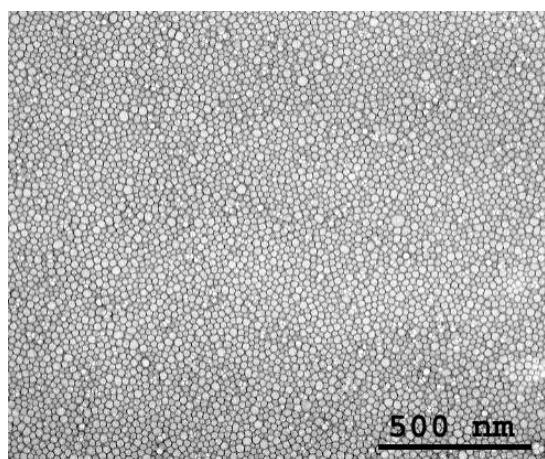
not regular over the complete length; a worm-like micelle should look straight. There is no reason for a “normal” block polydispersity of the copolymer to observe a segregation of the molecules; intramicellar segregation leading to cylindrical undulations was only observed for bimodal mixtures of considerably different block lengths [64]. In our case, the polydispersity of ABA molecules is only due to the polydispersity of initial PDMS block and have been measured by gel permeation chromatography at $M_n/M_w = 1.7$. [19] Furthermore, even if they would segregate, our molecules are not enough polydisperse to have a visible size difference such as the several nm undulations observed in the diameter of our nanotubes. The bulges corroborate thus the presence of a water-filled space inside the nanotube.



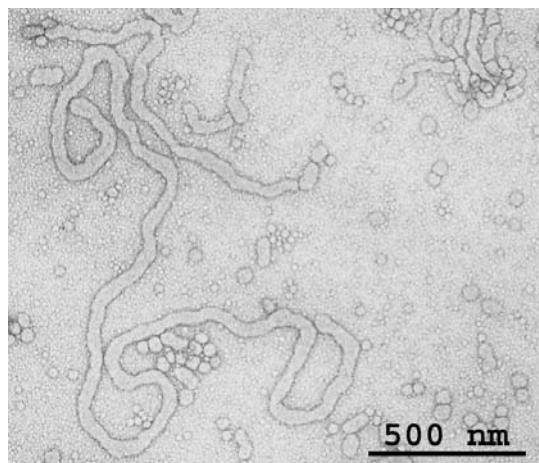
JW 08 method ethanol



JW 08 bulk dissolution



T 02 ethanol method



T 02 bulk dissolution

Figure 41: Morphology comparison of nanocontainers prepared with the ethanol method and the bulk dissolution for 3 ABA-copolymers

A schematic of the self-assembly of a water-filled nanotube is proposed in Figure 42; the wall of the nanotube is composed by copolymer membrane surrounding a water filled space.

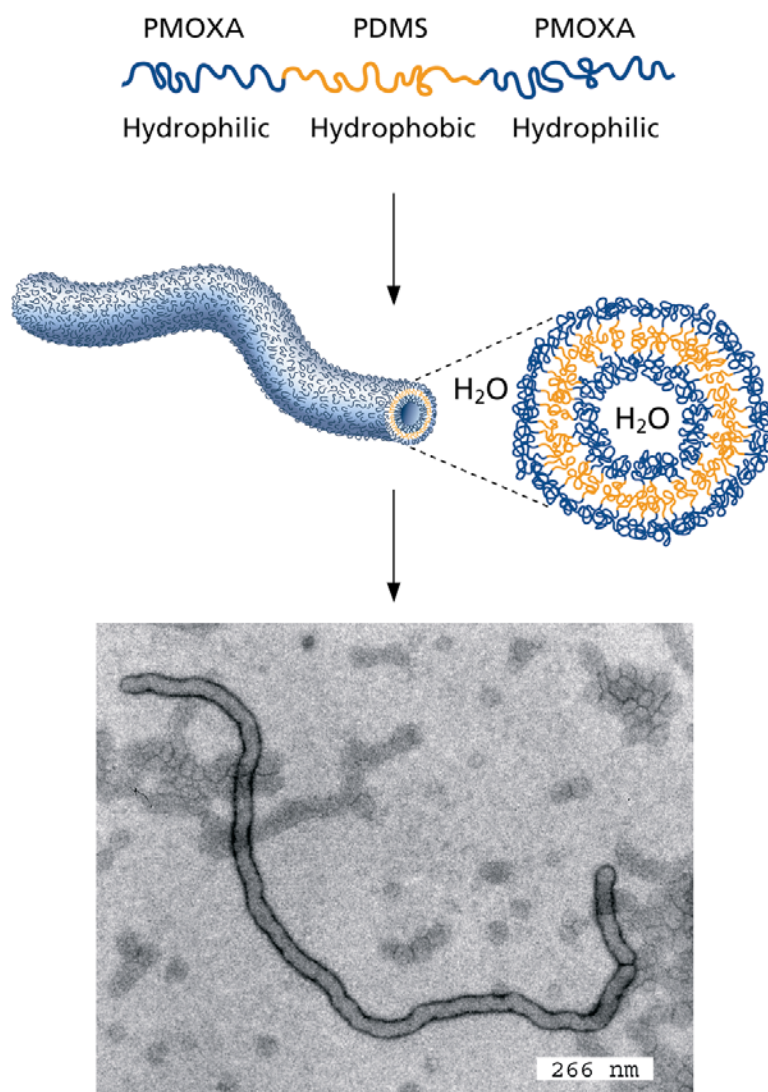


Figure 42: Self-assembly of ABA triblock copolymers in aqueous solution; TEM image of a polymer nanotube [65]

The addition of ethanol to a mixture of nanotube and nanovesicle leads to only nanovesicles in a very short time. We can suppose that the ethanol acts as a co-solvent for the polymer and thus modify its self-assembly in water. It could also act as a plasticizer.

Once demonstrated the ability to form polymer nanotubes via self-assembly of ABA-triblock copolymers in water, the next step was to produce nanotubes in large amount and to study their properties.

5.2 Film rehydration or film swelling

The method of film rehydration (or film swelling), common for liposome preparation and also already used for block copolymer vesicle preparation [46], resembles the bulk swelling method; the only difference being that the amphiphile is not hydrated as bulk powder but is hydrated as a thin film on a surface. To that end, A 1 % (wt/wt) solution of the copolymer in chloroform was dried under nitrogen in a test tube; by rotating the tube during drying a polymer film forms on the glass. Drying was completed by desiccation under vacuum overnight. In a second step, the film was rehydrated by water addition and stirring for 24 hours to yield a 1 wt% polymer solution, which is homogeneous and opaque.

After a 10-fold dilution with water, the samples have been investigated with TEM (chapter 7.9.2). As shown in Figure 43, this procedure yields to a mixture of vesicles and flexible nanotubes.

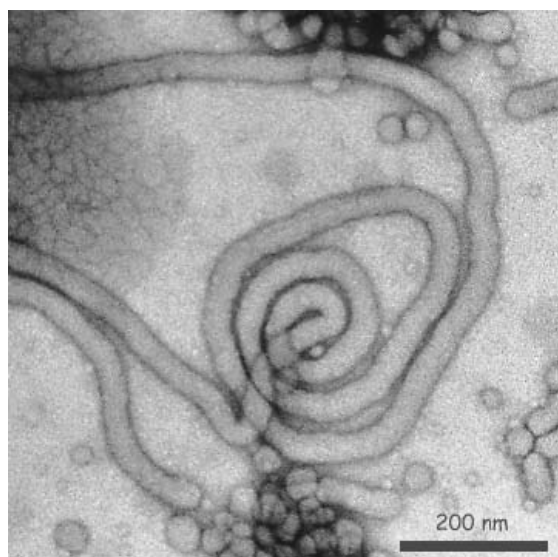


Figure 43: TEM picture of a soft nanotube formed by film rehydration of ABA-polymer (JW08)

The vesicles are quite polydisperse with diameters ranging from 40 to over 500 nm, but the tube diameter is astonishingly uniform at about 40 nm. The nanotubes extend up to several tens of microns in length and their concentration with respect to the number of vesicles depends on the copolymer used, that is, the formation of the tubes vs. vesicles depends on the relative block lengths of the hydrophilic PMOXA and hydrophobic PDMS blocks. Table 7 summarizes the nanotube formation results. A low PDMS/PMOXA wt/wt ratio (below ~ 1.5) favors vesicle formation and higher ratios (~ 2 and higher) increasingly favor nanotube formation. This tendency is qualitatively confirmed with a control experiment where the dry polymer was directly dissolved in water and imaged in the TEM (bulk dissolution method).

Table 7: Approximate volume fraction of tubes as a function of polymer composition and sample preparation

Copolymer ^a	PDMS/PMOXA	Tube volume	Tube volume
	Ratio (wt/wt)	fraction Rehydration	fraction Dissolution
A ₁₁ B ₆₂ A ₁₁	2.4	90 ± 5	30 ± 5
A ₁₆ B ₇₂ B ₁₆	2.1	85 ± 5	20 ± 5
A ₁₅ B ₆₂ B ₁₅	1.9	75 ± 5	25 ± 5
A ₂₁ B ₇₂ B ₂₁	1.5	5 ± 5	1 ± 5
A ₂₁ B ₆₉ B ₂₁	1.5	10 ± 5	5 ± 5

^a A: PMOXA, B: PDMS

Although we observe a trend in both sets of experiments, a quantification of this phenomenon is difficult from TEM data alone and the data in Table 7 thus have an error of about 10%. Nevertheless, these findings suggest that the formation of the nanotubes is largely controlled by the geometry of the PMOXA blocks: at a ratio of ~ 1.5 the PMOXA block is, relatively speaking, larger than the PMOXA block at a ratio of ~ 2 and more and hence it favors vesicles over tubes because each chain occupies a larger hydrodynamic volume. We can thus speculate that an even higher PDMS/PMOXA ratio will favor nanotube formation to an even higher extent.

It is possible to explain the role of the blocks geometry and the preparation methods if we consider the ABA molecules in “U” shape as diblock copolymer molecules, or if we assimilate an ABA membrane to a diblock bilayer.

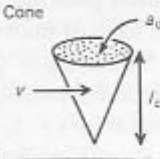


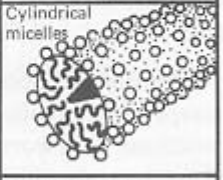

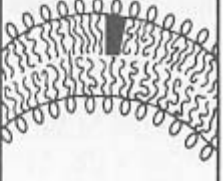

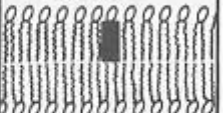

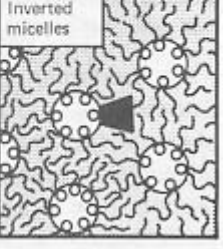
The geometry of amphiphilic molecules, such as surfactants, lipids, or copolymers, is currently believed to play a major role in defining its aggregation behavior [66]. In particular, those surfactants that possess a conical shape are expected to maximize intermolecular hydrophobic interactions by organizing into spherical micelles; those that are cylindrical form planar bilayers. The geometric packing properties of different lipids may be expressed in terms of the packing parameter

$$\frac{v}{a_0 l_c} \quad \text{Equation 10}$$

v is the volume and l_c the length of (hydrophobic) chain

a_0 is the (hydrophilic) head-group area

This parameter is characteristic for each lipid in a given solution environment, the value of which determines the type of aggregates [67]. Table 8 illustrates the structures formed by some common lipids, and how these can be modified by their ionic environment, temperature, chain unsaturation, etc.

Lipid	Critical packing parameter v/a_0l_c	Critical packing shape	Structures formed
Single-chained lipids (surfactants) with large head-group areas: <i>SDS in low salt</i>	$< 1/3$	Cone 	Spherical micelles 
Single-chained lipids with small head-group areas: <i>SDS and CTAB in high salt, nonionic lipids</i>	$1/3-1/2$	Truncated cone 	Cylindrical micelles 
Double-chained lipids with large head-group areas, fluid chains: <i>Phosphatidyl choline (lecithin), phosphatidyl serine, phosphatidyl glycerol, phosphatidyl inositol, phosphatidic acid, sphingomyelin, DGDG^a, dihexadecyl phosphate, dialkyl dimethyl ammonium salts</i>	$1/2-1$	Truncated cone 	Flexible bilayers, vesicles 
Double-chained lipids with small head-group areas, anionic lipids in high salt, saturated frozen chains: <i>phosphatidyl ethanolamine, phosphatidyl serine + Ca²⁺</i>	~ 1	Cylinder 	Planar bilayers 
Double-chained lipids with small head-group areas, nonionic lipids, poly (<i>cis</i>) unsaturated chains, high <i>T</i> : <i>unsat. phosphatidyl ethanolamine, cardiolipin + Ca²⁺, phosphatidic acid + Ca²⁺, cholesterol, MGDG^b</i>	> 1	Inverted truncated cone or wedge 	Inverted micelles 

^a DGDG, digalactosyl diglyceride, diglucosyl diglyceride.
^b MGDG, monogalactosyl diglyceride, monoglucosyl diglyceride.

Table 8: Mean dynamic packing shapes of lipids and the structures they form [67]

Because a nanotube is in fact a tubular vesicle, we can speculate that the geometry of the amphiphile molecule must be in between the one needed for a spherical vesicle and for a planar bilayer, i.e. with packing parameter between $1/2$ and 1 , to form a nanotube. Table 8 shows that the size of the (hydrophilic) head group is an important factor; large size favors spherical shape whereas small size favors planar bilayers. For our ABA molecules, hydrophilic head-group corresponds to PMOXA blocks; this explains that when they occupy a larger volume (higher hydrophobic/hydrophilic ratio), spherical vesicles are favored.

The factors influencing the size and shape of vesicles formed from amphiphilic molecules (lipids or diblocks) have been described in [68]. The formation of vesicles relies on the fact that the amphiphiles energetically prefer a parallel molecular arrangement; they form easily when the bilayer bending elasticity is low and the surface tension is high. An “equilibrium vesicle” size can be defined as the result of mixing entropy and molar bending energy. However, the standard polymer structures have such a low molecular solubility that the conformation and size is usually not a product of exchange and equilibrium processes but trapped by preparation conditions (so called “non equilibrium vesicles”). The actual vesicle size depends less on thermodynamics and more on non-equilibrium aspects of the formation process. Vesicles diameters can be tailored using different preparation procedures such as rehydration [69], electroformation [70], and direct dissolution in water. The shape of a vesicle is one that minimizes the bending energy for a given difference in the number of amphiphiles in the inner and outer monolayers, which depends on the preparation process. There are numerous shapes, including spherical, and tubular, as shown in the phase diagram in Figure 44.

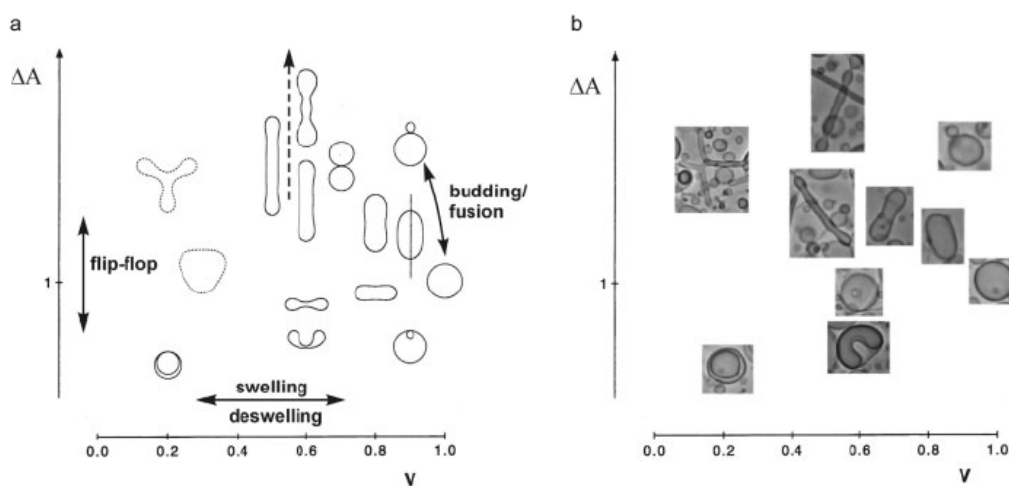


Figure 44: Phase diagram of theoretical (a) and observed (b) vesicle shape for amphiphilic block copolymers. Ways to change shape are indicated in (a). [68]

The phase diagram is parameterized in terms of dimensionless volume-to-area ratio $\nu = 6\pi^{1/2}VA^{-3/2}$ and the area difference $\Delta A = A_{in} - A_{out}$. The ratio ν is defined such that spherical vesicles have a maximum value of $\nu = 1$, i.e. that they possess the

highest possible volume-to area ratio. ΔA is the area difference between the inner and that outer parts of the bilayer and is proportional to the difference in the number of amphiphiles. A large area difference $\Delta A > 1$ tends to curve the membrane outward (upper part of the diagram, where we find the tubes), whereas a smaller or negative value $\Delta A < 1$ leads to inward curved shapes (lower part of the phase diagram). Other factors can also influence vesicle shapes, such as preparation process, temperature, or amphiphile composition. In our case, both polymer composition: high versus low hydrophobic/hydrophilic ratio, and preparation methods: film or bulk swelling versus electroformation (see appendix 8.1) or ethanol method, influences nanotube versus spherical vesicle formation.

The results in Table 7 also indicate also that film swelling is a more efficient pathway to polymer nanotubes than simple dissolution of the dry polymer in water (bulk swelling). We have just seen the importance of swelling methods in tubular vesicle formation (Figure 44). But we would point out the two main differences between bulk and film swelling. (i) We used chloroform to dissolve the polymer; we can envisage that this organic solvent yields to a spatial organization of the ABA molecules favoring the nanotube conformation. (ii) The polymer molecules are not in the same arrangement in a powder and in a film, we can speculate that in case of film swelling, the ABA molecules are already “organized” because of the interaction between the glass surface and the PMOXA blocks, helping the spontaneous formation of long tubes. Large area orientation of block copolymer microdomains in thin films has been already proved in [71]. Forming a film using a solution including a block copolymer and a solvent for the block copolymer; and rapid solidification from the solvent may include directional solidification and/or epitaxy to form patterns of microdomains in a film of block copolymer. Microdomains may include various structures formed by components of a block copolymer, such as vertical lamellae, in-plane cylinders, and vertical cylinders, and may depend on film thickness. We have also noticed an influence of film thickness in our experiments (data not shown). Indeed, the use of rotational evaporator to form a thin and homogeneous polymer film, which means a high proportion of polymer molecules in contact with glass surface and thus “organized”, favors formation of long nanotubes compared to a simple film formation in a glass tube (quite thick and inhomogeneous film), which leads to a higher proportion of spherical vesicles or short nanotubes.

This phenomenon could be compared with the nanotube formation observed in the subphase of a polymer monolayer after deposition and evaporation of a drop of polymer-chloroform solution onto a water surface (see appendix 8.2): ABA molecules are also here already oriented at the air-water interface.

As a control, we have confirmed that all those polymers form only nanovesicles with the ethanol and detergent methods. Indeed, in these two methods, the molecules are “dispersed” in the water by the ethanol (co-solvent) or the detergent. They do not adopt a special orientation between each other favorable to nanotubes. Furthermore, in that case, we have “equilibrium” vesicles, because the permeation of solvent through the bilayer is possible, allowing ν adjustment; most vesicles are thus spherical [68].

Nanotubes are resistant to multiple extrusions through Millipore filters and SEC. They also remain stable over months if stored at 4°C. The TEM image shown in Figure 45 has been taken after 8 months of storage at 4°C.

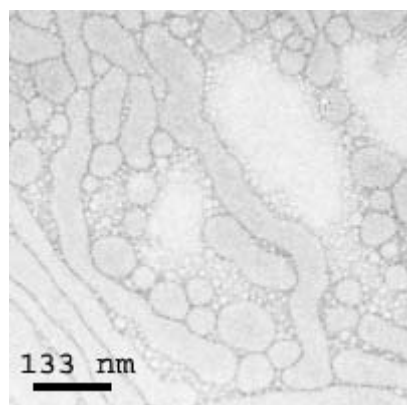


Figure 45: ABA-polymer nanotubes in water after 8 months of storage

We have also investigated nanotubes prepared at different pH. Figure 46 shows that they remain intact even at strong basic or acidic conditions. However, we see a change in the regularity of the outer surface of the nanotubes. Because the different samples have been prepared in different buffers (with different salts), we can speculate that salts interact with the PMOXA block and lead to different aspect of the shell.

This is of particular interest for biological applications, such as drug delivery; for example the pH of the stomach is 2 and it could be of great advantage to have nanocontainers able to protect a drug in such an environment.

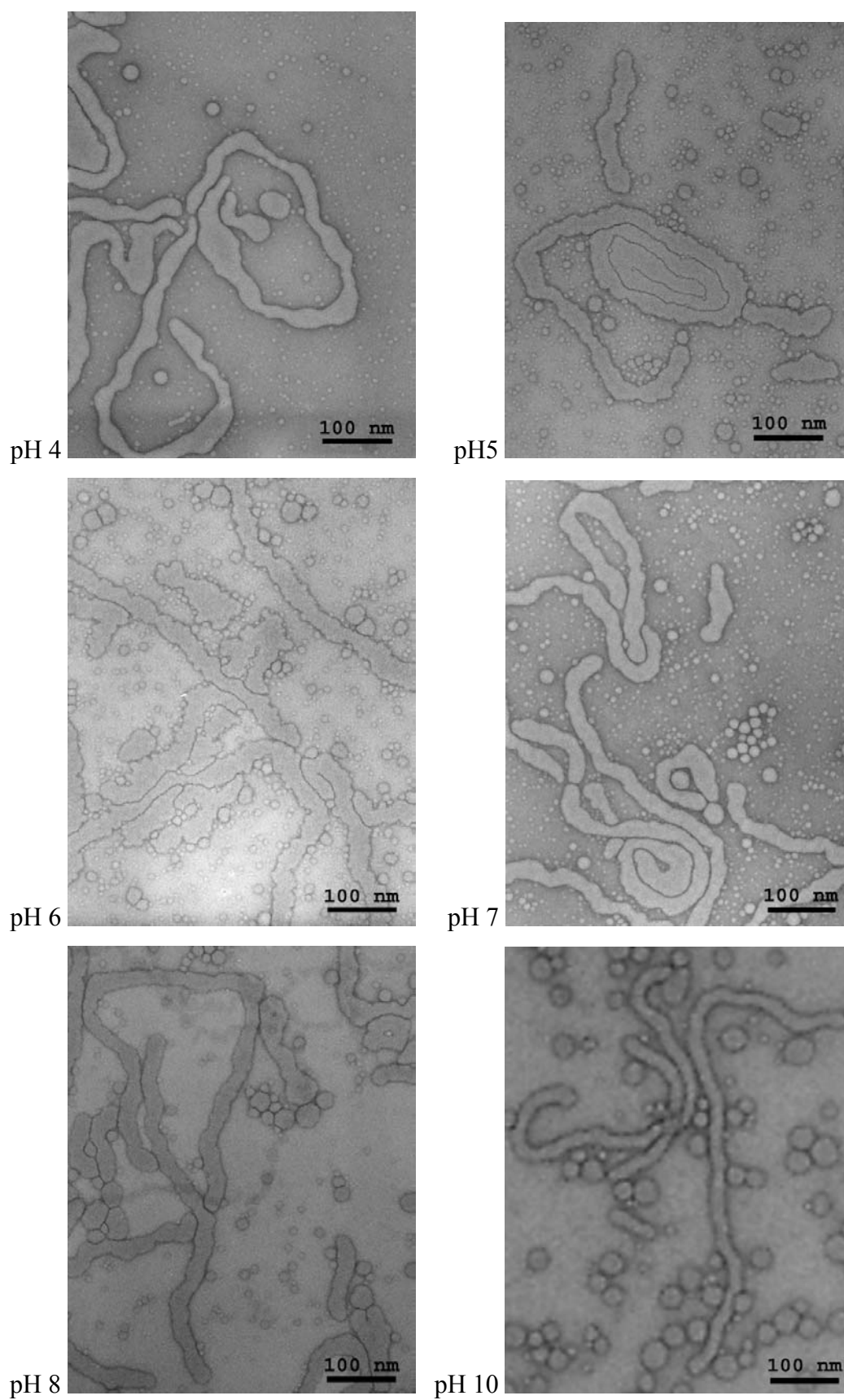


Figure 46: ABA-polymer nanotubes (JW 08) formed in aqueous buffers at various pH

As done previously for nanovesicles [19], the nanotubes can be prepared with a polymer functionalized with methacrylate end-group that polymerize upon UV-irradiation. 0.1% of a photo-initiator (Irgacure 2959 from Ciba) was added to the nanotube preparation and irradiated for 30 sec. We have checked by NMR spectroscopy that the conversion of the methacrylates is almost complete (data non shown); we can hence speculate that crosslinking could further stabilize the nanotubes for various applications involving for example the use of organic solvents or the stretching of the nanotubes, such as in optical tweezers manipulation.

Figure 47 demonstrates that the incorporation of methacrylate end groups and subsequent UV polymerization does not change the shape of the aggregates.

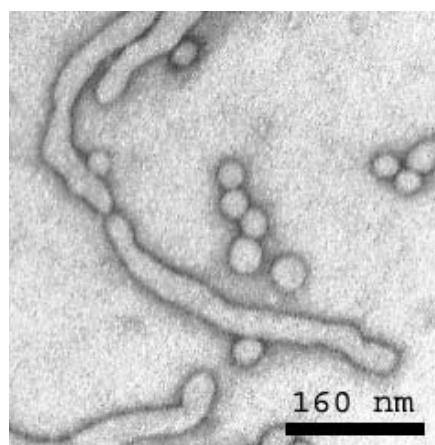


Figure 47: TEM image of cross-linked nanotubes and vesicles

We have employed different strategies to prove that the nanotubes are indeed water-filled nanotubes as opposed to rodlike micelles with a hydrophobic interior: cryo-TEM imaging, hydrophilic fluorescent dye encapsulation, and both hydrophilic and hydrophobic gold particles encapsulation.

5.3 Cryo-TEM

Cryo-TEM offers the great advantage that specimens are frozen and viewed in vitreous ice and therefore seen in a natural hydrated state, which is as close to their natural state as it is currently possible.

Figure 48 shows cryo-TEM images of self-assembled structures obtained via film rehydration of the copolymer JW08. We can distinguish nanovesicles of several hundreds nm diameters and also long tubes with a lower contrast.

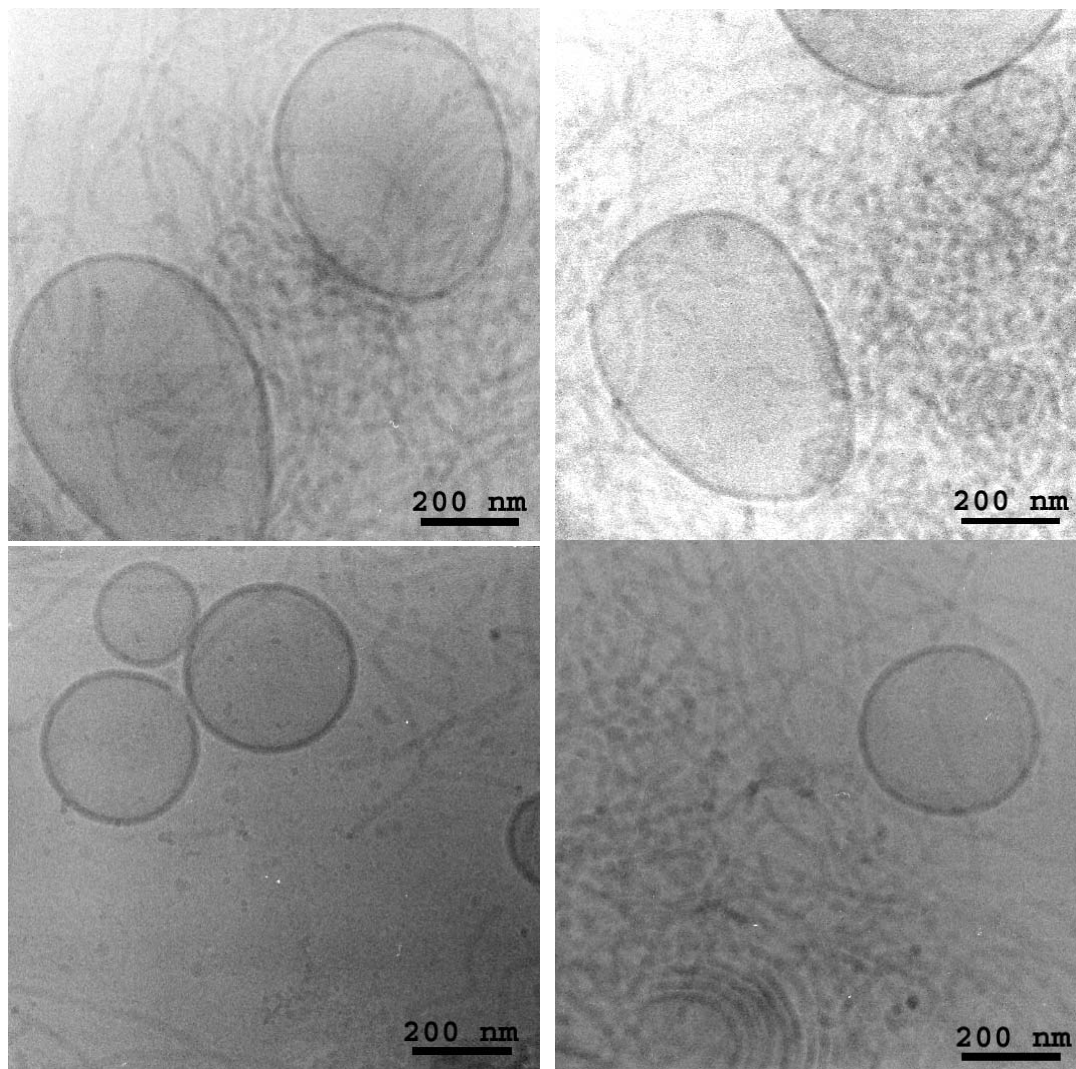


Figure 48: Cryo TEM images of nanocontainers (nanovesicles and nanotubes) prepared via film rehydration of ABA-copolymer (JW08)

Cryo-TEM, compared to other TEM techniques, offers the unique possibility to measure the real sizes in solution. In Figure 49, taking account of the low contrast of the nanotubes, we can measure the nanotube diameter: 20 ± 4 nm and the membrane thickness of the vesicles, 17 ± 4 nm.

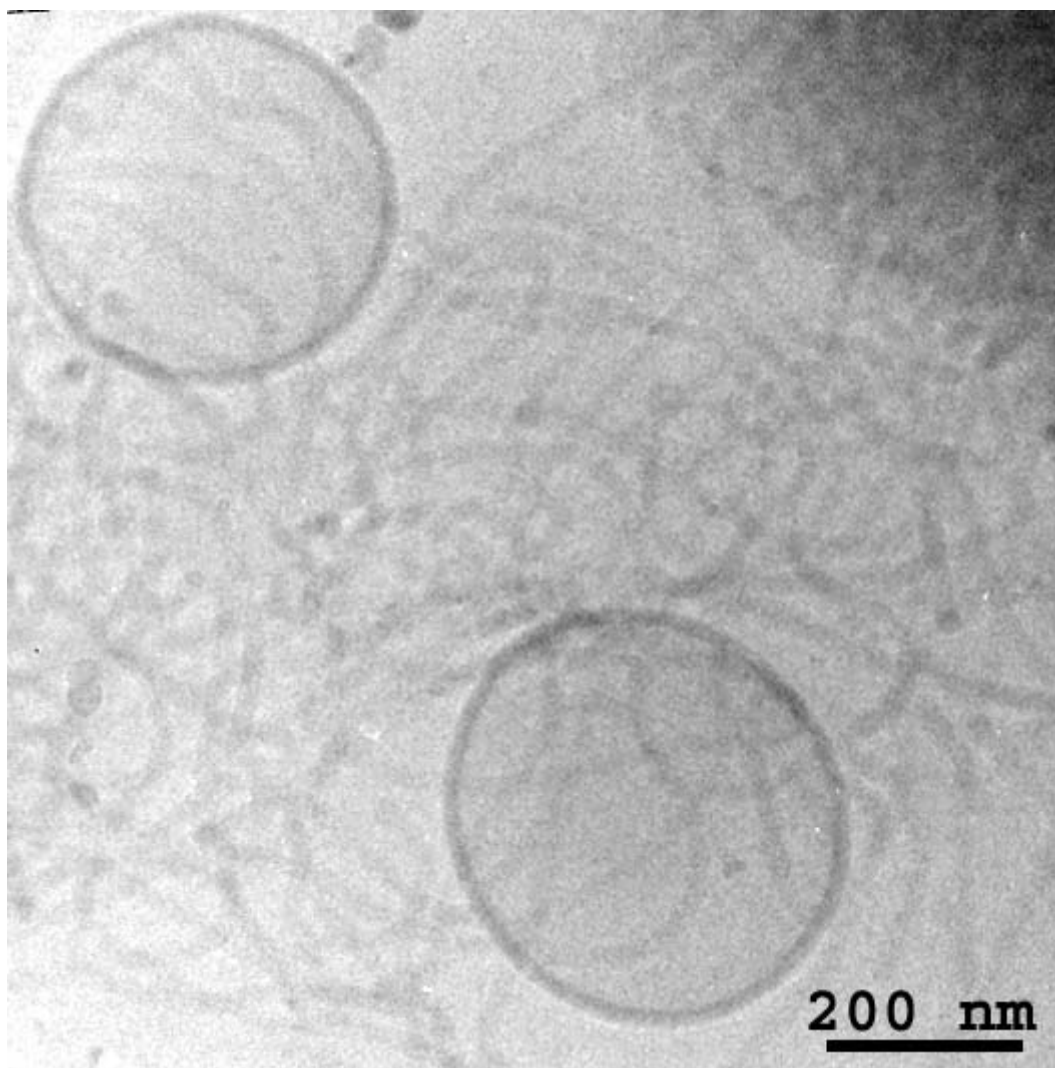


Figure 49: Cryo TEM image of nanocontainers (nanovesicles and nanotubes) prepared via film rehydration of ABA-copolymer (JW08)

The vesicle membrane thickness is larger as the one expected from previous studies. Indeed the thickness of the hydrophobic part of the ABA-membrane, which is usually more contrasted in cryo-TEM, has been evaluated to 10 nm by membrane capacitance [18]. The size difference (5-10 nm) observed in cryo-TEM could be explained if the density of PMOXA is enough to be imaged in the cryo-TEM and by the little defocus we used.

However, if the vesicle walls measure around 17 nm, we would expect to have at least 2 times the thickness membrane, i.e. at least 30 nm, for the nanotube diameter. Those images may thus suggest the presence of worm-like micelles and not tubes. This would explain their low contrast compared to vesicles, as shown in Figure 50. Indeed, only the vesicular shape can produce a strong contrast in cryo-TEM; polymer

thickness is strongly different between the side and the center of a vesicle; a hollow shape is thus visualizable. In the case of worm-like micelles, the polymer thickness is the same over all the length of the worm; no contrast can be produced. A nanotube is elongated vesicle and should also be seen in cryo-TEM.

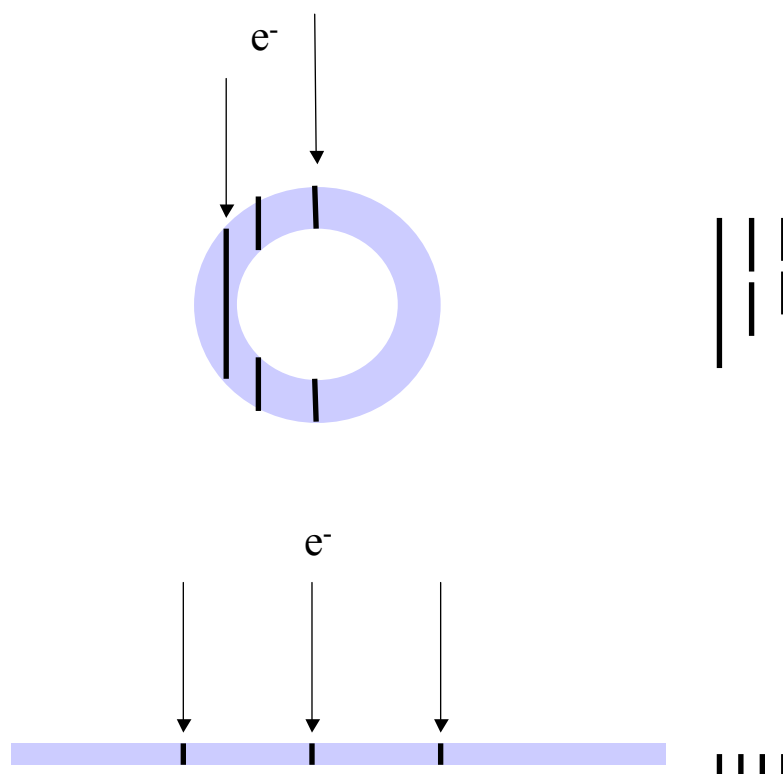


Figure 50: Contrast in cryo-TEM

However the “worm” hypothesis does not fit with standard TEM images, interpreted as nanotube (diameter > 40 nm and bulges). And we should not forget that diameter of nanotubes are extremely low compared to the vesicles observed here. We explained that the contrast results from the accumulation of electron density in the vesicle wall: thus a bigger vesicle will produce a higher contrast than a small. The limited diameter of the nanotubes is probably the reason why we do not distinguish their vesicular shape; this will also explain why we do not observe on the cryo-TEM pictures the small vesicles always observed in standard TEM beside nanotubes (see for e.g. Figure 43).

Figure 51 demonstrates also the formation of multilamellar vesicles. The vesicles walls are composed of several layers with water filled space in between. We can

observe vesicle membrane deformation leading to coalescence (vesicle growing). This proves the dynamics of the vesicles and the ability for the membrane to be deformed; this corroborates the possibility for ABA-molecules to form various superstructures, including nanotubes.

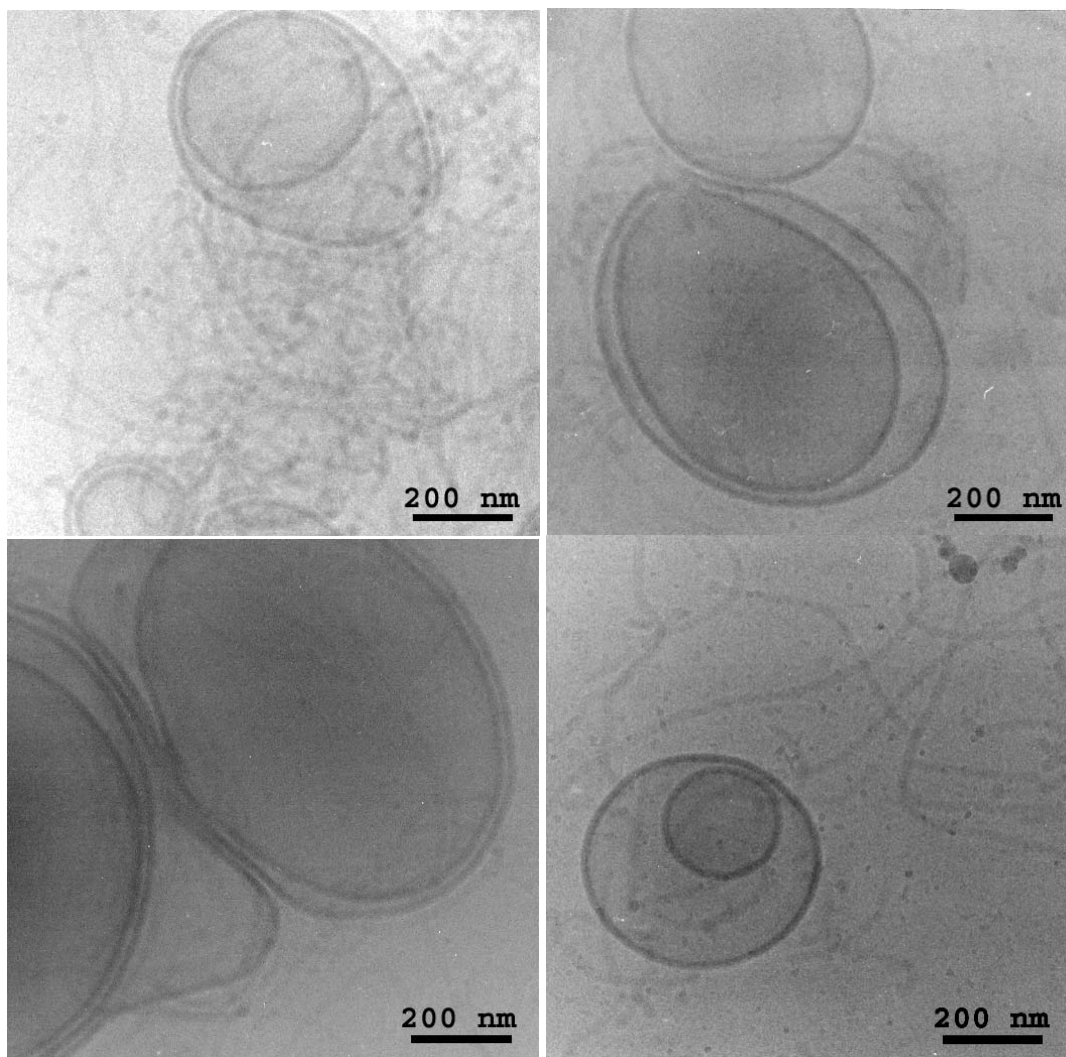


Figure 51: Multilamellar vesicles obtained by film rehydration method

The formation of vesicles is clearly shown by cryo-TEM, but this technique is not able to definitively prove the hollow nature of the nanotubes. Therefore a second strategy was employed, which consists of encapsulating a hydrophilic fluorescent dye within the nanotubes.

5.4 Fluorimetry

Nanocontainers (nanovesicles + nanotubes) were prepared via film rehydration with an aqueous solution containing the hydrophobic fluorescent dye carboxyfluorescein (CF). Non-encapsulated dye is removed from the sample by SEC prior to fluorescence measurements. Fluorescence intensity of the CF-loaded nanocontainers (nanovesicles + nanotubes) has been measured with a fluorimeter (see chapter 7.11.2). We used a detergent (*o*-POE) to destabilize the membrane and observe the release of the dye into the external medium.

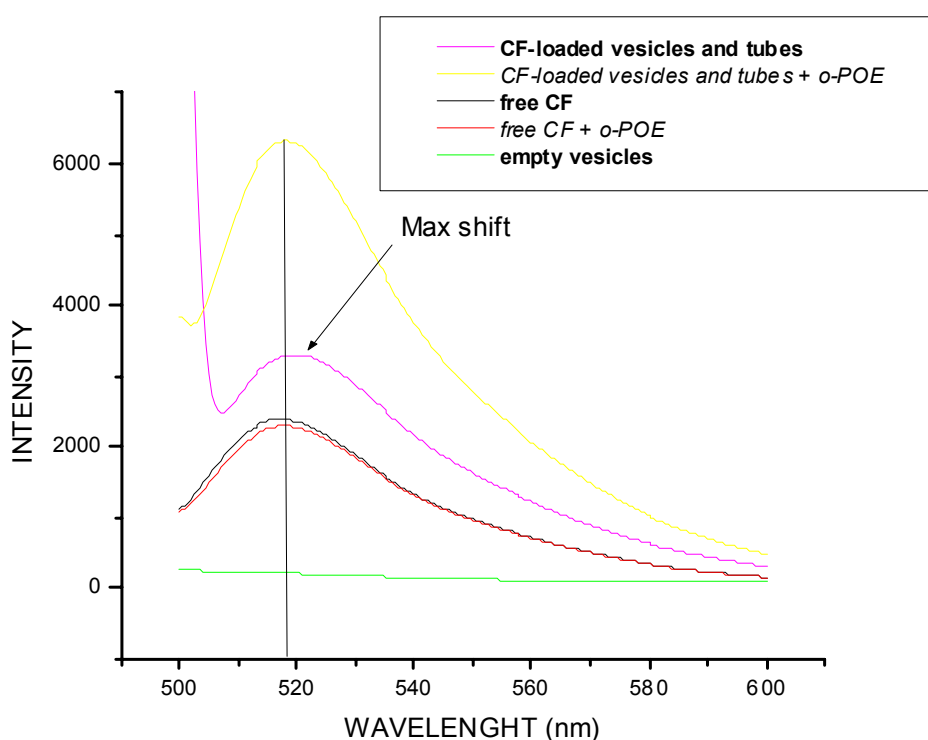


Figure 52: Fluorescence intensity of CF loaded nanocontainers

Figure 52 shows clearly an increase of the fluorescence intensity after detergent addition. CF encapsulation leads to self-quenching which is corroborated by an increase in fluorescence intensity upon polymer membrane destabilization with detergent. As controls, free CF in solution and ABA-copolymer vesicles without dye, have been measured under the same conditions. We have confirmed that the detergent does not have an influence on the intensity of the CF and that the polymer does not have a significant fluorescence at this wavelength. The absorption maximum of the free CF is around 518 nm. This peak is slightly shifted to higher wavelength (523 nm)

when CF is encapsulated into nanocontainers. This shift is not due to the presence of the detergent (see the free CF curves where the o-POE has no influence). It is probably due to an interaction between the ABA copolymer and the dye (when they are close to each other) leading to a change of the dye's electronic environment. After release in solution, the maximum is close to that of the free dye, showing that the polymer and the dye molecules do not interact anymore. We have seen the same kind of shift for encapsulation of dye in nanovesicles alone, prepared via the detergent method, thus without nanotubes (data not shown).

This experiment proves that we have encapsulated CF in the nanocontainers. However we have always a mixture of vesicles and tubes, and we cannot completely avoid the possibility for the CF to be only encapsulated into vesicles.

Fluorescence microscopy (see chapter 7.11.1) of CF-loaded nanocontainers has thus been done, after SEC cleaning and several weeks of storage. Figure 53 shows a CF-loaded nanotube beside a nanovesicle. No intensity was measured outside. This proves that the inside of the tubes really contains water and CF. This in turn rules out the formation of rodlike micelles. This also shows that no permeation of the dye through ABA-polymer membrane occurred over weeks.

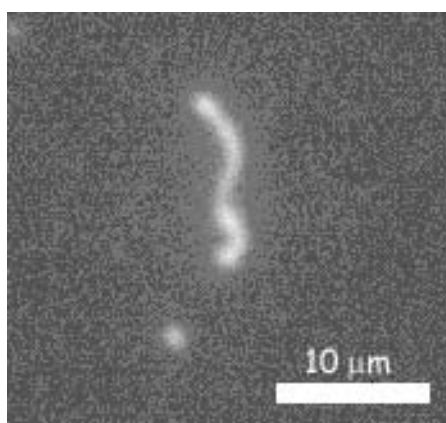


Figure 53: Fluorescence micrograph of a CF-loaded nanotube

However this kind of picture was hard to reproduce because of the fast bleaching of CF and also the resolution limit of the optical microscope. A third strategy was thus employed to image the interior of the nanotubes; we tried to encapsulate gold particles, common markers for TEM experiments.

5.5 Gold loaded nanotubes

5.5.1 Gold particles encapsulation

In order to distinguish rod-like micelles from nanotubes (and at the same time spherical micelles from spherical vesicles) one approach was to simply encapsulate pre-synthesized gold nanoparticles.

We have used hydrophobic and hydrophilic gold particles. In principle, the hydrophobic particles will be inside if we have micelles and the hydrophilic particles will be encapsulated into water filled vesicles or tubes.

Nanotubes are prepared with the film rehydration method. The hydrophobic gold particles are dispersed in the chloroform/polymer solution before drying and should therefore be uniformly distributed in the polymer film. The hydrophilic particles are dispersed in the water used for rehydration of the polymer film. In both cases, after rehydration, non-encapsulated gold is removed by SEC and samples are examined in TEM. Because of the hydrophobicity of the gold, gold-filled aggregates must be micelles

As shown in Figure 54 some hydrophobic gold particles are encapsulated into spheres, that must be spherical micelles, and no gold particles were found inside nanotubes, that contributes to eliminate the rod-like micelle hypothesis. However, those spherical micelles could be due to the presence of the particles during rehydration, leading to assembly of the PDMS blocks around the hydrophobic gold. It does not prove that micelles are formed without hydrophobic gold particles in the solution during polymer film rehydration.

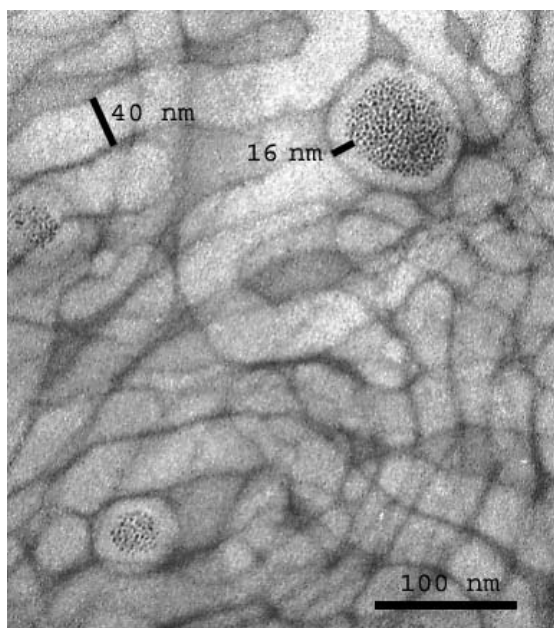


Figure 54: TEM picture of hydrophobic gold particles encapsulated into nanocontainers prepared via film rehydration of JW08

Unfortunately, we were unable to encapsulate the hydrophilic gold particles that would demonstrate the hollowness of the tubes. Our experiments and published studies indicates that colloidal gold particles are not suited for encapsulation into liposomes and polymer vesicles, because they will precipitate at high concentration necessary to load a large fraction of liposomes [72] and also because they are not stably entrapped in the liposomes do to their high density [73]. As a result, this experiment was not conclusive.

In a second attempt, we thus tried to encapsulate a gold solution, rather than gold particles, into nanotubes; the particle formation could then be initiated after the nanotube formation. Gold formation is thus templated by polymer superstructures.

5.5.2 Gold templated formation

Method 1: NaAuCl₄

According to Sato [74], particle formation into liposomes can be induced from gold salt (NaAuCl₄) solutions by UV irradiation that initiates the gold reduction. We have thus prepared nanotubes via film rehydration of JW08 in a gold salt solution. Unfortunately, gold reduction starts without any control (i.e. without UV irradiation).

After cleaning with SEC, gold particles with different shapes are observed in TEM: spheres, triangles (or tetrahedrons), and rods, as shown in Figure 55.

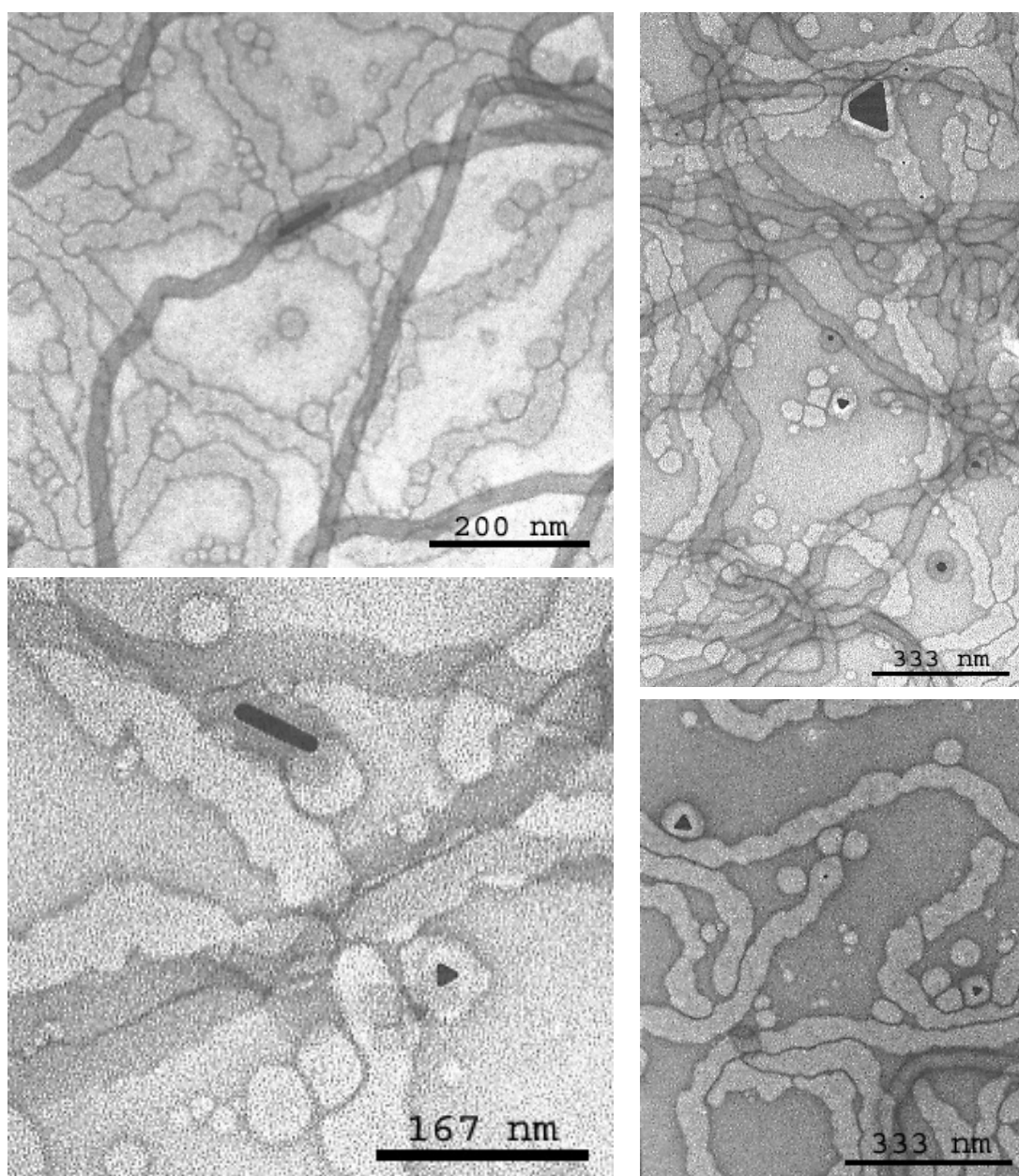


Figure 55: Gold particles encapsulated into nanotubes and vesicles after NaAuCl_4 reduction

A lot of methods have been developed for synthesis of colloidal gold, but the shape mainly observed is spherical. Colloidal gold preparations with a diameter greater than 25 nm exhibit eccentricity (ratio of major-minor axes) and various geometrical shapes; in general these alterations from the normal spherical shape cannot be avoided and reflect the crystalline nature of the colloidal particle. Over reported values, a colloidal gold preparation showing greater heterogeneity is often representative of an

irregular rate of nucleation. [75] Because here the nucleation was not induced with UV, only a few particles have been formed. They have grown slowly and with all the available ions. This explains their quite big size (> 25 nm) and thus their non-spherical shape. The shape disparity could be due to an irregular rate of nucleation but furthermore to different local concentration in gold ions, accrediting the encapsulation inside polymer containers. Furthermore, gold particles are all encapsulated in polymer containers (because of the size of gold particles, they have no reason to be separated from the polymer in SEC). In particular, gold rods are encapsulated into the tubes; their formation may thus be templated by the tubular shape of the self-assembled polymer.

Method 2: HAuCl_4 , pH 3

According to Hong [72] and Huang [76] particle formation can be induced from gold chloride (HAuCl_4) solutions by adjusting pH and temperature. Particularly, acidic conditions must prevent precipitation. We have thus prepared nanotubes by rehydration of polymer films into aqueous HAuCl_4 solutions at pH 3. Unfortunately, in our case, acidic conditions (pH 3 versus pH 6) only limited the reaction and did not completely avoid nucleation. The rehydration takes several hours, during which gold ion reduction occurred spontaneously. After SEC purification, as shown in Figure 56, we obtained clearly encapsulated gold, in spheres and in tubes; most particles have a hexagonal shape and have a similar size (around 40 nm of diameter). A better homogeneity in size and shape compared to the previous method is probably due to the acidic conditions that slow the reaction. However, even if the reaction was slow, we still cannot be sure that the gold is reduced inside the containers or if already reduced gold particles are simply entrapped during nanotube formation.

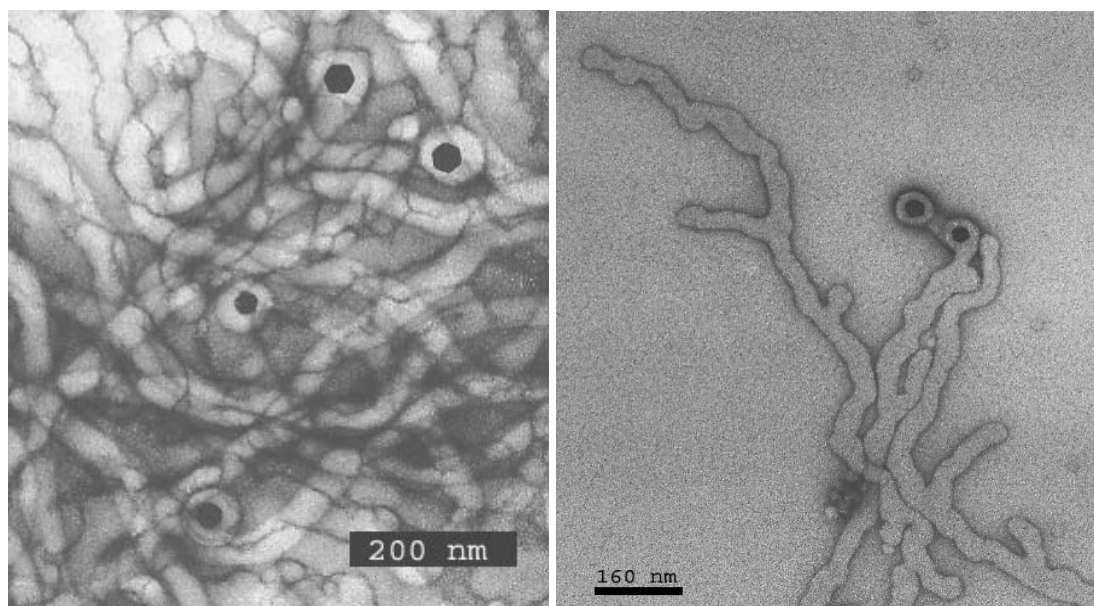


Figure 56: Gold particles encapsulated into nanotubes and vesicles after HAuCl_4 reduction (pH 3)

Method 3: HAuCl_4 in pure water

We still needed to find a way to control the initiation of the gold reduction in order to be sure that all gold particles observed are formed after complete rehydration of the polymer. We have observed that when the nanotubes are prepared in gold chloride (HAuCl_4) dissolved in pure water, rather than in buffer, the solution remains yellow (gold ions) over days. The presence of salt in the buffer seems to be the reason of premature gold precipitation. Because SEC necessitates the use of buffers leading to gold precipitation, the samples were only irradiated in UV without any previous purification. Other techniques of purification like ultracentrifugation and dialysis have been tried but lead also to gold precipitation.

In earlier experiments of UV irradiation of gold colloids stabilized by rod-like micelles [77] or polymers [78, 79], the concentration of both stabilizer and gold ions has been demonstrated to play a role in final gold particle shape. We have thus prepared nanotubes via film rehydration in aqueous gold chloride solutions varying between 0.5 mM and 40 mM of HAuCl_4 . A control sample, i.e. HAuCl_4 0.4 mM in water without polymer, was also prepared.

Samples were observed in TEM before UV irradiation. In rare cases they exhibit a few gold particles shown in Figure 57 that have similar shapes (hexagon, rod,

triangle) as the one present with method 1 and 2. They are also probably due to some nucleation occurred spontaneously, due to the presence of an impurity for example.

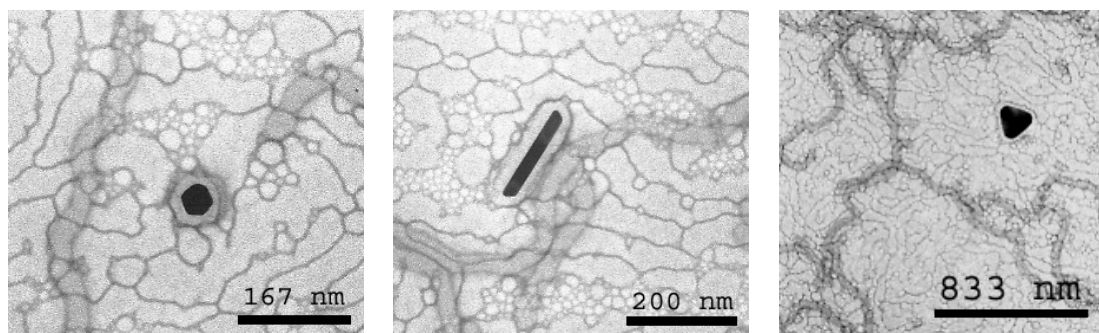


Figure 57: 0.5 mM gold chloride loaded nanocontainers before irradiation

Samples have then been irradiated with UV to initiate precipitation. TEM after 48 h of UV irradiation of 0.5 mM HAuCl_4 loaded nanocontainers (Figure 58) shows that a lot of spherical gold particles have been formed. This demonstrates that here the precipitation was well controlled: many nucleation sites have been formed and nucleation rate was homogeneous (small spheres).

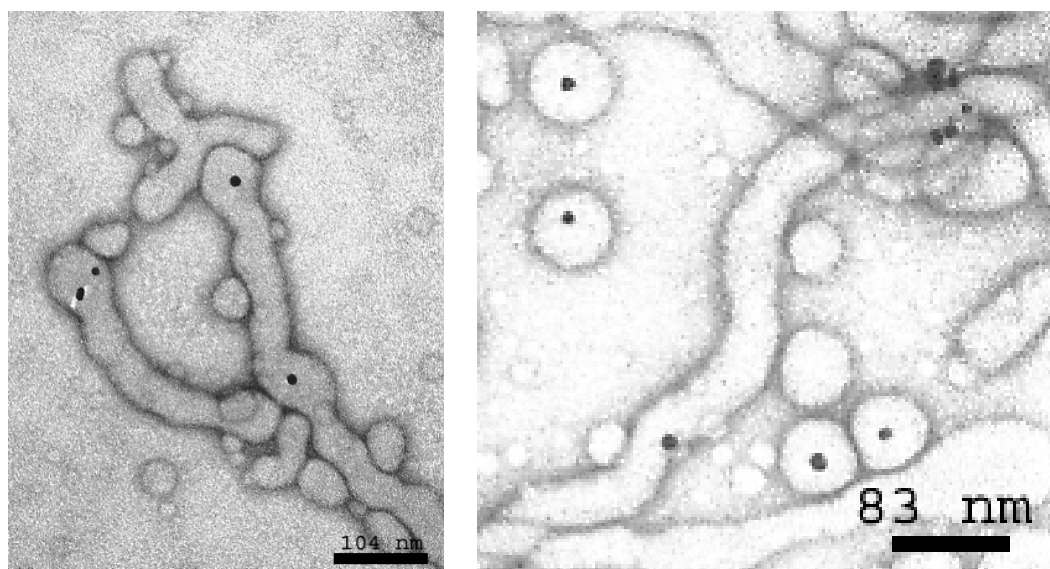


Figure 58: 0.5 mM gold chloride loaded nanocontainers after 48 h irradiation

We expect an interaction of the gold ions with the PMOXA block of the polymer, as already described between HAuCl_4 and vinylpyridine [80]. The presence of HAuCl_4 most probably results in local complexation of some amide groups of PMOXA units

with the AuCl_4^- ions. As a consequence, and despite the sample were not cleaned with SEC, all the gold particles are inside (or stuck to the outside shell) of a nanocontainer.

The reduction of the gold ions is followed by UV spectroscopy over time. After 26 h, it was not possible to record the optical density anymore because samples (polymer and/or gold particles) precipitated. High concentrated samples precipitated also fast.

Results for the control sample at 0.5 mM HAuCl_4 (without polymer) are shown in Figure 59.

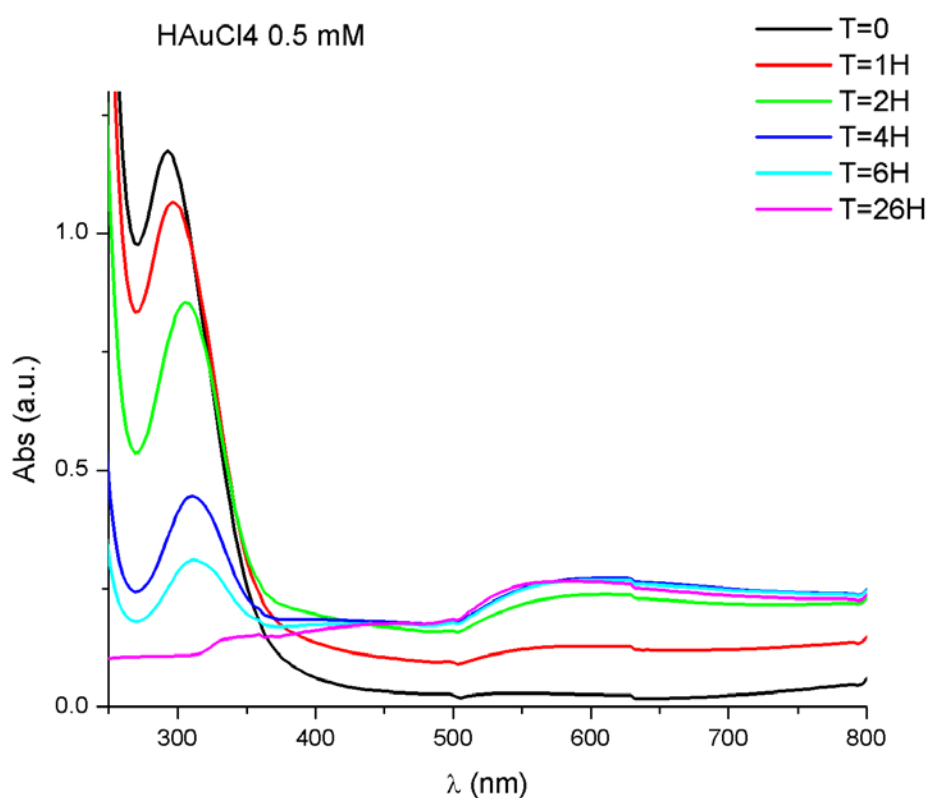


Figure 59: UV – vis spectra of gold chloride solution as a function of irradiation time

As expected, the absorption band at 320 nm, assigned to the gold ions AuCl_4^- , disappears and a plasmon band at around 520-550 nm, corresponding to the gold metal, appears with UV irradiation time. The intensity of the plasmon band increases and reaches a maximum after 4h. However, this maximum does not indicate that all the gold ions are reduced, because the 320 nm band continues to decrease. We can

suppose that the metallic gold particles precipitate when their size increase, and are thus not anymore in the beam.

Results for the samples of polymer film rehydrated in 0.5 mM HAuCl_4 solution are shown in Figure 60.

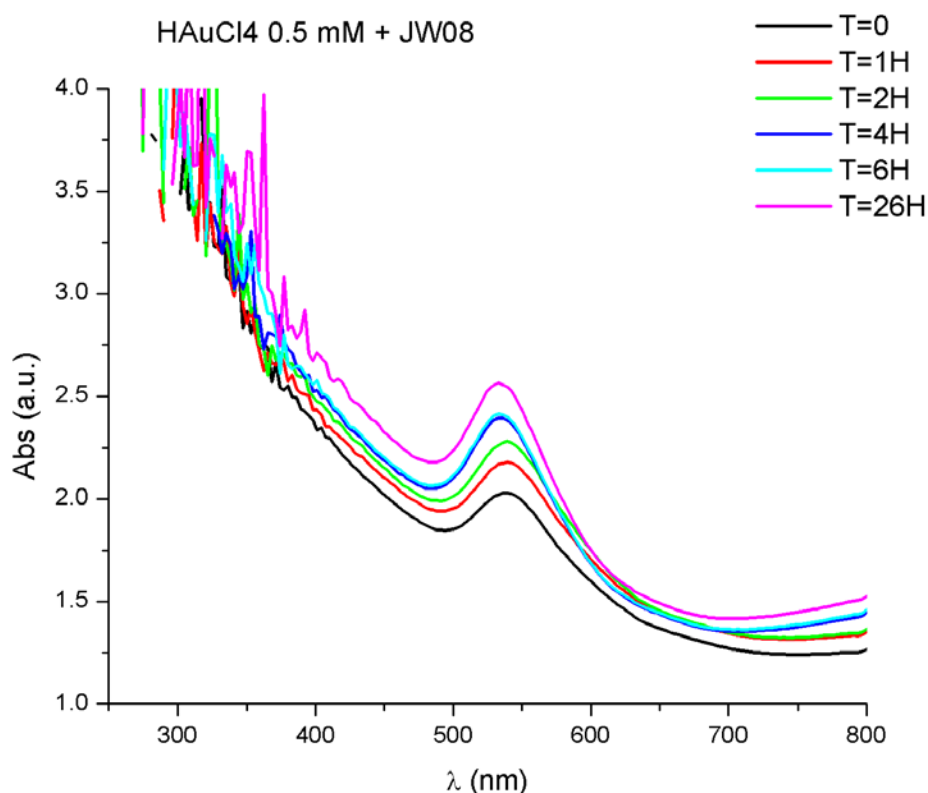


Figure 60: UV – vis spectra of gold chloride loaded nanocontainers in function of irradiation time

The polymer, like many organic molecules, absorbed a lot around 300 nm and thus masked the AuCl_4^- band. However, we could follow the formation of gold particles; the intensity of the plasmon band around 540 nm increased over time. Furthermore, this plasmon band shifted to shorter wavelengths with increasing UV irradiation time. This could be correlated to the aspect ratio of the spheroids, i.e. the particle size and shape, as done in [81] for spherical, and rod-like gold particles. Calculated absorption spectra [82] for spherical gold particles show that in a longitudinal resonance the band moves quickly to longer wavelength as the aspect ratios of the spheroids increase, while the band remains near the wavelength of the spherical particle absorption band in the transverse resonance. At the beginning of the experiment (before irradiation),

we observed a few rodlike particles (having large aspect ratios). During irradiation, spherical particles are formed: the proportion of rod-like one thus decreases versus irradiation time. We observed thus logically a shift to shorter wavelengths.

Figure 61 shows the maximum of the gold particle plasmon band (540 nm) intensity over the time for the 2 samples (with and without polymer); the absorbance before irradiation has been normalized to zero for a better comparison.

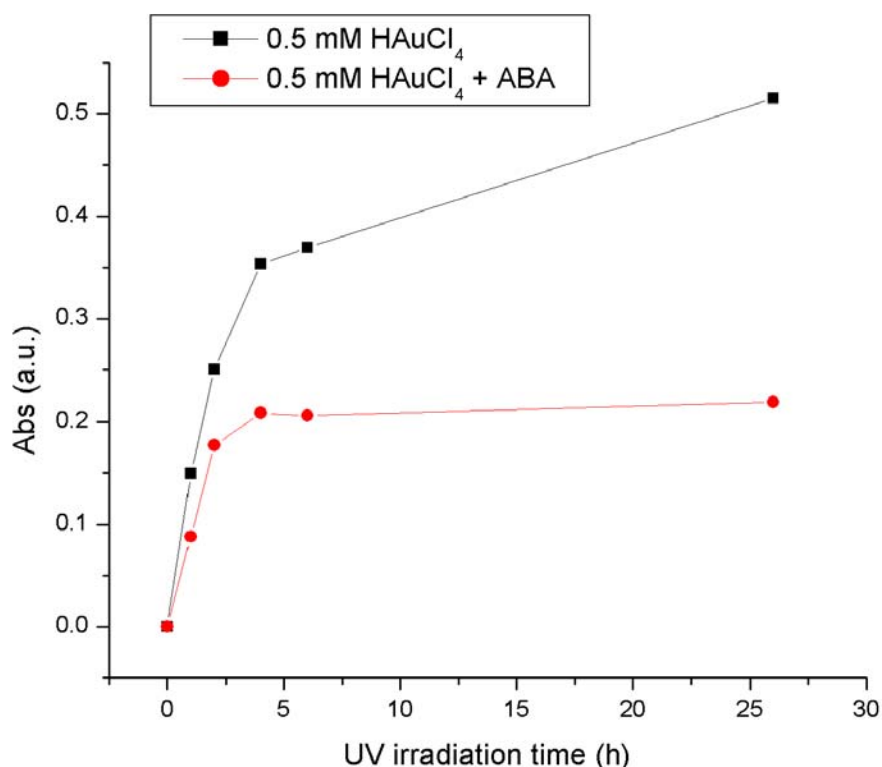


Figure 61: Absorption of gold particles at 540 nm over irradiation time, for 0.05 mM HAuCl₄ with and without polymer.

The UV intensity increases until a plateau is reached after around 4 h of irradiation for the aqueous gold solution without polymer. As explained before, this is due to precipitation of the gold particles. We do not reach this plateau in presence of polymer, even if the intensity increase is considerably slower after 4 h. This leads to the conclusion that most gold particles are stabilized by the polymer and do not precipitate: they stay in solution, thus in the beam. Encapsulation of the gold colloid in individual nanocontainers cannot be proven by the absence of precipitation, but the

absence of precipitation is a necessary condition. This confirmed previous observations in TEM (Figure 58).

We expected to observe many gold rods templated by the nanotube shape [77] by increasing gold ion concentration. Unfortunately, the complexation also around the nanocontainers leads to aggregation and precipitation of the samples at higher concentrations (5, 20, 40 mM H_{AuCl}₄) after few hours of irradiation. Because we cannot clean the samples without initiating the reduction of gold, increasing the gold concentration inside the vesicles/tubes is difficult. One perspective is to better control non-desired nucleation. For that we can envisage to use sterile water (to avoid any contaminant) and to perform experiments, including SEC purification, at 4°C. Indeed, temperature is known to play a role in the initiation of gold reduction [76] and we have not modified this parameter in our experiments.

5.6 Reminder of main results

Using new preparation methods for PMOXA-PDMS-PMOXA triblock copolymer self-assemblies, we have complemented the phase diagram of those polymers in dilute aqueous solution. We have demonstrated that (1) it is possible to form nanotubes besides nanovesicles using bulk dissolution of the copolymers; (2) the film rehydration method is a reproducible method to produce nanotubes in high proportion, and (3) it is possible to encapsulate hydrophilic substances and synthesize *in situ* inorganic particles into the interior of the nanotubes.

6 Conclusion and outlooks

The self-assembly of PMOXA-b-PDMS-b-PMOXA triblock copolymers in dilute aqueous solution has been studied for various polymer compositions and preparation methods. Both factors have an influence on the morphology of the superstructures, i.e. on the formation of micelles, vesicles, and/or nanotubes.

The established ethanol method is a short and easy way to produce nanovesicles. Furthermore, a new method using detergents and bio-beads has been shown to be a powerful alternative to co-solvent use for nanovesicles preparation and to render possible the functional reconstitution in polymer nanovesicles of fragile membrane proteins, such as Complex I.

Illustrating the influence of the polymer block lengths and the preparation method on the morphology of the ABA copolymer self-assembled structures, we have demonstrated that it is possible to form also nanotubes using bulk dissolution of the copolymers. Furthermore, the film rehydration is a reproducible preparation method for nanotubes in high proportion. The hollowness of the polymer nanotubes has been proved by encapsulation of hydrophilic substances and *in situ* synthesis of inorganic particles into the interior of the nanotubes.

Because of the poor mechanical stability of most membrane proteins, a lot of reconstitutions were not successful with the ethanol method in the past. As we have presented, the preparation of functional Complex I proteovesicles with the bio-beads method developed in this thesis was successful and possibly opens a way for the incorporation of a wide range of membrane proteins. This could allow the preparation of new smart drug delivery systems and nanoreactors. The ability of the ABA triblock copolymer to be chemically modified could also be used to attach specific groups to the nanovesicles for drug targeting.

Soft polymer nanotubes are also of great interest for various fields of applications [55]. Made from biocompatible organic polymers, they can find application in miniature

electronics for biotechnology and medicine. They have thus an advantage over carbon nanotubes, which are not biocompatible and cannot be degraded by living organisms. Another interesting application has been introduced with in situ templated synthesis of gold particles; this could be extended to various metallic particles but also to nanotube templated biomineralization.

7 Material and Methods

7.1 Polymers

The organic chemists of the group, following the route presented in Figure 62, have synthesized various batches of PMOXA-b-PDMS-b-PMOXA

Synthesis of Amphiphilic ABA-Triblock Copolymer Carrying Polymerizable Groups:

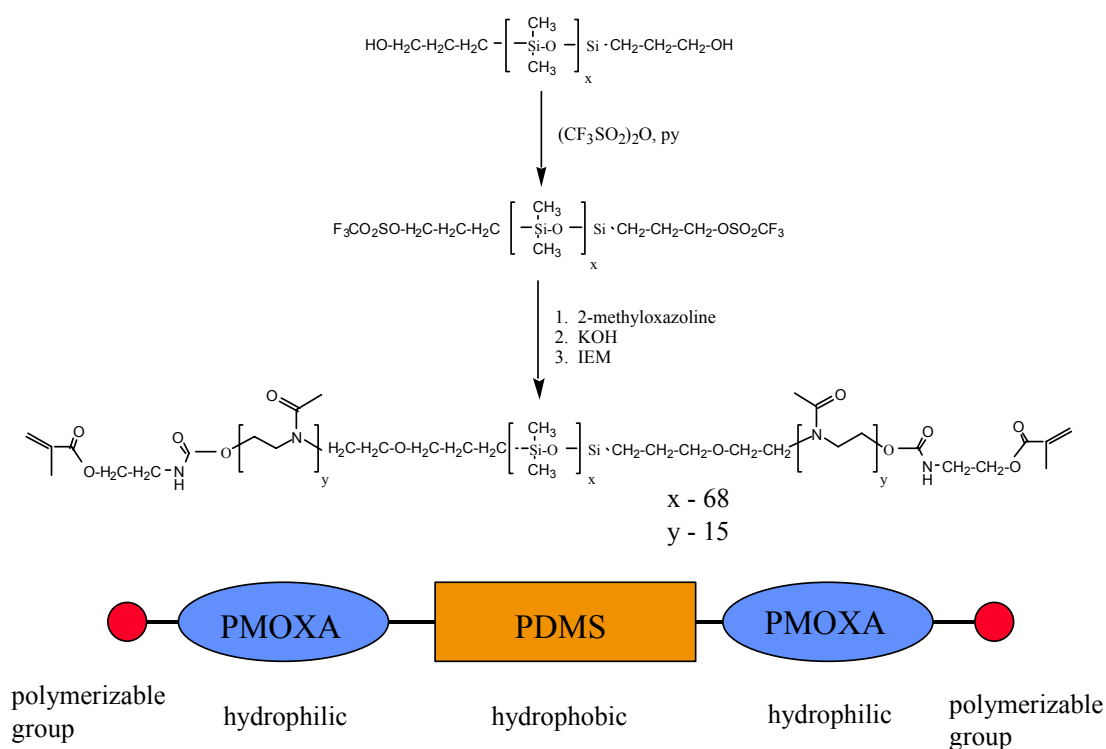


Figure 62: Synthesis of PMOXA-b-PDMS-b-PMOXA

The PMOXA block length is estimated from ^1H NMR spectra (Bruker 400 MHz) with respect to the known PDMS block length. The composition and corresponding names of the polymer used are summarized in Table 9.

Table 9: ABA-triblock copolymers used in the studies

Name	Mn	End group	Formula	Chemist
HP 708	9000	Methacrylate	A ₂₁ B ₆₉ A ₂₁	Ciba Vision
JW 08	7500	OH	A ₁₅ B ₆₂ A ₁₅	J. Widmer
JW 03	4150	Methacrylate	A ₂₆ B ₄₈ A ₂₆	J. Widmer
T 02	8500	OH	A ₁₆ B ₇₂ A ₁₆	T. Haefele
TD 01	8500	Methacrylate	A ₁₆ B ₇₂ A ₁₆	D. Streich
TD 02	8500	Methacrylate	A ₁₆ B ₇₂ A ₁₆	D. Streich
S 125	9300	OH	A ₂₁ B ₇₂ A ₂₁	S. Benito
S 104	6700	OH	A ₁₁ B ₆₂ A ₁₁	S. Benito
S 131	8660	OH	A ₁₈ B ₇₂ A ₁₈	S. Benito

^a A: PMOXA, B: PDMS

7.2 Complex I reconstitution experiments

E. coli Complex I was isolated from a strain overproducing Complex I [83] kindly provided by T. Friedrich. The protein was stored in 50 mM MES/NaOH, 50 mM NaCl, 0.15 % DDM solution at pH 6.

Complex I was reconstituted in ABA-polymer vesicles via the bio-beads method with the polymer S125. Triton X100 detergent at 0.5 % final concentration was used to solubilize the polymer in Tris/HCl buffer at pH 8; 1h stirring and two sonication cycles of 10 sec were performed to help the dissolution. 80 µl of protein stock solution (1 mg.mL⁻¹) was added to 5 ml the polymer/detergent mixture and stirred for 3-6 hours before detergent removal with bio-beads (see chapter 7.4).

Complex I was also reconstituted via the ethanol method (see chapter 7.3). 80 µl of protein stock solution (1 mg.mL⁻¹) was added dropwise at the same time than 250 µl of ethanol/polymer S125 solution to 4.75 ml of Tris/HCl buffer at pH 8.

The enzymatic activity test was performed on samples containing 0.3 mL of (proteo) vesicles solution, 0.185 mL of Tris/HCl buffer at pH 8, and 5 µl of 0.1 M ferricyanide solution. 10 µl of a freshly prepared 10 mM NADH solution was added to initiate the reduction of ferricyanide. Control measurement with “free” Complex I was performed

on samples containing 1.5 μl of a 10 $\text{mg}\cdot\text{ml}^{-1}$ protein stock solution and 0.485 mL of Tris/HCl buffer at pH 8 containing 0.1 % Triton X100 [84].

7.3 Ethanol method

The polymer is dissolved in ethanol by magnetic stirring. Under magnetic stirring this ethanolic solution is added dropwise to an aqueous buffer until a final concentration of 1% of polymer was reached. Multiple extrusions through filters with decreasing pore sizes (0.5, 0.2 and 0.1 μm) are performed to control the diameter of the vesicles.

7.4 Detergent removal with Bio-Beads

- Preparation of Bio-Beads SM-2 Adsorbent (20-50 mesh) from BIO-RAD

The bio-beads quantity needed for one reconstitution essay was weighted. The beads were washed 2 times with methanol, and 3 times with distilled water or the buffer used for the protein storage. The beads were finally immersed in 3 mL of the buffer. Humid beads were stored at 4°C in 0.02% of sodium azide, with carefully avoiding any bead dry.

- Removal procedure

The polymer (1%) was dissolved in a detergent-containing buffer (3% OG) until the solution becomes transparent (~1 h stirring).

For reconstitution: the protein is added (between 10 and 100 μl for 1 ml of polymer-detergent solution) and mixed 1 h.

The tip extremity of a micropipette was cut and 1/3 volume of the bead suspension was taken. The excess of liquid was removed by quickly blotting the tip on a wipe. The beads were never completely dry because they should be humid to be efficient. The beads were introduced in the sample and stirred at least 3 h. This was repeated 2 times until all the beads were introduced.

After sedimentation or centrifugation of the sample, the supernatant was recuperated and purified on a SEC column to eliminate the bead dust and eventual residual detergent.

7.5 Atomic force microscopy

The vesicles prepared with the ethanol method were deposited from aqueous solution onto freshly cleaved mica. Measurements were done in the dry state, after evaporation of the solvent. A Nanoscope III was used in the tapping mode, with a standard non-contact cantilever from μ -Mash, with a resonance frequency of 150 kHz.

7.6 Dialysis

7.6.1 Dialysis membranes

Dialysis was performed using membranes with a molecular weight cut-off (MWCO) of 8 kDa (Spectra/Por[®] Biotech), that have been previously soaked in a large volume of distilled water for 30 min at room temperature to remove the sodium azide preservative agent, and thoroughly rinsed in distilled water. 1 ml of sample was loaded in the bag and inserted in 1 L of buffer, which was changed several times during the dialysis.

7.6.2 Temperature-controlled, continuous open-flow dialysis apparatus

As shown in Figure 63, the dialysis chamber (stainless steel) consists of 2 buffer reservoirs, the first being used to equilibrate the temperature of the dialysate. A planar dialysis membrane separating the Teflon sample chamber (6 mm diameter, 100 μ l) from the second buffer reservoir allows the passage of soluble detergent molecules and salts. Sample chambers are sealed with a transparent plastic membrane fixed with an aluminum plate and thermally isolated by a glass plate. A pre-set sequence of linear temperature gradients is executed by a microprocessor that also controls the peristaltic pump responsible for continuous-flow dialysis.

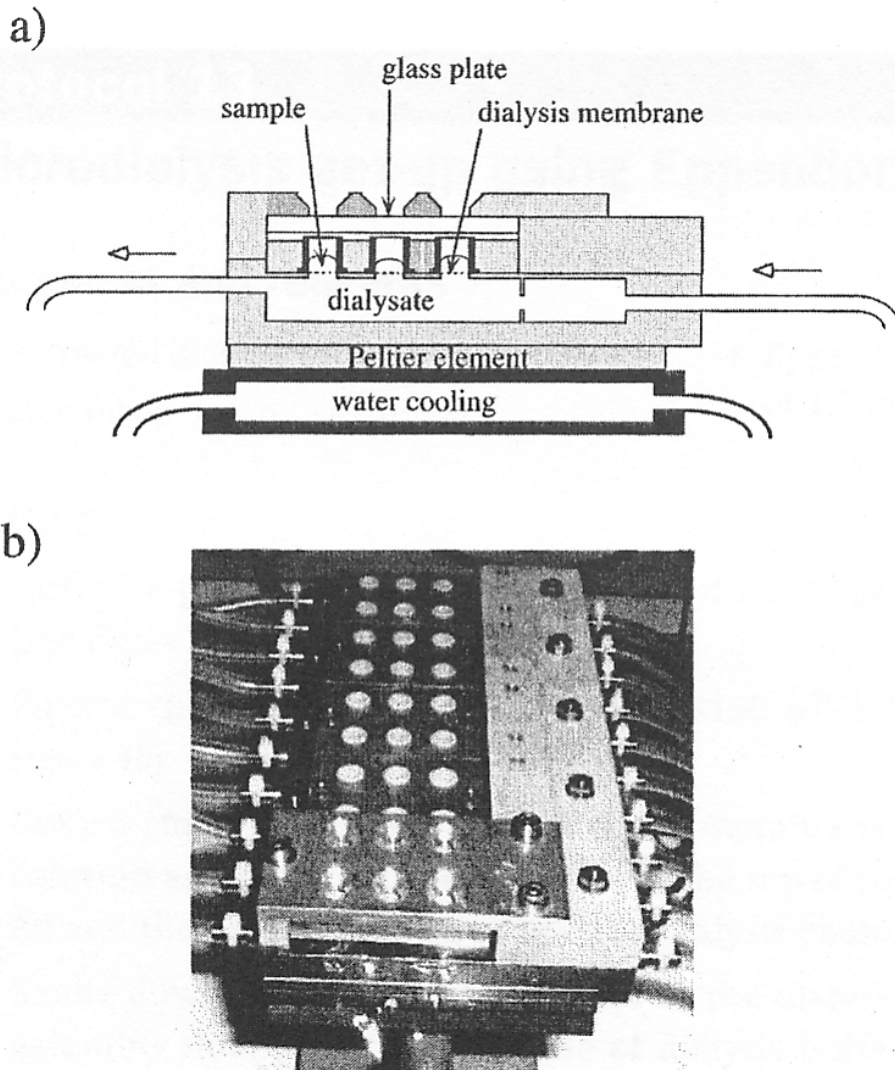


Figure 63: Temperature-controlled, continuous open-flow dialysis apparatus; a) Schematic, b) Photograph of the apparatus showing 30 sample chambers with 6 closed in front; [85] p 252

7.7 Dilution method

7.7.1 The dilution cell with optical detector

The cuvette is made of Teflon and has a volume of 450 μl (Figure 64 a). Two transparent plastic coverslips (CrystalClene, Molecular Dimensions, Florida, USA) are used to close this V-shaped cell, allowing a 670 nm laser beam to traverse the solution (Imatronic, Berkshire, UK). The chamber is temperature-regulated by a sensor and a Peltier element (Peltron, Fürth, Germany) working in a feedback loop controlled by a microcontroller linked to a computer. The dilution buffer flow is set

by the opening rate of a micro-valve (Lee, Westbrook, USA) combined with a home-built syringe pump controlled by a computer. Each opening/closing cycle of the solenoid can last from 40 ms to several seconds. The buffer volume injected during each opening of the solenoid ranges from 0.05 to 1.5 μl , depending on the syringe. The minimum volume for an experiment is 15 μl . This is required to enable the laser beam to illuminate the reaction volume without interference with the liquid surface. Also it permits a paddle to stir the mixture. The light sensor is a photodiode (Centronic, Croydon, UK) equipped with a small axial tube mounted at the centre of the diode to absorb the unscattered light. The collected scattered light is a direct measure of the structures assembled.

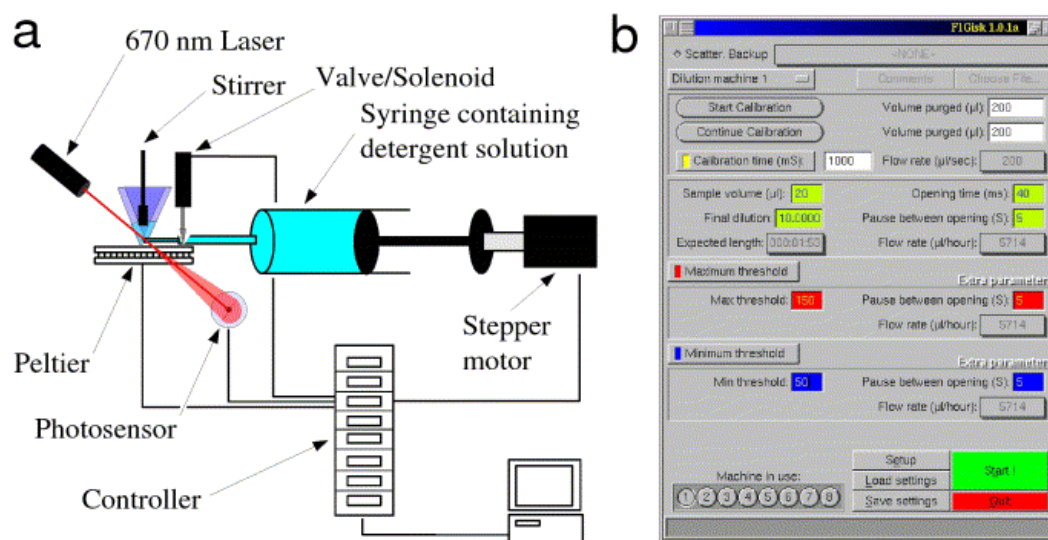


Figure 64: Dilution machine. a: The dilution buffer (with or without detergent) is supplied to the triangular cuvette by a microsyringe that is driven by a screw mounted on the stepper motor. The valve prevents diffusion between cuvette and reservoir. Proteoliposome assembly is monitored using a photodiode that collects the scattered laser light. A Peltier element controls the temperature of the cuvette. **b:** A graphical user interface allows all pertinent parameters of the eight channels to be individually set and monitored during a dilution run. Final results are automatically stored in a protocol and printed.

7.7.2 Control unit

The eight channels of the dilution machine are controlled by a Motorola 68000 microcontroller. The state of the sensors is recorded every 20 μs , and integrated by the embedded software of the microcontroller. From time to time, the computer retrieves these data and also sends the commands and parameters to the microcontroller that

ensures the temperature changes or dilutions to be made at the required rates and final volume. A Linux-based ix86 PC is used to hold the Graphical User Interface (GUI, Figure 64 B), and to print the final dilution/scattering curves. All the software modules needed to run the dilution machine were assembled into a package called GISK, available at www.sourceforge.net. GISK is under the GNU general public license and is entirely written in C. This interface allows all parameters needed to manage a dilution experiment to be set and the system to be calibrated. A flow calibration procedure is required for each channel. After calibration, the initial sample volume, the final dilution, the pause between valve openings and the temperature are set for each channel. Two optional fields can be activated. They change the rate of dilution or the temperature according to a defined scattering threshold or a preset dilution value. These parameters are entered for each of the eight channels. At the bottom of the GUI, eight buttons activate or inactivate each channel. The period over which the computer has to integrate the signal, i.e. the degree of smoothing, can be set (typically 30 s). Extra features permit the settings of the communication port (in case more than eight channels are used), the rate of the data flow, the printers, the debugging level and the automatic resetting of the microcontroller to be defined. The software is multithreaded so that each channel is controlled separately in order to have not only experimental flexibility but also the most accurate dilution rate and reproducibility. The data, additional comments and the settings are saved in a default (based on the current date) or a defined file. This file can be automatically printed, showing the final dilution curves. During the experiment a table shows the current light scattering values and the remaining time.

7.8 Determination of the free detergent concentration using the sitting-drop method

A piece of parafilm was placed on the socket. 20 μ l water droplet was deposited and the focus of the camera is adjusted (software). 20 μ l sample droplet was placed on the socket on a new piece of parafilm (on the illuminated spot). A photograph was taken with a video recorder (this should be done quickly to avoid evaporation from the drop). After 30 second we got 3 pairs of focus point values and the mean value. Solutions for a standard curve were made with buffer or water as diluents in the range

of 0.1 to 3 times the CMC and allow equilibrating overnight at the temperature at which the measurements will be made.

7.9 Transmission Electronic Microscopy

7.9.1 Preparation of carbon-parlodion* composite polymer films on copper grids

A relatively large drop of 2% parlodion* in n-butylacetate solution was spread on a large (20 cm diameter) distilled water surface, prepared in a round Petri dish. About 50 copper grids (200-400 mesh/in from Electron Microscopy Science) were placed on the surface of the flat floating parlodion* surface with the darker copper grid surface facing the parlodion. The grids were covered with a hydrophilic paper (usually recycled) and the entire paper surface is allowed to soak. The piece of paper was removed with attached grids and parlodion* and let dry on the bench at least 1 h. A uniform sheet of carbon (50 nm thick) was evaporated on these grids using a vacuum evaporator at $7 \cdot 10^{-5}$ mbar and a graphite contact point heated by 30 V and 35 A for 6 sec.

* Parlodion is Pyroxylin purified strips from Electron Microscopy Science, $C_{12}H_{16}N_4O_{18}$, which is highly purified from cellulose nitrate and specially prepared foreembedding tissue for sectioning and for preparing semi-permeable membranes.

7.9.2 Negative staining

Carbon/parlodion-coated grids were deposited on a glass block covered with Parafilm into a glow-discharge unit and current was applied for 10 sec under vacuum. Grids should be used within the next 30 min.

The specimen grid was hold horizontally with precision forceps and 5 μ l of the specimen solution was deposited on the carbon-coated side of the grid. After 30-60 sec adsorption, the excess of liquid was blotted by touching the grid surface with a filter paper. The grid was then washed on a drop of distilled water for 2 sec and blotted again (3 times).

The specimen was stained by lowering the specimen grid on to a drop of negative stain solution (1-2 % uranyl acetate) for 20 sec (2 times).

Grids were stored in plastic boxes until inspection in a Hitachi H7000 electron microscope operating at 100 kV. Micrographs were recorded on Kodak SO-163 films.

7.9.3 Cryoelectron microscopy (Cryo-EM)

A 4 μ l aliquot of sample was adsorbed for 30 sec onto holey-carbon film 400 mesh grids, blotted with Whatman 4 filter paper and frozen into liquid ethane at -178 °C. Frozen grids were transferred onto a Philips CM200-FEG electron microscope using a Gatan 626 cryo-holder. Electron micrographs were recorded at an accelerating voltage of 200 kV and a magnification of 50000 x, using a low-dose system. Defocus was -2 μ m. Micrographs were recorded on Kodak SO-163 films.

7.9.4 Freeze Fracture preparations for electron microscopy.

A droplet of copolymer suspension was placed between a thin copper holder and a thin copper plate before quenching in liquid propane, as described by Aggerbeck and Gulik-Krzywicki [86]. The frozen sample was fractured at -125°C in a vacuum of about 10^{-7} torr by removing the upper plate with a knife that had been cooled in liquid nitrogen in a Balzers 301 freeze-etching unit. The fractured sample was replicated with a 1 nm-thick platinum-carbon deposit. The replica was washed with distilled water, adsorbed on the EM grid and observed with a Hitachi 7000 electron microscope operating at 100 kV. Micrographs were recorded on Kodak SO-163 films.

7.10 Dynamic Light Scattering

Samples are examined into 10 mm diameter quartz cells mounted in a thermostatic optical matching vat ($T = 293 \pm 0.02$ K). Dynamic Light Scattering was performed using a ALV-Langen goniometer equipped with a frequency-doubled Nd:YAG laser (ADLAS, $\lambda=532$ nm). Measurements were performed at scattering angles from 30° to 150° for each sample and 6 successive dilutions. Cumulant analysis was performed from the photon intensity autocorrelation function $g^2(t)$, using an ALV-5000/E correlator.

7.11 Fluorescence measurements

7.11.1 Fluorescence microscopy

10 μl of sample were deposited on a rectangular glass slide, covered with a square cover slip, and sealed with clear nail polish. Samples were examined with a Leica DMIRE2 fluorescence microscope; Phase contrast; 40, 63, and 100 x; Filtercube L5 (Excite BP 460-500, Dichroic 505, Emitter BP 512-542).

7.11.2 Fluorimetry

Fluorescence measurements were performed using a spectrofluorimeter JASCO F-P-773. Slits for emission and excitation were adjusted at 2, 5, 10, or 20 nm. Temperature can be controlled by a thermostatic bath (from 15° to 60°C); the majority of measurements was done at room temperature.

8 Appendix I: Other ABA-triblock copolymer superstructures

8.1 GIANT VESICLES

Electroformation is the most suitable technique to achieve homogenous unilamellar giant polymersomes with diameters above one micrometer [45, 46, 48]. This size is suitable for some applications, which require optical microscopy, such as patch-clamp (electrophysiological recording) or optical tweezers manipulation.

This method is akin to the film rehydration method, however, instead of using any solid surface, the amphiphile film is spread on a pair of metallic electrodes. After addition of a buffer, an electric current (either AC or DC) is applied to facilitate hydration. The electric field affects the vesicle formation by decreasing membrane tension (and therefore leading to the increased number of defects in the layers), by inducing periodic motions (mechanical stress) through electroosmotic effects (only AC) and by increasing interlayer repulsion through electroviscous/electrostatic effects (mainly in the case of charged amphiphiles) [87].

Diameters in the micrometer range and excellent monodispersity achieved by this method compete with low yields with respect to self-assembled particles as well as total volume attainable.

We have prepared giants as followed. The polymer was first dissolved into chloroform (10 mg/mL). 100 μ l of this solution was sprayed onto the surface of 2 electrodes; the thin film formed was dried by blowing over a stream of nitrogen and by following one night desiccation under vacuum. The 2 adjacent electrodes are then immersed into 1 mL aqueous buffer in a sealed chamber. Giant vesicles were formed applying an alternating current of 10V at a frequency of 10 Hz for 2 h followed by 1 h at 5V and 1 Hz. Samples were investigated in Phase contrast microscopy. Figure 65 shows vesicles with diameters around 1 μ m.

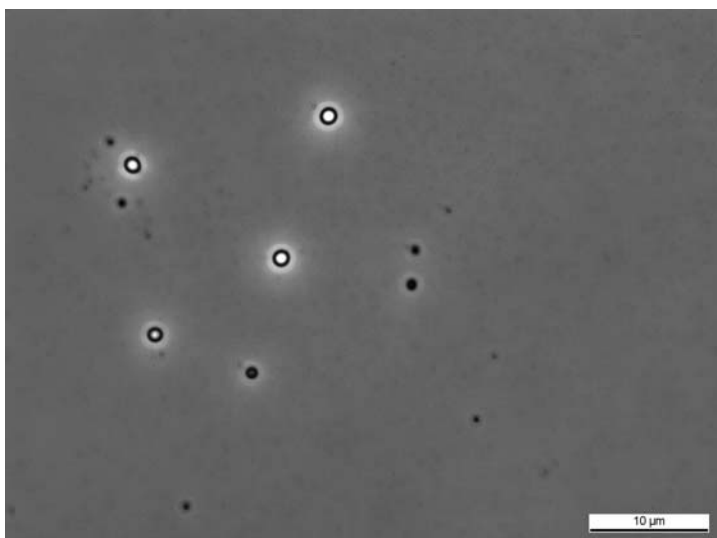


Figure 65: Phase contrast microscopy of ABA-triblock copolymer giant vesicles

Even if the set-up only allows the preparation of a small sample volume, this technique is an efficient production method of giant vesicles, also with the new polymer batches.

To obtain giant vesicles in higher yields, a slightly modified set-up based on a 2-electrode cell (originally designed for EPR studies) can be used [23].

8.2 MONOLAYERS

In order to determine protein insertion in ABA-triblock copolymer membrane, Langmuir monolayer experiments [21] were performed. Because of the amphiphilic behavior of ABA-triblock copolymer, it is possible to form a Langmuir film at the air-water interface. Insertion of the protein in this film will induce a surface pressure increase. However this experiment does not test functionality of the inserted protein.

Surface pressure measurements

We used a NIMA film balance (series 601 BAM) with a surface area set at 360 cm² for open barriers. The Teflon trough (300 ml of volume) was filled with freshly purified water (bi-distilled water filtered through 0.45 μm Millipore filters) and the water surface was repeatedly cleaned by aspiration before the isotherms were measured during continuous compression of the polymer film. In a typical

measurement, 20 μl of a polymer stock solution (10 mg dissolved in 10 ml of chloroform) was spread dropwise on the water surface with a syringe. 20 minutes were allowed for solvent evaporation before compression. The surface pressure Π was measured with a Wilhelmy plate at room temperature and with a barrier speed of 100 cm^2/min .

Because of the limited trough area, which is usually optimized for small surfactant spreading, and large molecular area of the polymer molecules, it was not possible to record the whole compression isotherm during one run. Therefore a few steps with different initial surface concentrations were done. Figure 66 shows the complete isotherm consisting on an overlap of the individual isotherms obtained with different spreading volumes.

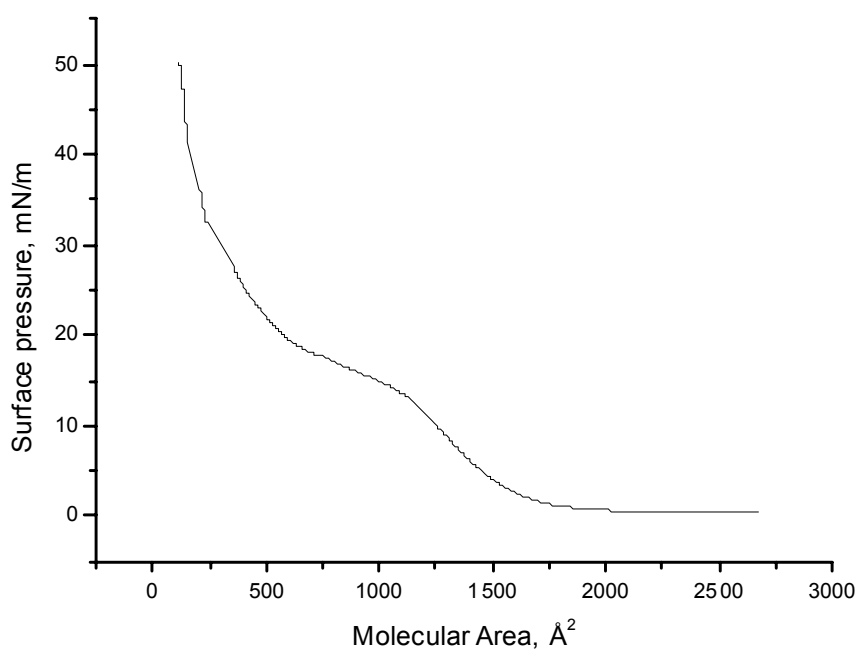
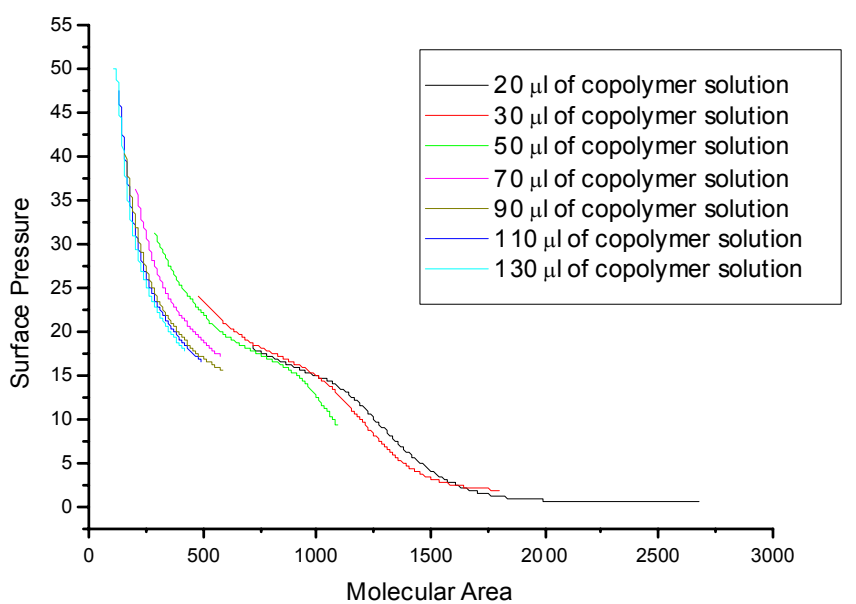


Figure 66: Construction of a pressure isotherm of an ABA triblock copolymer (HP 708)

The behavior reassembles the one of common low molecular weight amphiphiles, although the starting molecular area is much higher in the case of polymer amphiphiles. During compression the Langmuir isotherm of the ABA-copolymer HP708 shows a liquid-expanded state up to 15 mN/m and a solid phase (condensed state) at around 50 mN.m⁻¹. No collapse was observed because the polymer used

shows a high degree of flexibility and some water solubility (partial solubilization occurs).

Moreover, a very distinct phase transition is visible at 15 mN/m. In low molecular amphiphiles this type of plateau region of the surface pressure-area isotherm in most cases represents a two-phase coexistence region between a fluid-like low-density phase and a condensed phase [88]. The steep pressure increase after the transition region indicates the ability of the polymer to form very tightly packed films. As a result of compression of monolayer film, amphiphilic triblock copolymers at the air-water interface are expected to undergo conformational changes, as illustrated in Figure 67. We expect for symmetrical molecules with hydrophobic middle block a loose or coiled conformation at low surface pressures. In the gas-like phase (a) the molecules are lying flat adsorbed on the surface (pancake conformation), whereas in liquid expanded region (b) mushroom or hemispherical conformation occurs. Upon compression the molecules adopt more packed structures in the condensed states. [89, 90] In the liquid condensed phase (c), the polymer adopts a “U” shape with the middle block immersed in the subphase in a brush-like conformation. In the solid form (d) the stretching of polymer is maximal.

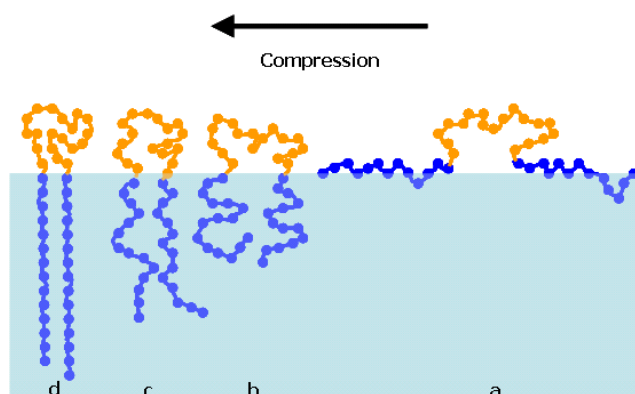


Figure 67: Effects of the compression on the possible conformation of ABA block-copolymer monolayers; a) low compression or gas region, b) liquid expanded phase, c) liquid condensed phase, d) solid condensed phase. [91]

Similar experiments have been reproduced with several new ABA batches (JW03, S125, TD02). They have the same behavior as HP708 with solid phase occurring around $50 \text{ mN}\cdot\text{m}^{-1}$, as shown in Figure 68. We can notice that the intermediate transitions occur at the same pressures but with different corresponding molecular

areas; those small differences are however included in the experimental error, for e.g. the volume of spread polymer solution is not perfectly reproducible.

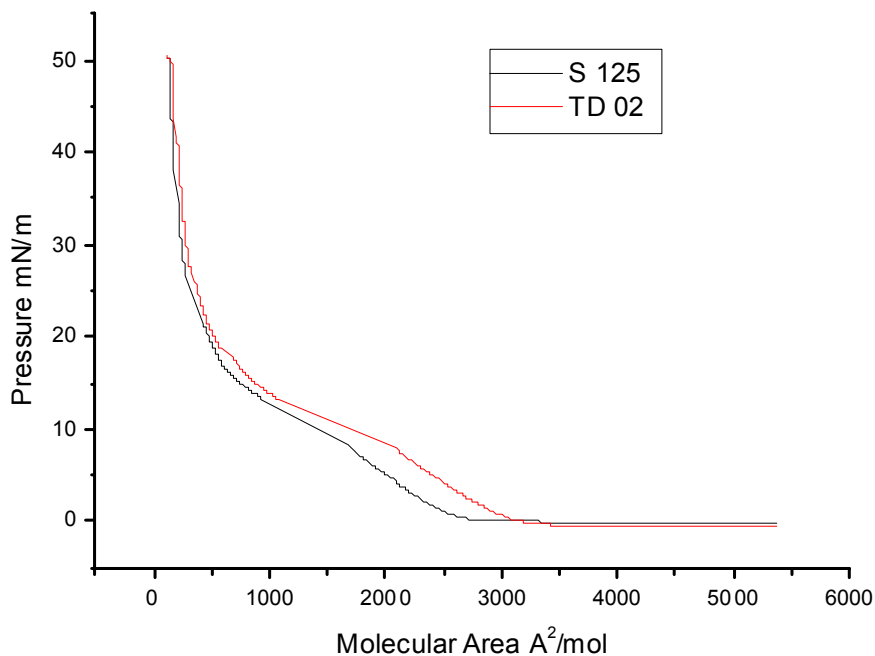


Figure 68: Pressure isotherms for 2 ABA copolymers

Figure 69 shows the comparison between compression and successive decompression. Depending on the initial surface concentration, the compression-expansion curves have different patterns. At low surface concentration, hysteresis is observed, whereas at higher surface concentration the isotherms indicate aggregation of the material at high pressure and difficulties with re-spreading of aggregates upon expansion. We can also suppose an exchange of molecules between the interface and ABA aggregates present in the subphase.

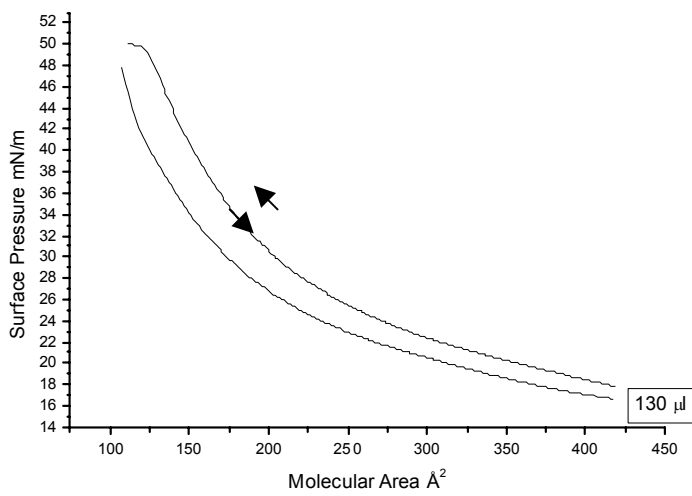
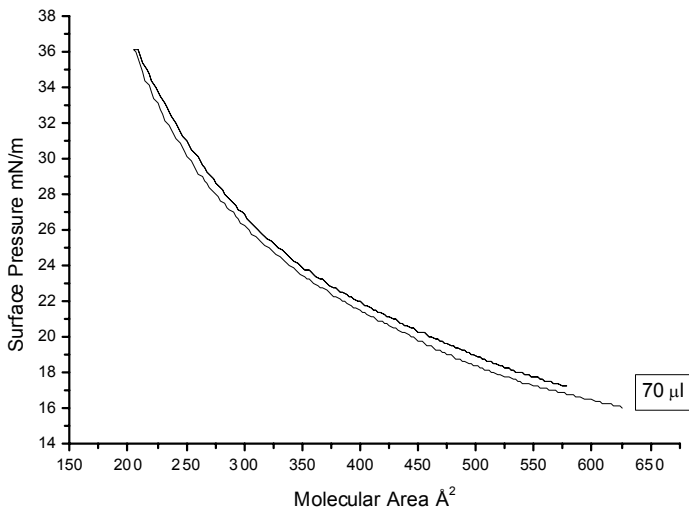
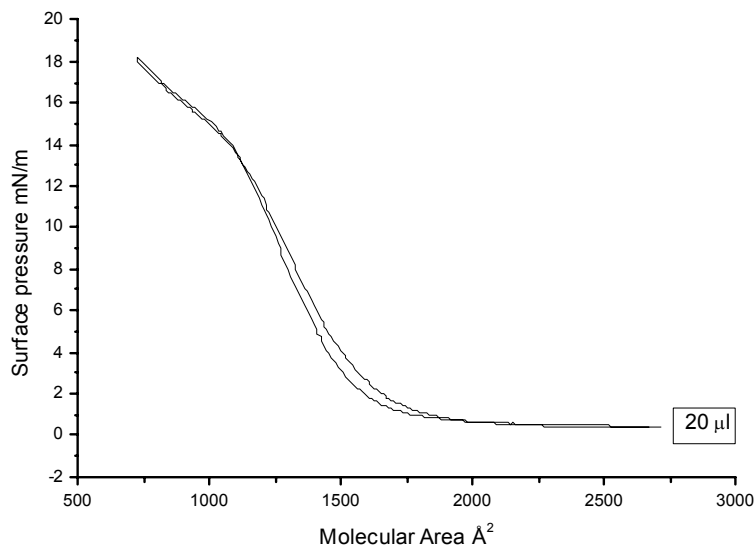


Figure 69: Compression-Decompression isotherms at different initial concentrations

Protein insertion

The protein interaction with a copolymer film was studied at an initial surface pressure of $9 \text{ mN}\cdot\text{m}^{-1}$; the copolymer film is thus in the liquid phase of the isotherm and will enable protein incorporation. OmpF protein was injected with a microsyringe directly to the buffer solution subphase (10mM Hepes, 100mM NaCl, pH 7.40). After stabilization of the pressure, compression of the polymer-protein film was performed.

Figure 70 shows the pressure isotherms during protein incorporation. The addition of OmpF to the subphase induced a shift toward higher surface pressure and larger effective molecular area in the compression isotherms, increasing with the protein concentration (injected volume).

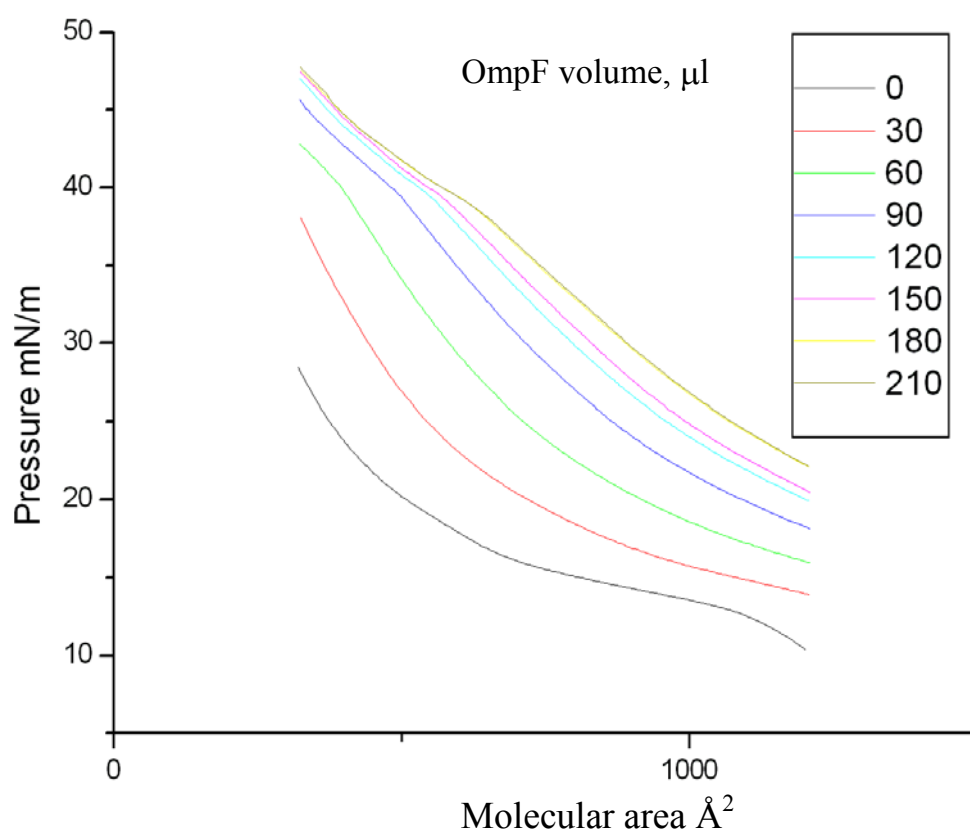


Figure 70: Pressure isotherm of OmpF / ABA copolymer (S125) hybrid Langmuir film for different OmpF protein volumes (μl) injected in the subphase at an initial pressure of $9 \text{ mN}\cdot\text{m}^{-1}$

This indicates successful protein interaction with the polymer molecules. When the maximal protein incorporation is reached, no more changes in pressure increase are observed, as observed in Figure 71.

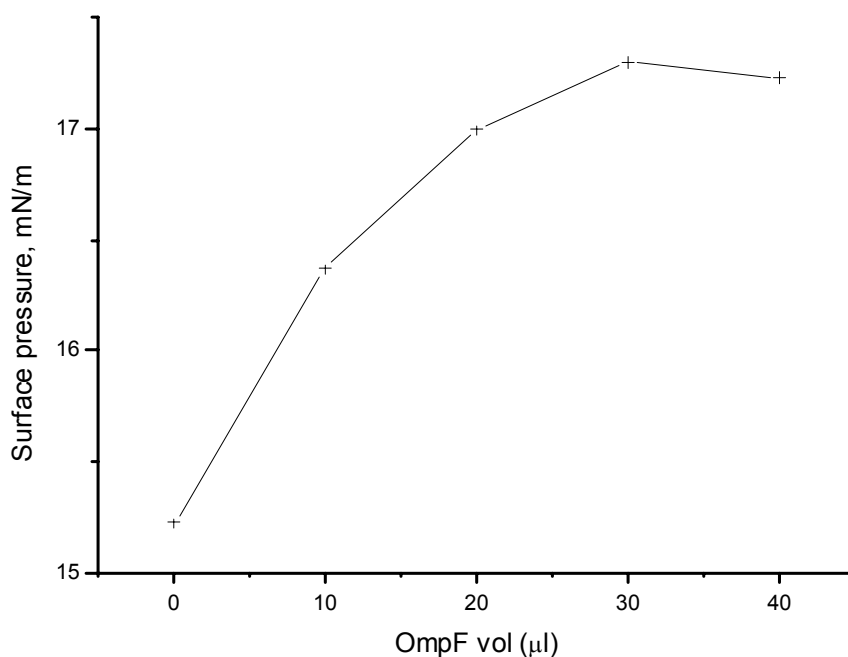


Figure 71: Change of surface pressure versus OmpF protein insertion for HP 708 polymer monolayer (initial molecular area set at 600 \AA^2)

TEM imaging

A Teflon setup, schematized in Figure 72, was used to transfer Langmuir films onto TEM grids. It contains 8 wells of 60 ml, with a 4 mm diameter, i.e. the same size as the electron microscopy carbon-coated grids, which are deposited on the drop for the transfer of the structures formed at the interface. On the side of each well, an injection hole allows addition of micellar protein solutions or Bio-Beads under the lipid layer.

[92]

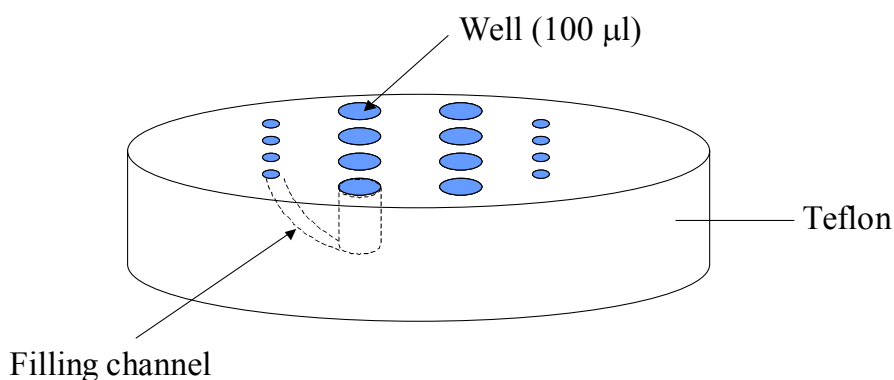


Figure 72: Teflon plate for LB film formation

The wells were filled with distilled water and a drop of the polymer solution in chloroform was deposited on the surface. The organic solvent was allowed to evaporate overnight (in a humid atmosphere to avoid loss of water). The film was transferred to a TEM grid by lowering the specimen grid on to the top of the drop for 30-60 sec.

Various polymer concentrations were used to form spread films. TEM images are shown in Figure 73. Unfortunately we were unable to visualize the film; it means that the film is collapsed or homogeneous. However we observed structures formed by the ABA copolymer in the subphase: vesicles and single or interconnected nanotubes (they are attracted on the grid because of the glow discharge that renders the grid surface hydrophilic). This confirms that a film of ABA favors the subsequent formation of nanotubes, as we have seen in film hydration method [5.2]. The length and the proportion of nanotubes seem to increase with the polymer-spread volume, i.e. with the surface pressure.

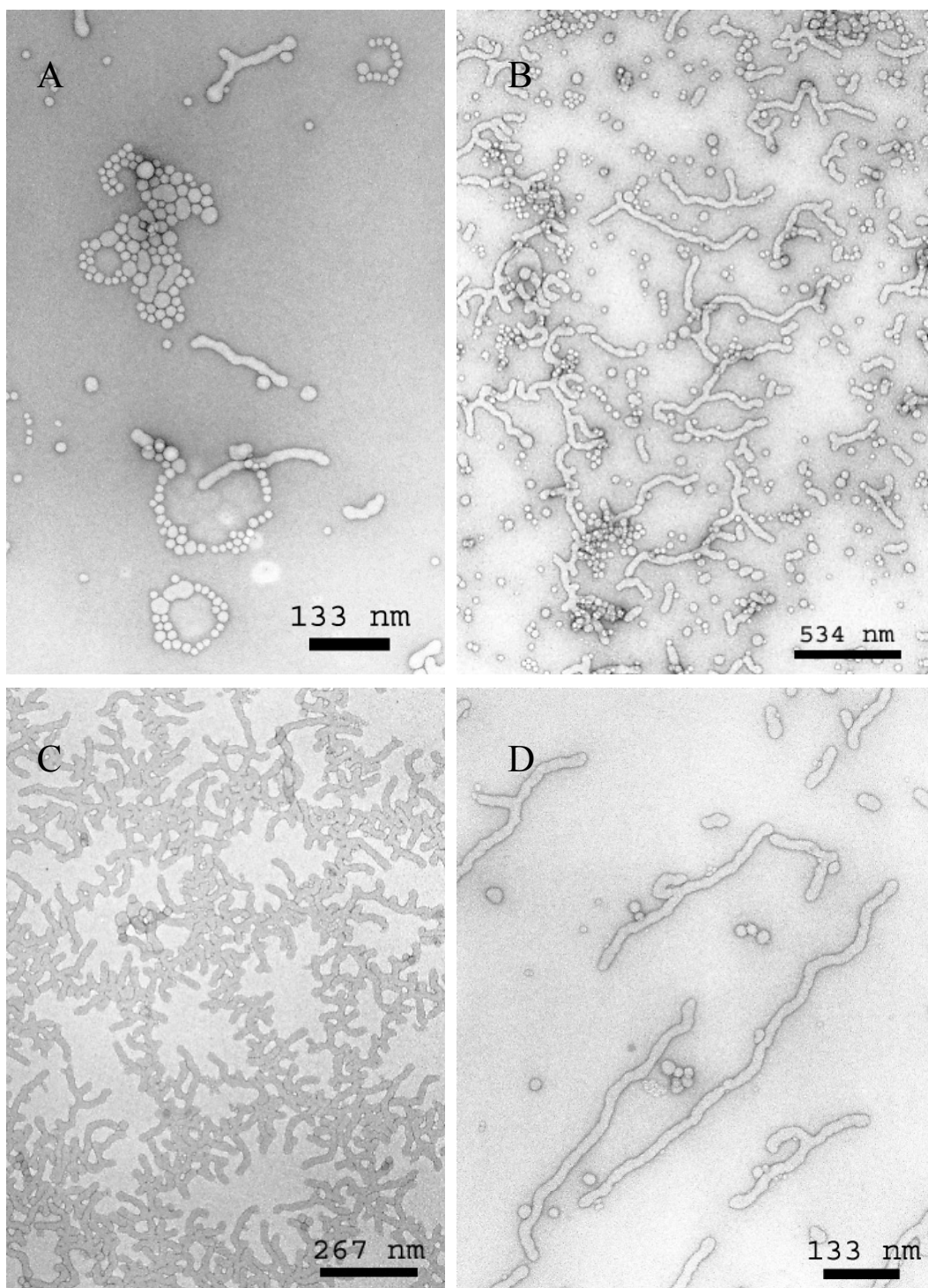


Figure 73: TEM pictures obtained after lowering a grid on ABA spread film after deposition of a 0.5 μl (A), 0.75 μl (B) and 1 μl (C, D) of TD02 (1 mg/ml).

We can approximate the surface pressure by comparing the ratio between polymer solution spread volume and area in both cases: Teflon setup for TEM imaging (well area = 200 mm²) and previous NIMA balance experiments (open barrier area = 360 cm²). Starting from the polymer solution volume spread in TEM imaging

experiments, we can calculate the corresponding volume that must be spread in NIMA balance to have the same ratio. Corresponding surface pressure and polymer film state can thus be estimated from the compression isotherm shown in Figure 66. Results are summarized in Table 10. The polymer concentrations in chloroform were the same (1 mg/ml) in both experiments.

Table 10: Spread volumes in NIMA balance calculated to have the same polymer solution spread volume / area ratio than in TEM imaging experiments and corresponding surface pressure and state of the polymer film

TEM imaging spread volume μl	NIMA balance spread volume μl	Surface pressure mN/m	State of the polymer film
0.5	90	10	gas region
0.75	135	17	liquid expanded phase
1	180	> 20	liquid condensed phase

If we compare those calculated values to the polymer solution volumes spread to build the complete pressure isotherm of the polymer (Figure 66), we see clearly that we have imaged in the Figure 73 the 3 polymer film states before solid condensed region, i.e. gas region (picture A), liquid expanded region (picture B) and liquid condensed region (pictures C and D). The superstructures observed in the subphase, formed by self-assembly of the molecules ejected from the Langmuir film, could thus be related directly to the compression of the film and the conformation of the polymer (Figure 67). A more packed structure in the film favors nanotube formation in the subphase; this confirms the hypothesis of microdomains arrangement at the surface favoring nanotube versus vesicle formation (see film method p62).

The next step will be to use an ABA-triblock copolymer functionalized with Ni-NTA end-groups recently synthesized in the group. This end-group will allow specific binding of His-tag proteins, and furthermore specific attachment of a lipid layer containing 2D crystallized His-tag proteins. This would be interesting to stabilize the crystals for observation in TEM and afterwards in AFM. We can also imagine the possibility to stretch the layer in order to study pressure dependant channels, such as the Large mechanosensitive channel (MscL) presented in the next chapter, and image their structure in the open state.

9 APPENDIX II: Free-standing films – Bilayers

9.1 Introduction

Biological membranes are mainly composed of lipids, which form a fluid matrix for membrane proteins. Those proteins have various functions such as specific transport. For biotechnological or pharmaceutical applications it would be interesting to immobilize proteins in an artificial membrane and ensure that they keep their functionality. Various membrane proteins have already been reconstituted in polymer vesicles [19, 21, 23].

In this work we focused on the large conductance mechanosensitive channel (MscL), which plays an essential role in osmoregulation in bacteria [93]. MscL is well known to open and close in response to mechanical stress in the lipid bilayer. To test the functionality of MscL in a polymer membrane we wanted to use Back Lipid Membrane (BLM) technique, which has successfully been used to fabricate large freestanding films from amphiphilic copolymers [18] and to reconstitute OmpF protein [94]. The first step of this project was to characterize Tb-MscL in a conventional lipid bilayer by the BLM technique.

9.2 Experimental

- Tb-MscL purification

The *Mycobacterium tuberculosis* mechanosensitive channel of large conductance (MscL) was purified from a stab culture of the plasmid (Tb-MscL in pET19b) in the strain (MscL knockout with DE3 lysogen) as given by Chang et al.[95] After growth and extraction (french press) MscL is eluted on a Ni-NTA column. We obtain typically 1 mg/ml of MscL with a sufficient purity (Figure 74 shows the SDS-page gel after each purification step).

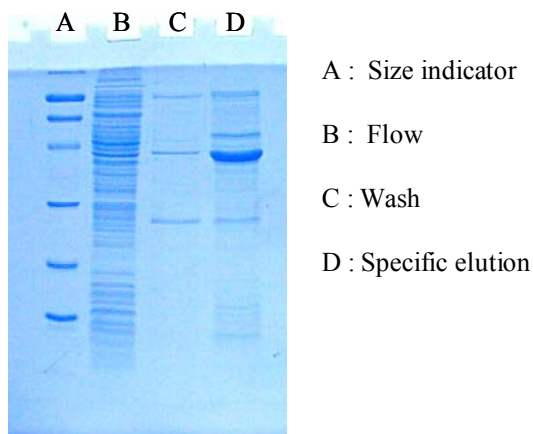


Figure 74: SDS-Page BioRad minigel

- BLM recording

Solvent-free membranes were prepared as described by Montal and Müller.[96] The experimental set-up used to record the conductance across the membrane is described in Figure 75. (Bilayer Membrane Amplifier BLM-120 BioLogic, Digital Tape Recorder DTP-1204 BioLogic, 100 Ms/sec oscilloscope (DSO) 450 Gould, Ag/AgCl electrodes World precision instruments).

Hexadecane in hexane (2%) was used for aperture prepainting. The 2 compartments were filled with a salt solution (1M KCl, 10 mM Tris pH 7.5, 1mM CaCl₂). The membrane forming solutions were Diphytanoylphosphatidylcholine (DPHPC) at 3.8 mg/ml in hexane/chloroform (60/40) or E. Coli extract lipids (Avanti Polar Lipids) at 2 mg/ml in hexane/chloroform (90/10). 10 µl of lipid solution is deposited on the surface of each bath. The 2 compartments were filled with a salt solution (1M KCl, 10 mM Tris pH=7.5, 1mM CaCl₂). In order to create an osmotic gradient we have used Polyethylenglycol 2000 (Aldrich) at 5% and 20% (w/w) in 1M KCl. For protein reconstitution we added 1 µl of protein solution in each bath and applied tension from 50 to 100 mV to destabilize the membrane and facilitate insertion.

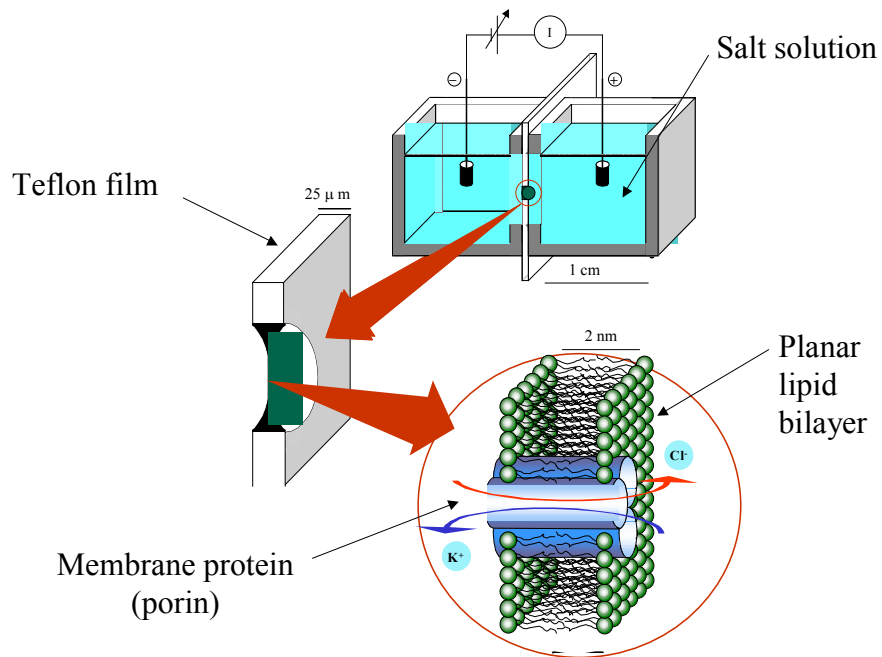


Figure 75: BLM set-up

9.3 Results

First experiments were performed with DPHPC lipids. We have obtained membranes with a capacitance between 120 and 230 pF and a rupture voltage between 200 and 400 mV, typical values for bilayers.

In order to insert MscL we have applied step-by-step tension voltage of +/- 50 mV, +/- 100 mV, +/- 150 mV, and +/- 200 mV. Figure 76 shows the conductance recorded at + 200 mV.

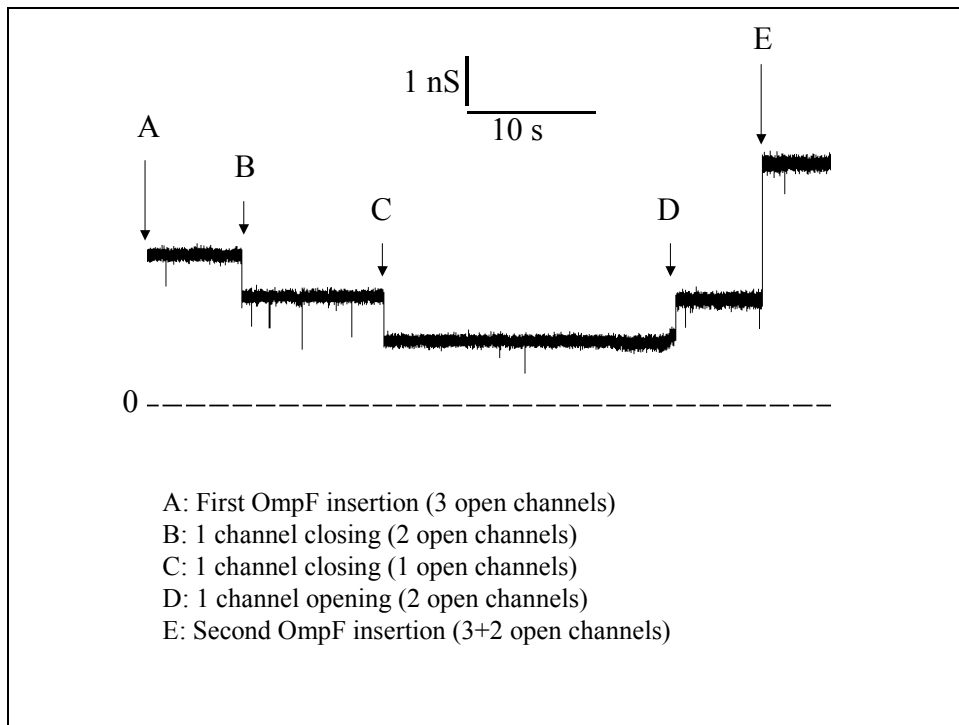


Figure 76: Conductance observed at +200 mV

We observed a conductance of 3 nS due to the insertion of a channel in the membrane. It is typical gating observed at high voltage for OmpF channels [97]; the protein solution was not perfectly pure and this method allows detecting single protein.

The MscL channel is normally closed. We have thus not observed the corresponding signal (at least 10 times the conductance of OmpF in accordance with patch-clamp recording [93]). As indicated by its name, MscL is sensible to a mechanical stress. In patch-clamp experiments the channel is open by pipette suction on proteoliposome or directly on membrane cell.

We have tried different ways to open the channels. Firstly we have applied a hydrostatic pressure by using different volumes on both sides of the bilayer. Secondly we have replaced in one side the buffer by PEG solution in order to create an osmotic pressure on the membrane. No significant conductance was observed.

We have repeated the same experiments with E.Coli extract lipids normally used in 2D crystal reconstitution. But the membrane is hard to form and not very stable. After rupture it is difficult to reform a membrane in presence of PEG in one bath.

9.4 Conclusion and perspectives

The BLM technique was used to test the functional reconstitution of MscL in membranes. Before using polymer membranes, we should know the conductance values of this channel in lipid bilayers. Until now we have not obtained significant results.

This could be due to several reasons. First MscL is not inserted in the BLM. Secondly, MscL is inserted in the BLM, but the hydrostatic or osmotic pressure created is not sufficient to open the channels.

It will be interesting to test another type of MscL, particularly E.Coli-MscL, which needs less than 100 mm Hg [98] to open, whereas Tb-MscL needs ~200 mm Hg pipette pressure from patch-clamp experiments to be opened.[99]. We can also imagine a system to apply not a pressure but a real mechanical stress to the membrane because MscL is in fact sensible to tension.

We should also try in a polymer membrane that can reticulate. The cross-linked membrane is more rigid and would thus transmit better tensions, facilitating opening of MscL. In order to perform those experiments on polymer we should use a second BLM system that we have already tried on our polymer [18].

10 APPENDIX III: Polymer nanocontainers for selective immobilization at surfaces

Reactive, water-soluble and filled polymer nanocontainers have been developed in our group using a two-step emulsion polymerization via core-shell latexes (Figure 77). In the future, the outer surface of nanocontainers will be modified with functional groups that couple them covalently at surfaces.

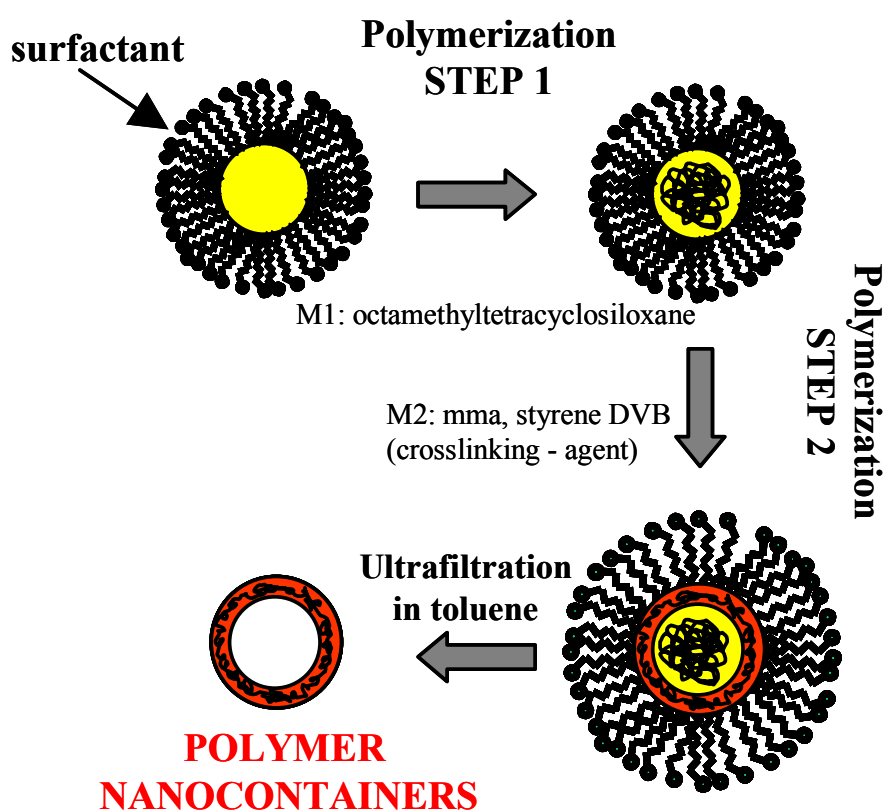


Figure 77: Schematic representation of the polymer nanocontainer production via core-shell latexes

Figure 78 shows systematic TEM study of the morphologies obtained, allowing the control of each step of the nanocontainer preparation.

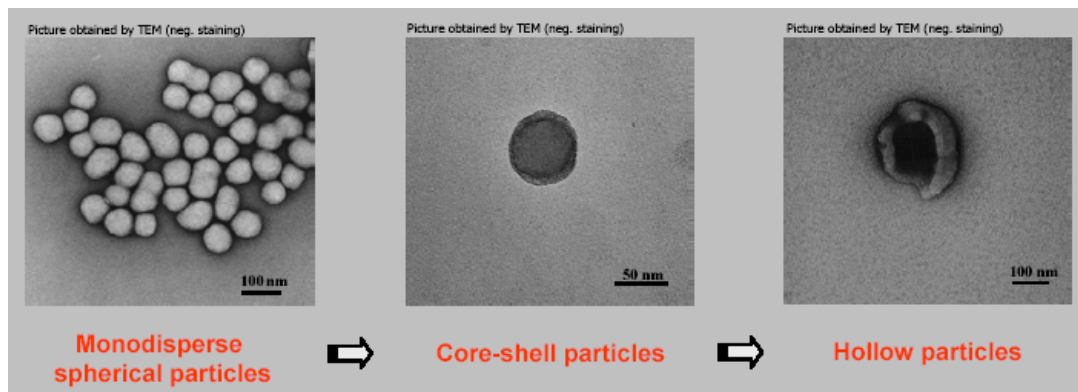


Figure 78: Morphology of particles studied by TEM

11 Publications and Posters

A part of this work has been already published or presented in poster sessions.

POSTER PRESENTATIONS

- 2003 Nanotubes and vesicles from ABA-triblock copolymers: Biomimetic membranes for protein reconstitution, J. Grumelard, S. Benito and W. Meier, Swiss Chemical Society Fall Meeting, Lausanne, Switzerland
- 2003 Influence of preparation method on self-assembly of block copolymers, J. Grumelard and W. Meier, National Center of Competence in Research Nanoscale Science Review panel, Basel, Switzerland
- 2004 Hollow nanotubes and vesicles: From copolymers to biomimetic membranes, J. Grumelard and W. Meier, Polymer Group of Switzerland Spring Meeting, Polymer in Life Sciences, Basel, Switzerland
- 2004 Polymer nanocontainers for selective immobilization at surfaces, S. Poux, J. Grumelard and W. Meier, World Polymer Congress MACRO 2004, 40th IUPAC International Symposium on Macromolecules, Paris, France

PUBLICATION LIST

- 2003 Poster Abstract 293, Physical Chemistry session of SCS Fall meeting, *Chimia*, 57, p 454
- 2004 Soft nanotubes from amphiphilic ABA triblock macromonomers, J. Grumelard, A. Taubert, W. Meier, *Chemical Communications*, 13, p 1462-3
- Submitted Block copolymer vesicles – Using concepts from polymer chemistry to mimic biomembranes, K. Katarzyna, J. Grumelard, T. Haeffele, W. Meier, *Polymer*

Soft nanotubes from amphiphilic ABA triblock macromonomers

Julie Grumelard, Andreas Taubert and Wolfgang Meier*

Department of Chemistry, University of Basel, Klingelbergstrasse 80, CH-4056 Basel, Switzerland.

E-mail: Wolfgang.meier@unibas.ch; Fax: +41 61 267 3850; Tel: +41 61 267 3802

Received (in Cambridge, UK) 16th April 2004, Accepted 7th May 2004

First published as an Advance Article on the web 25th May 2004

Soft, water-filled polymer nanotubes of several tens of μm in length have been prepared *via* self-assembly of amphiphilic ABA-triblock macromonomers in aqueous media; the tubes are mechanically and chemically stable and can be loaded with water-soluble substances.

Nanotube research is currently one of the most active areas of Nanoscience.¹ Carbon nanotubes could have applications in miniature electronics and for hydrogen storage, but as they are stiff, difficult to process and purify, not biocompatible, and cannot be degraded by living organisms they are not well suited for biological applications; soft nanotubes made from biocompatible organic molecules and polymers however could find application in biotechnology and biomedicine.² Typical examples include self-assembled lipid nanotubes,³ and peptide-based nanotubes.⁴ Recently also block copolymers have been used to prepare vesicles and spherical or rod-like micelles.⁵ Polymer nanotubes however have so far only been described in organic solvents where their fabrication often requires elaborate procedures;^{6–8} however, the controlled preparation of water-filled polymer nanotubes in aqueous media has remained elusive. This communication introduces a simple method for the preparation of mechanically stable, water-filled, and soft nanotubes *via* the self-assembly of amphiphilic triblock copolymers.

Amphiphilic poly(2-methylloxazoline-*block*-dimethylsiloxane-*block*-2-methylloxazoline) (PMOXA-*b*-PDMS-*b*-PMOXA) ABA triblock copolymers were synthesized *via* cationic ring-opening polymerization of 2-methylloxazoline onto an activated telechelic PDMS block.⁹ The length of each block can be adjusted by the amount of monomer added to the reaction mixture and the -OH end groups of the PMOXA blocks allow for the functionalization with methacrylic acid. These triblock macromonomers form supramolecular assemblies in aqueous solution that can be chemically crosslinked *via* polymerization of the methacrylic acid groups. For the current study, we have used symmetric triblock copolymers with molecular weights ranging from 7000 to 9000 g mol^{-1} and a PDMS block of roughly 5000 g mol^{-1} .

Polymer nanotubes were fabricated *via* film rehydration. A 1% (wt/wt) solution of the copolymer in chloroform was dried under nitrogen in a test tube; by rotating the tube during drying a polymer film forms on the glass. Drying was completed by desiccation under vacuum overnight. The film was then rehydrated by water addition and stirring for 24 hours to yield a 1 wt% polymer solution, which is homogeneous and opaque. After a 10-fold dilution with water, the samples were examined with transmission electron microscopy (TEM, Hitachi H-7000). Experiments without dilution and with 1000-fold dilution yielded the same morphologies but the TEM imaging conditions were best at 10-fold dilution.

Fig. 1 shows a schematic of a self-assembled nanotube and a typical sample; the TEM image shows that the solution contains a mixture of vesicles and flexible nanotubes. The vesicles are quite polydisperse with diameters ranging from 40 to over 500 nm, but the tube diameter is astonishingly uniform at about 40 nm. The nanotubes extend up to several tens of microns in length and their concentration with respect to the number of vesicles depends on the copolymer used, that is, the formation of the tubes *vs.* vesicles depends on the relative block lengths of the hydrophilic PMOXA and hydrophobic PDMS blocks.

Table 1 summarizes the nanotube formation results. A low PDMS/PMOXA wt/wt ratio (below ~ 1.5) favors vesicle formation and higher ratios (~ 2 and higher) increasingly favor nanotube formation. This tendency is qualitatively confirmed with a control experiment where the dry polymer was directly dissolved in water and imaged in the TEM.

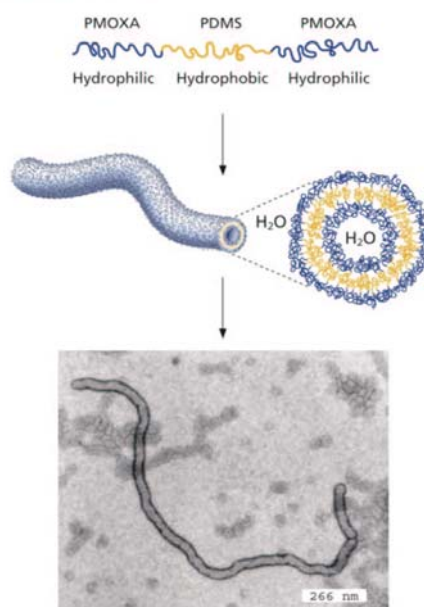


Fig. 1 Self-assembly of ABA triblock copolymers in aqueous solution; TEM image of a polymer nanotube.

Table 1 Approximate volume fraction of tubes as a function of polymer composition and sample preparation^a

Copolymer ^b	PDMS/PMOXA Ratio (wt/wt)	Tube volume fraction	
		Rehydration	Dissolution
A ₁₁ B ₆₂ A ₁₁	2.4	90 ± 5	30 ± 5
A ₁₆ B ₇₂ B ₁₆	2.1	85 ± 5	20 ± 5
A ₁₅ B ₆₂ B ₁₅	1.9	75 ± 5	25 ± 5
A ₂₁ B ₇₂ B ₂₁	1.5	5 ± 5	1 ± 5
A ₂₁ B ₆₂ B ₂₁	1.5	10 ± 5	5 ± 5

^a Volume fractions were estimated from TEM images by assuming that the area occupied by tubes is directly related to their volume fraction. ^b A: PMOXA, B: PDMS.

Although we observe a trend in both sets of experiments, a quantification of this phenomenon is difficult from TEM data alone and the data in Table 1 thus have an error of about 10%. Nevertheless, these findings suggest that the formation of the nanotubes is largely controlled by the geometry of the PMOXA blocks: at a ratio of ~ 1.5 the PMOXA block is, relatively speaking, larger than at a ratio of ~ 2 and more and it hence favors vesicles over tubes because each chain occupies a larger hydrodynamic volume.

The results in Table 1 also indicate that not only the PDMS/PMOXA ratio but also the preparation procedure influences the formation of the nanotubes; film rehydration is thus a more efficient pathway to polymer nanotubes than simple dissolution of the dry polymer in water. It is hence an elegant additional method to enhance nanotube over vesicle formation.

A major reason for the interest in polymer vesicles and nanotubes is their high mechanical stability compared to lipid nanotubes. For example, our nanotubes are resistant to repeated filtration through 0.45 μm filters and to size exclusion chromatography. The nanotubes also remain stable over 8 months if stored at 4 $^{\circ}\text{C}$.

As the polymers can be functionalized with methacrylate end groups that polymerize upon UV-irradiation, chemical cross-linking can further increase nanotube stability. As in earlier experiments¹⁰ we have seen by Nuclear Magnetic Resonance that the conversion of the methacrylates is almost complete and that the nanotube shapes are therefore permanently fixed. This is also confirmed by dissolution experiments: only the crosslinked nanotubes preserve their structural integrity after dispersion in ethanol or chloroform (which are good solvents for both blocks of the polymers). This is confirmed in Fig. 2 that shows polymerized nanotubes isolated from ethanol. Obviously the incorporation of methacrylate end groups and subsequent UV polymerization does not change the shape of the aggregates but yields a mechanically even more stable structure.

To prove the formation of water-filled tubes (as opposed to rodlike micelles with a hydrophobic interior) we have encapsulated carboxyfluorescein (CF), a water-soluble fluorescent dye, into the nanotubes. To that end, a copolymer film was prepared as before, but was rehydrated with a 10 mM solution of CF in PBS buffer.[†] The final copolymer concentration was again 1 wt%. Non-encapsulated CF was removed by size exclusion chromatography (Sephacrose[®] 4B, Sigma). The purified sample was re-concentrated by centrifugation (Centricon[®] YM-100, 100'000 Da nominal molecular weight limit cut-off) and examined with fluorescence microscopy (Leica DMIRE2).

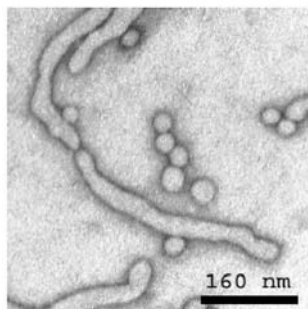


Fig. 2 TEM image of cross-linked nanotubes and vesicles.

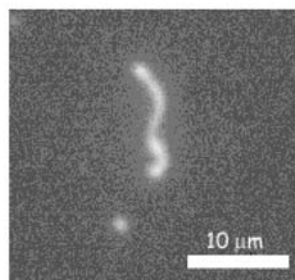


Fig. 3 Fluorescence micrograph of a CF-loaded nanotube.

Fig. 3 shows an intense fluorescence from the interior of a tube (and a vesicle), but no measurable intensity outside. This proves that the inside of the tubes really contains water and CF. This in turn rules out the formation of rodlike micelles. The fluorescence microscopy also demonstrates the exceptional stability and low permeability of the nanotubes because the fluorescence dye CF was kept in the tube during the whole purification process.

In conclusion, we have demonstrated the direct formation of soft water-filled nanotubes from ABA-triblock copolymers by direct self-assembly from a dry film. The nanotubes are mechanically stable and can be loaded with water-soluble substances. The possibility to add reactive groups to the copolymer enables further stabilization by chemical cross-linking; other functional groups may enable specific targeting or molecular recognition. Self-assembled polymer nanotubes may thus find applications as smart drug delivery devices, as highly specific templates for inorganic synthesis, and in nanofluidics, where they could act as connections between different, spatially separated compartments. As an extension of this current study, we are exploring asymmetric ABC triblock copolymers for the fabrication of nanotubes with chemically different inner and outer surfaces.¹¹

We thank Professor A. Engel, Dr T. Braun, and Dr M. Chami for providing the TEM equipment and for help with experiments and image analysis, S. Benito, T. Haefele, and J. Widmer for polymer synthesis, and R. Pfalzberger for the sketch in Fig. 1. Financial support from the National Center for Competence in Research "Nanoscale Science" and the Swiss National Science Foundation is gratefully acknowledged.

Notes and references

[†] PBS – Phosphate Buffer Saline, pH = 7.4.

- 1 M. L. Cohen, *Mater. Sci. Eng., C*, 2001, **C15**, 1.
- 2 C. R. Martin and P. Kohli, *Nature Rev. Drug Discovery*, 2003, **2**, 29.
- 3 A. I. Smirnov and O. G. Poluektov, *J. Am. Chem. Soc.*, 2003, **125**, 8434.
- 4 J. M. Buriak and M. R. Ghadiri, *Mater. Sci. Eng., C*, 1997, **C4**, 207.
- 5 Y.-Y. Won, A. K. Braman, H. T. Davis and F. S. Bates, *J. Phys. Chem. B*, 2002, **106**, 3354.
- 6 S. Stewart and G. Liu, *Angew. Chem. Int. Ed.*, 2000, **39**, 340.
- 7 K. Yu and A. Eisenberg, *Macromolecules*, 1998, **31**, 3509.
- 8 J. Ruez, R. Barjovani, J. A. Massey, M. A. Winnik and I. Manners, *Angew. Chem. Int. Ed.*, 2000, **39**, 3862.
- 9 C. Nardin, T. Hirt, J. Leukel and W. Meier, *Langmuir*, 2000, **16**, 1035.
- 10 W. Meier, T. Hirt and C. Nardin, *PCT Int. Appl.*, 2001, 28.
- 11 R. Stoescu and W. Meier, *Chem. Commun.*, 2002, 3016.

12 Acknowledgments

This PhD thesis has been prepared in the **Department of Chemistry of the University of Basel** under the supervision of **Pr. Wolfgang Meier**. I would like first to gratefully acknowledge him for offering me this position, and for his scientific help during those 3 years. I had the chance to work on a subject combining polymers and membrane proteins, which looks to be very promising for Nanoscience (the Nobel Prize 2003 recompenses discoveries concerning channels in cell membranes!).

I am grateful to **Pr. Marcus Textor** from ETH of Zurich for accepting to be my co-referee.

I would like to thank especially **Pr. Andreas Engel**, from the **Biocenter of Basel**, who offers me the possibility to collaborate strongly with his group. It allows me to go back over my first scientific formation in biology. I thank all Engel's group members for their kindness, and especially **Dr. Thomas Braun** for protein reconstitution, **Dr. Mohamed Chami** for TEM, **Thomas Kaufmann** for MscL purification, and **Dr. Hervé Rémigy** for dilution machine.

Thanks to **Dr. Leo Merz** from the **Department of Physics of Basel** for AFM experiments and his kindness.

I thank **Pr. Matthias Winterhalter** from **CNRS of Toulouse** (France), who invited me to spend 1 month in his laboratory, and **Dr. Christophe Danelon** for teaching me the Black Lipid Membrane technique.

Meier's group is now really huge: we were 7 when I arrived... and more than 30 when I finish! So I thank everybody for the stimulating ambiance; I have learned that it is perhaps not always easy, but even always interesting to work in a multinational environment! (9 countries were represented!)

For introducing me all the experiments in the lab I thank sincerely Alexandra! Thanks also to Michael for the time he spent to solve my computer problems. For our joint

experiments I thank Alexandra, Caroline, Samantha, Sandrine and Sven. For their help in my experiments I thank Daniel, Roxana, Stefan Graber (trainee) and Thomas. For the articles jointly written I thank Andreas and Kasia.

I also gratefully thank Andreas and Per for corrections of the thesis.

I do not forget all the persons of the Institute of PC who contribute, by their help and their good mood, to render this PhD so pleasant.

I would like to finish my thanks by my parents, who always encourage me to do what I like and support me in all my ventures!

13 REFERENCES

1. Voet, D. and J.G. Voet, *Biochemistry: Second Edition*. 1995. p. 1361 pp.
2. Zhang, Y.-P., B. Ceh, and D.D. Lasic, *Liposomes in drug delivery*, in *Polymeric Biomaterials (2nd Edition)*. 2002. p. 783-821.
3. Vanlerberghe, G., *Liposomes in cosmetics: how and why?*, in *Handbook of Nonmedical Applications of Liposomes*. 1996. p. 77-89.
4. Lasic, D.D. and Editor, *Liposomes in Gene Delivery*. 1997. p. 320 pp.
5. Winterhalter, M. and D.D. Lasic, *Liposome stability and formation: experimental parameters and theories on the size distribution*, in *Chemistry and physics of lipids*. 1993: Ireland. p. 35-43.
6. Ringsdorf, H., B. Schlarb, and J. Venzmer, *Molecular architecture and function in polymeric oriented systems. Models for the study of organization, surface recognition, and dynamics in biomembranes*, in *Angewandte Chemie*. 1988. p. 117-62.
7. Lasic, D.D., E. Bolotin, and R.N. Brey, *Polymerized liposomes: from biophysics to applications. Part I*, in *Chimica Oggi*. 2000. p. 48-51.
8. Silvander, M., *Steric stabilization of liposomes - a review*, in *Progress in Colloid & Polymer Science*. 2002. p. 35-40.
9. Lasic, D.D., *Sterically stabilized vesicles*, in *Angewandte Chemie*. 1994. p. 1765-79, (See also *Angew. Chem., Int. Ed. Engl.*, 1994, 33(17), 1685-90).
10. Neumann, R. and H. Ringsdorf, *Peptide liposomes from amphiphilic amino acids*, in *Journal of the American Chemical Society*. 1986. p. 487-90.
11. Neumann, R., et al., *Preparation and characterization of long chain amino acid and peptide vesicle membranes*, in *Biochimica et biophysica acta*. 1987: Netherlands. p. 338-48.
12. Tirrell, D.A., D.Y. Takigawa, and K. Seki, *Interactions of synthetic polymers with cell membranes and model membrane systems. Part 7. pH sensitization of phospholipid vesicles via complexation with synthetic poly(carboxylic acid)s*, in *Annals of the New York Academy of Sciences*. 1985. p. 237-48.
13. Takigawa, D.Y. and D.A. Tirrell, *Interactions of synthetic polymers with cell membranes and model membrane systems, 9. Reversal of magnesium(2+)*

- induced structural changes in dipalmitoylphosphatidylglycerol bilayers by adsorbed poly(ethyleneimine)s*, in *Makromolekulare Chemie, Rapid Communications*. 1985. p. 653-7.
14. Gero Decher, E.K., Helmut Ringsdorf, Joachim Venzmer, Dieter Bitter-Suermann, Christoph Weisgerber, *Interaction of amphiphilic polymers with model membranes*. *Angewandte Makromolekulare Chemie*, 1989. **166**(1): p. 71-80.
 15. Meier, W., et al., *Stabilization of planar lipid membranes: A stratified layer approach*, in *Physical Chemistry Chemical Physics*. 2000. p. 4559-4562.
 16. Graff, A., M. Winterhalter, and W. Meier, *Nanoreactors from Polymer-Stabilized Liposomes*, in *Langmuir*. 2001. p. 919-923.
 17. Nardin, C., et al., *Nanoreactors based on (polymerized) ABA-triblock copolymer vesicles*, in *Chemical Communications (Cambridge)*. 2000. p. 1433-1434.
 18. Nardin, C., M. Winterhalter, and W. Meier, *Giant Free-Standing ABA Triblock Copolymer Membranes*, in *Langmuir*. 2000. p. 7708-7712.
 19. Nardin, C., et al., *Polymerized ABA Triblock Copolymer Vesicles*, in *Langmuir*. 2000. p. 1035-1041.
 20. Nardin, C. and W. Meier, *Hybrid materials from amphiphilic block copolymers and membrane proteins*, in *Reviews in Molecular Biotechnology*. 2002. p. 17-26.
 21. Graff, A., et al., *Virus-assisted loading of polymer nanocontainer*, in *Proceedings of the National Academy of Sciences of the United States of America*. 2002. p. 5064-5068.
 22. Nardin, C. and W. Meier, *Polymerizable amphiphilic block copolymers: From nanostructured hydrogels to nanoreactors and ultrathin films*, in *Chimia*. 2001. p. 142-146.
 23. Sauer, M., et al., *Ion-carrier controlled precipitation of calcium phosphate in giant ABA triblock copolymer vesicles*, in *Chemical Communications (Cambridge, United Kingdom)*. 2001. p. 2452-2453.
 24. Tuzar, Z. and P. Kratochvil, *Micelles of block and graft copolymers in solutions*, in *Surface and Colloid Science*. 1993. p. 1-83.
 25. Willison, J.H.M. and A.J. Rowe, *Practical Methods in Electron Microscopy, Vol. 8: Replica, Shadowing and Freeze-Etching Techniques*. 1980. p. 300 pp.

26. Nguyen-Misra, M., S. Misra, and W.L. Mattice, *Bridging by End-Adsorbed Triblock Copolymers*, in *Macromolecules*. 1996. p. 1407-15.
27. Wang, Y., W.L. Mattice, and D.H. Napper, *Simulation of the self-assembly of symmetric triblock copolymers in dilute solution*, in *Macromolecules*. 1992. p. 4073-7.
28. Soo, P.L. and A. Eisenberg, *Preparation of block copolymer vesicles in solution*, in *Journal of Polymer Science, Part B: Polymer Physics*. 2004. p. 923-938.
29. Luo, L. and A. Eisenberg, *Thermodynamic Stabilization Mechanism of Block Copolymer Vesicles*, in *Journal of the American Chemical Society*. 2001. p. 1012-1013.
30. Luo, L. and A. Eisenberg, *Thermodynamic Size Control of Block Copolymer Vesicles in Solution*, in *Langmuir*. 2001. p. 6804-6811.
31. Choucair, A.A., A.H. Kycia, and A. Eisenberg, *Kinetics of Fusion of Polystyrene-*b*-poly(acrylic acid) Vesicles in Solution*, in *Langmuir*. 2003. p. 1001-1008.
32. Nardin, C., et al., *Amphiphilic block copolymer nanocontainers as bioreactors*, in *European Physical Journal E: Soft Matter*. 2001. p. 403-410.
33. Rigaud, J.L., et al., *Use of detergents in two-dimensional crystallization of membrane proteins*, in *Biochimica et Biophysica Acta*. 2000. p. 112-128.
34. Rigaud, J.L., et al., *Detergent removal by non-polar polystyrene beads. Applications to membrane protein reconstitution and two-dimensional crystallization*, in *European Biophysics Journal*. 1998. p. 305-319.
35. Engel, A., et al., *Assembly of 2-D membrane protein crystals: dynamics, crystal order, and fidelity of structure analysis by electron microscopy*, in *Journal of structural biology*. 1992: United States. p. 219-34.
36. Pata, V., et al., *Membrane Solubilization by Detergent: Resistance Conferred by Thickness*, in *Langmuir*. 2004. p. 3888-3893.
37. Dolder, M., A. Engel, and M. Zulauf, *The micelle to vesicle transition of lipids and detergents in the presence of a membrane protein: towards a rationale for 2D crystallization*, in *FEBS letters*. 1996: Netherlands. p. 203-8.
38. Remigy, H.W., et al., *Membrane protein reconstitution and crystallization by controlled dilution*, in *FEBS Letters*. 2003. p. 160-169.

39. Rigaud, J.L., et al., *Bio-Beads: an efficient strategy for two-dimensional crystallization of membrane proteins*, in *Journal of structural biology*. 1997: United States. p. 226-35.
40. Levy, D., et al., *Phospholipid vesicle solubilization and reconstitution by detergents. Symmetrical analysis of the two processes using octaethylene glycol mono-n-dodecyl ether*, in *Biochemistry*. 1990: United States. p. 9480-8.
41. Levy, D., et al., *A systematic study of liposome and proteoliposome reconstitution involving Bio-Bead-mediated Triton X-100 removal*, in *Biochimica et biophysica acta*. 1990: Netherlands. p. 179-90.
42. Rotenberg, Y., L. Boruvka, and A.W. Neumann, *Determination of surface tension and contact angle from the shapes of axisymmetric fluid interfaces*, in *Journal of Colloid and Interface Science*. 1983. p. 169-83.
43. Rigaud, J.L., M.T. Paternostre, and A. Bluzat, *Mechanisms of membrane protein insertion into liposomes during reconstitution procedures involving the use of detergents. 2. Incorporation of the light-driven proton pump bacteriorhodopsin*, in *Biochemistry*. 1988: United States. p. 2677-88.
44. Kahya, N., et al., *Reconstitution of membrane proteins into giant unilamellar vesicles via peptide-induced fusion*, in *Biophysical Journal*. 2001. p. 1464-1474.
45. Discher, B.M., et al., *Polymersomes: Tough vesicles made from diblock copolymers*, in *Science (Washington, D. C.)*. 1999. p. 1143-1146.
46. Lee, J.C.M., et al., *Preparation, stability, and in vitro performance of vesicles made with diblock copolymers*, in *Biotechnology and Bioengineering*. 2001. p. 135-145.
47. Discher, B.M., et al., *Cross-linked Polymersome Membranes: Vesicles with Broadly Adjustable Properties*, in *Journal of Physical Chemistry B*. 2002. p. 2848-2854.
48. Dimova, R., et al., *Hyperviscous diblock copolymer vesicles*, in *European Physical Journal E: Soft Matter*. 2002. p. 241-250.
49. Bermudez, H., et al., *Molecular Weight Dependence of Polymersome Membrane Structure, Elasticity, and Stability*, in *Macromolecules*. 2002. p. 8203-8208.

50. Pata, V. and N. Dan, *The effect of chain length on protein solubilization in polymer-based vesicles (polymersomes)*, in *Biophysical Journal*. 2003. p. 2111-2118.
51. Graff, A., *Insertion of membrane proteins in artificial polymer membranes*, in *Department of Chemistry*. 2004, University of Basel: Basel.
52. Friedrich, T., *The NADH:ubiquinone oxidoreductase (complex I) from Escherichia coli*, in *Biochimica et Biophysica Acta*. 1998. p. 134-146.
53. Leif, H., et al., *Isolation and characterization of the proton-translocating NADH:ubiquinone oxidoreductase from Escherichia coli*, in *European Journal of Biochemistry*. 1995. p. 538-48.
54. Stoenescu, R. and W. Meier, *Vesicles with asymmetric membranes from amphiphilic ABC triblock copolymers*, in *Chemical Communications (Cambridge, United Kingdom)*. 2002. p. 3016-3017.
55. Cohen, M.L., *Nanotubes, Nanoscience, and Nanotechnology*, in *Materials Science & Engineering, C: Biomimetic and Supramolecular Systems*. 2001. p. 1-11.
56. Martin, C.R. and P. Kohli, *The emerging field of nanotube biotechnology*, in *Nature Reviews Drug Discovery*. 2003. p. 29-37.
57. Smirnov, A.I. and O.G. Poluektov, *Substrate-supported lipid nanotube arrays*, in *Journal of the American Chemical Society*. 2003. p. 8434-8435.
58. Buriak, J.M. and M.R. Ghadiri, *Self-assembly of peptide based nanotubes*, in *Materials Science & Engineering, C: Biomimetic Materials, Sensors and Systems*. 1997. p. 207-212.
59. Won, Y.-Y., et al., *Cryogenic Transmission Electron Microscopy (Cryo-TEM) of Micelles and Vesicles Formed in Water by Poly(ethylene oxide)-Based Block Copolymers*, in *Journal of Physical Chemistry B*. 2002. p. 3354-3364.
60. Stewart, S. and G. Liu, *Block copolymer nanotubes*, in *Angewandte Chemie, International Edition*. 2000. p. 340-344.
61. Yu, K. and A. Eisenberg, *Bilayer Morphologies of Self-Assembled Crew-Cut Aggregates of Amphiphilic PS-b-PEO Diblock Copolymers in Solution*, in *Macromolecules*. 1998. p. 3509-3518.
62. Raez, J., et al., *Self-assembled organometallic block copolymer nanotubes*, in *Angewandte Chemie, International Edition*. 2000. p. 3862-3865.

63. Mela, P., et al., *Nanofluidics*, in *Encyclopedia of Nanoscience and Nanotechnology*. 2004. p. 739-755.
64. Jain, S. and F.S. Bates, *Consequences of Nonergodicity in Aqueous Binary PEO-PB Micellar Dispersions*, in *Macromolecules*. 2004. p. 1511-1523.
65. Grumelard, J., A. Taubert, and W. Meier, *Soft nanotubes from amphiphilic ABA triblock macromonomers*, in *Chemical communications (Cambridge, England)*. 2004: England: United Kingdom. p. 1462-3.
66. Hirano, K., H. Fukuda, and S.L. Regen, *Polymerizable ion-paired amphiphiles*, in *Langmuir*. 1991. p. 1045-7.
67. Israelachvili, J.N., *Intermolecular and Surface Forces*. 1991. p. 291 pp.
68. Antonietti, M. and S. Foerster, *Vesicles and liposomes: A self-assembly principle beyond lipids*, in *Advanced Materials (Weinheim, Germany)*. 2003. p. 1323-1333.
69. Evans, E. and D. Needham, *Physical properties of surfactant bilayer membranes: thermal transitions, elasticity, rigidity, cohesion and colloidal interactions*. *Journal of Physical Chemistry*, 1987. **91**(16): p. 4219-4228.
70. Angelova, M.I., et al., *AC field controlled formation of giant fluctuating vesicles and bending elasticity measurements*, in *Springer Proceedings in Physics*. 1992. p. 178-82.
71. Thomas, E.L., et al., *Large area orientation of block copolymer microdomains in thin films*, in *U.S. Pat. Appl. Publ.* 2003, (USA). US. p. 42 pp.
72. Hong, K., et al., *Liposomes containing colloidal gold are a useful probe of liposome-cell interactions*, in *Biochimica et Biophysica Acta*. 1983. p. 320-3.
73. Gao, K. and L. Huang, *Solid core liposomes with encapsulated colloidal gold particles*, in *Biochimica et Biophysica Acta*. 1987. p. 377-83.
74. Sato, T., et al., *Photochemical deposition of noble metal ultrafine particles onto liposomes*, in *Journal of Materials Chemistry*. 1997. p. 1837-1840.
75. Hayat, M.A. and Editor, *Colloidal Gold: Principles, Methods, and Applications, Vol. 1*. 1989. p. 536 pp.
76. Huang, S.K., et al., *Light microscopic localization of silver-enhanced liposome-entrapped colloidal gold in mouse tissues*, in *Biochimica Et Biophysica Acta*. 1991: Netherlands. p. 117-21.

77. Esumi, K., K. Matsuhisa, and K. Torigoe, *Preparation of Rodlike Gold Particles by UV Irradiation Using Cationic Micelles as a Template*, in *Langmuir*. 1995. p. 3285-7.
78. Zhou, Y., et al., *A Novel ultraviolet irradiation technique for shape-controlled synthesis of gold nanoparticles at room temperature*, in *Chemistry of Materials*. 1999. p. 2310-2312.
79. Esumi, K., et al., *Preparation of Gold Colloids with UV Irradiation Using Dendrimers as Stabilizer*, in *Langmuir*. 1998. p. 3157-3159.
80. Sidorov, S.N., et al., *Influence of Metalation on the Morphologies of Poly(ethylene oxide)-block-poly(4-vinylpyridine) Block Copolymer Micelles*, in *Langmuir*. 2004. p. 3543-3550.
81. Hughes, A.E. and S.C. Jain, *Metal colloids in ionic crystals*, in *Advances in Physics*. 1979. p. 717-828.
82. Creighton, J.A. and D.G. Eadon, *Ultraviolet-visible absorption spectra of the colloidal metallic elements*, in *Journal of the Chemical Society, Faraday Transactions*. 1991. p. 3881-91.
83. Spehr, V., et al., *Overexpression of the Escherichia coli nuo-Operon and Isolation of the Overproduced NADH:Ubiquinone Oxidoreductase (Complex I)*, in *Biochemistry*. 1999. p. 16261-16267.
84. Friedrich, T., et al., *A small isoform of NADH:ubiquinone oxidoreductase (complex I) without mitochondrially encoded subunits is made in chloramphenicol-treated Neurospora crassa*, in *European journal of biochemistry / FEBS*. 1989: GERMANY, WEST: Germany, Federal Republic of. p. 173-80.
85. Baldwin, S.A. and Editor, *Membrane Transport: A Practical Approach*. 2000. p. 320 pp.
86. Aggerbeck, L.P. and T. Gulik-Krzywicki, *Studies of lipoproteins by freeze-fracture and etching electron microscopy*, in *Methods in enzymology*. 1986: United States. p. 457-72.
87. Angelova, M. and D. Dimitrov, *Swelling of charged lipids and formation of liposomes on electrode surfaces*, in *Molecular Crystals and Liquid Crystals*. 1987. p. 89-104.
88. Vollhardt, D., *Phase transition in adsorption layers at the air-water interface*. *Advances in Colloid and Interface Science*, 1999. **79**(1): p. 19-57.

89. Munoz, M.G., et al., *Monolayers of symmetric triblock copolymers at the air-water interface. 1. Equilibrium properties*. Langmuir, 2000. **16**(3): p. 1083-1093.
90. Munoz, M.G., et al., *Monolayers of symmetric triblock copolymers at the air-water interface. 2. Adsorption kinetics*. Langmuir, 2000. **16**(3): p. 1094-1101.
91. Benito, S., *PhD thesis*. 2004.
92. Levy, D., M. Chami, and J.L. Rigaud, *Two-dimensional crystallization of membrane proteins: the lipid layer strategy*, in *FEBS Letters*. 2001. p. 187-193.
93. Hamill, O.P. and B. Martinac, *Molecular basis of mechanotransduction in living cells*, in *Physiological Reviews*. 2001. p. 685-740.
94. Meier, W., C. Nardin, and M. Winterhalter, *Reconstitution of channel proteins in (polymerized) ABA triblock copolymer membranes*, in *Angewandte Chemie, International Edition*. 2000. p. 4599-4602.
95. Chang, G., et al., *Structure of the MscL homolog from Mycobacterium tuberculosis: a gated mechanosensitive ion channel*, in *Science (Washington, D. C.)*. 1998. p. 2220-2226.
96. Montal, M. and P. Mueller, *Formation of bimolecular membranes from lipid monolayers and a study of their electrical properties*, in *Proceedings of the National Academy of Sciences of the United States of America*. 1972: United States. p. 3561-6.
97. Rostovtseva, T.K., E.M. Nestorovich, and S.M. Bezrukov, *Partitioning of differently sized poly(ethylene glycol)s into OmpF porin*, in *Biophysical Journal*. 2002. p. 160-169.
98. Hase, C.C., A.C. Le Dain, and B. Martinac, *Purification of functional reconstitution of the recombinant large mechanosensitive ion channel (MscL) of Escherichia coli*, in *Journal of Biological Chemistry*. 1995. p. 18329-34.
99. Moe, P.C., G. Levin, and P. Blount, *Correlating a protein structure with function of a bacterial mechanosensitive channel*, in *Journal of Biological Chemistry*. 2000. p. 31121-31127.